DISSERTATION

STRUCTURE-FUNCTION RELATIONSHIPS UNDERLYING GLUA2 MECHANISMS OF DEACTIVATION, DESENSITIZATION, AND MODULATION

Submitted by

Jonathan E. Harms

Department of Biomedical Sciences

In partial fulfillment of the requirements

For the Degree of Doctor of Philosophy

Colorado State University

Fort Collins, Colorado

Spring 2013

Doctoral Committee:

Advisor: Kathryn M. Partin

Gregory C. Amberg
Ashok Prasad
Michael M. Tamkun

ABSTRACT

STRUCTURE-FUNCTION RELATIONSHIPS UNDERLYING GLUA2 MECHANISMS OF DEACTIVATION, DESENSITIZATION, AND MODULATION

Glutamate is the primary excitatory neurotransmitter in the central nervous system, where it is principally responsible for mediating excitatory neurotransmission. Ligand-gated receptors to glutamate, such as the a-amino-3-hydroxy-5-methyl-isoxazole-propionic acid (AMPA) receptor, are responsible for many cognitive processes; with the AMPA receptor showing an essential role in learning, memory, and synaptic plasticity. As many mental illnesses and diseases show underlying cognitive complications, therapeutic drugs that can alleviate these cognitive deficits show tremendous potential benefit. However, despite great interest and continued advancement, progress of drugs through clinical trials into available treatments has been slow and problematic.

One potential reason for the slow progress of drug development is a lack of basic understanding for how compounds bind to AMPA receptors and upregulate their function. Presented here are several studies aimed to better understand how structural interactions regulate AMPA receptor mechanisms of gating and modulation. These studies combine fast-perfusion electrophysiology capable of simulating synaptic events with structural information obtained from x-ray crystallography studies to analyze potential mechanisms of allosteric modulation. Promisingly, we have identified potential patterns relating modulator properties such as size and rigidity with their observed physiological effects. Such patterns suggest that information from these studies can facilitate design of more

targeted and efficacious cognition enhancing drugs. In addition to this drug analysis, we identify a new potential drug target site: the AMPA receptor outer vestibule near the ion-conducting pore. We further characterize that alteration to this site acts independently of other modulators, providing a site for modulators that may accompany current pharmacological therapies. Together, these studies demonstrate that structural information can be successfully applied to the process of drug design, with the added benefit of enhancing our understanding for molecular mechanisms of AMPA receptor function.

ACKNOWLEDGEMENTS

This work was funded through an NIH R01 grant of Dr. Kathryn Partin, whose level of patience rivals the persistence she claims me to have. I can only imagine how frustrating it is to have a graduate student motivated more by desire than deadlines. Your knowledge, understanding and acceptance has made everything possible. I thank the other members of the Partin lab: Dr. Leslie Stone, who's time in the lab has mirrored my own, you have been a great source of guidance; Jacob Meyers, you motivate me to do more, and may you find patching success; and other members to have come and gone, I appreciate all of your contributions. I thank all of the collaborators who have assisted with the publication of manuscripts. To John, I am glad to hear you are doing well and thank you for your artwork. Thank you, committee members, for your suggestions and guidance (and for not asking too many questions); and to Erin Bisenius and Nancy Graham, who have helped in so many ways to ensure my graduation. And finally, I thank my family, who has supported me so much emotionally and financially, and always been there for me, even if thousands of miles away. Thank you everyone for your contributions and support.

TABLE OF CONTENTS

LIST OF TABLES

LIST OF FIGURES

CHAPTER 1: INTRODUCTION

1.1 AMPA receptor physiology

Glutamate is the primary excitatory neurotransmitter of the central nervous system (CNS), and essentially involved in neural communication. As a ligand in the CNS, glutamate binds to and activates several different types of receptors, including several classes of ionotropic glutamate receptors. These ionotropic receptors, named for the synthetic agonists they are selective for, include AMPA, NMDA, Kainate, and the recently identified δ receptors. In particular, AMPA and NMDA receptors are expressed post-synaptically, responding to pre-synaptically released glutamate. While both receptors bind agonist, NMDA receptors are blocked by extracellular magnesium at physiological resting membrane potentials. Thus, the initial AMPA receptor dependent depolarizing current is critical for NMDA receptor activation, providing the Ca^{2+} influx necessary to drive CAMKII dependent post-synaptic remodeling that governs synaptic plasticity. It is through these mechanisms that AMPA receptors play a key role in many cognitive processes, including learning and memory. Not surprisingly, AMPA receptors are expressed in areas of the brain involved in learning and memory, including the hippocampus, forebrain, and cortex (Traynelis et al., 2010).

Due to the essential role they play in cognition and memory, AMPA receptors are of great clinical interest as a therapeutic target for cognitive disorders. Several studies have shown an ability of drugs facilitating AMPA receptor function to improve memory in both animal models and human patients (Staubli et al., 1994b, Lynch et al., 1997, Hampson et al.,

1998). Additionally, new evidence has linked AMPA receptor activity to drugs having anti-depressant properties (Auer et al., 2000, Berman et al., 2000, Koike et al., 2011), suggesting AMPA reeptors as an avenue for treating chronic depression. In addition to the benefits of enhanced AMPA receptor activity, drugs that reduce AMPA receptor function may also show clincal potential for treating certain disorders. Specifically, AMPA receptor antagonists have shown promise in treating epilepsy and seizure disorders (Rogawski, 2011, Bialer et al., 2013). However, despite continued design and refinement of AMPA receptor modulatory compounds, adoption of these drugs into clinical trials and subsequent therapeutics has been slow for positive modulators (Ward et al., 2010, Chang et al., 2012).

Given their involvement in memory and cognition, as well as their clinical potential for treating prevalent neurlogical conditions, the design and refinement of more specific AMPA receptor modulatory compounds is of great interest and importance. As such, it is necessary to better understand the molecular mechanisms of AMPA receptor function, incuding how molecular interactions within the receptor and with modulatory drugs govern and alter physiolgical function.

1.2 AMPA receptor composition

AMPA receptors are comprised of four individual subunits, forming a tetramer featuring four distinct domains: an amine-terminal domain (ATD) believed to play a role in subunit organization (Jin et al., 2009, Sukumaran et al., 2012); the ligand-binding domain (LBD), where glutamate or other agonist binds (Armstrong and Gouaux, 2000); a transmembrane domain (TMD), made up of helical coils that span the cell membrane and

form the channel pore (Sobolevsky et al., 2009); and a c-terminal tail region, shown to be involved in receptor trafficking (Bedoukian et al., 2006) and kinetics (Suzuki et al., 2005). There are four subtypes of AMPA receptor subunits, designated GluA1-4, whose homomers differ in kinetic properties (Swanson et al., 1997), agonist binding (Kessler and Arai, 2006, Kessler et al., 2008), and modulation by accessory protieins (Suzuki et al., 2008, Montgomery et al., 2009, Traynelis et al., 2010). Further evidence suggests that subtypes differ in preference for one another (Ayalon et al., 2005, Greger et al., 2007, Sukumaran et al., 2012), with heteromeric receptors selectively reflecting specific properties of their composite subtypes (Swanson et al., 1997). Additionally, alternative splicing results in "flip" and "flop" isoforms for each receptor subtype (Sommer et al., 1990). Though only differing by a few amino acids, these isoforms nonetheless display distinct differences in channel kinetics (Koike et al., 2000, Timm et al., 2011), agonist affinity (Kessler and Arai, 2006), and modulation by drug compounds (Partin et al., 1996, Kessler et al., 2000, Timm et al., 2011). Finally, additional RNA editing sites are found along the receptor, including the Q/R editing site controlling Ca^{2+} permeability through the channel pore (Greger et al., 2002). This post-transcripional modification of glutamine to arganine occurs in the majority of GluA2 subunits, and attributes both to Ca^{2+} impermeability of GluA2 containing receptors, as well as preference to form heterotetramers (Greger et al., 2002). The later could either result from the Q/R site occuring at a subunit interface, or affecting GluA2 escape from the endoplasmic reticulum, making it more likely to contact other subunits (Greger et al., 2002). Another site of post-transcriptional editing, the R/E editing site along the ATD to LBD linker, is also believed to play a role in subunit interaction and

dimerization (Greger et al., 2003). These interactions drive subunit assembly into dimers, and further dimerization into a "dimer-of-dimers" structure.

1.3 AMPA receptor mechanisms

One of the most revealing research tools over the past decade of AMPA receptor research has been x-ray crystallography. While a mostly intact GluA2 homomer was recently crystallized and published by Sobolevsky, Rosconi, and Gouaux in late 2009, the isolated GluA2 ligand binding core crystal structure (S1S2) first published by Armstrong and Gouaux in 2000 has been prominently featured and replicated under a variety of receptor conditions. Though these crystal structures only represent "snapshots" of the receptor at a given state and time, their use in describing biochemical interactions underlying agonist and modulator binding and function has been valuable for understanding energy exchange involved in glutamate receptor gating. Further, crystallographic information has produced a structural template from which to base targeted mutagenesis studies. These mutagensis studies, which often involve targeted cysteine mutations, have allowed for the physiological assesment of specific structural interactions. This interplay between structure and physiological function has defined the method through which receptors have been studied in the past as well as the following studies herein.

The ligand binding core of AMPA receptors represents and is commonly refered to as a "clamshell," with agonoist binding between hinged upper (D1) and lower (D2) lobes of the binding domain (Armstrong and Gouaux, 2000). This action of agonist is believed to cause the D2 lobes of the cleft to swing upward, pulling on linker regions betweeen the LBD

and transmembrane helices, resulting in opening of the channel pore (figure 1.1). The extent to which the channel pore opens seems to be dependent on agonist affinity and the degree of cleft closure (Armstrong and Gouaux, 2000, Armstrong et al., 2003, Jin et al., 2003, Robert et al., 2005). This process of "activation" causes receptor strain and instability, which is relieved in one of two ways. First, the receptors can "deactivate" in essentially the reverse process of activation, which is believed to first require channel closure allowing for the "clamshell" to reopen and agonist to dissociate. The other process to decrease strain and increase receptor stability is through "desensitization," a secondary conformational rearrangement of the ligand binding core. Here, the upper lobes of the ligand binding core dissociate, allowing the receptor to take on a closed channel-like state with agonist still bound (figure 1.1). Indeed, the nondesensitizing L483Y mutation is believed to strenthen the connection between back-to-back D1 lobes of the dimer, preventing the receptor from transitioning to a desensitized conformation (Stern-Bach et al., 1998, Sun et al., 2002).

While it would be convenient to think of receptor deactivation as dependent on D2 movement and desensitization dependent on D1 movement, other studies of AMPA receptor mutants suggest more complex interactions governing AMPA receptor gating. One surprise is that the L483Y mutation in D1 also slows receptor deactivation (Sun et al., 2002, Horning and Mayer, 2004, Harms, unpublished data). Further, other mutations made outside of the LBD region, including the *Lurcher* mutant in the pore-region (Klein and Howe, 2004) and the GluA2 linker mutant, R628E (Yelshansky et al., 2004), show the ability to modulate agonist affinity and desensitization. Ultimately, these studies suggest that the isolated ligand binding core (S1S2), while it has been an immensely useful tool for

AMPA receptor research, is not sufficient for understanding the full scope of AMPA receptor mechanisms of gating. Therefore, further study of mutations outside of the S1S2 region, as facilitated by the more recent, mostly-intact GluA2 structure (Sobolevsky et al., 2009), could be essential for elucidating AMPA receptor mechanisms.

1.4 AMPA receptor modulation

The potential clinical significance for a heightened understanding of AMPA receptor structure and function manifests in the form of more specific and efficacious modulatory drugs. Many such allosteric modulatory compounds have been identifeid, including both potentiators (positive) and inhibitors (negative). Positive allosteric modulators have been shown to reproduce many of the effects observed in LTP, including potentiation of neuronal currents (Staubli et al., 1994a, Arai et al., 2000, Arai et al., 2004), and increasing BDNF expression (Lauterborn et al., 2000, Jourdi et al., 2009). Further, these positive effects have shown measurable memory improvements in animal models (Staubli et al., 1994b, Hampson et al., 1998), and human subjects (Lynch et al., 1997). However, despite their vast potential for treating cognitive disorders, progression of these compounds through clinical trials has remained slow and discouraging (Ward et al., 2010). Thus, the development of positive allosteric modulators, including structurally guided design of modulatory compounds (Jamieson et al., 2011, Ward et al., 2011, Harms et al., 2013), remains of key interest for investigation.

In much the same way that access to crystal structure data has informed the understanding of AMPA receptor mechanisms, so too it has guided the understanding and development of allosteric modulators. Structural data is available for some of the more

extensively studied allosteric modulators, including the benzothiadiazides such as CTZ (Sun et al., 2002), and the pyrrolidinines, including CX614 (Jin et al., 2005). An interesting structural observation is that these two compounds, which are believed to alter receptor kinetics through different mechanisms (CTZ slows onset of desensitzation while CX614 slows deactivation), nonetheless bind at the same pocket between dimer interfaces (figure 1.2). Upon a closer inspection of this modulator binding pocket, Ptak, Ahmed, and Oswald (2009) proposed the existence of five specific subsites that modulators differentially occupy. These include a central A subsite, the hydrophobic C and C' subsites in the upper region near D1, and the water containing B and B' pocket. Reconsidering CTZ and CX614 structural data, it is observed that CTZ binds as two molecules, occupying the B and C or B' and C' subsites, while CX614 binds along the dimer backbone occupying only the A subsite (figure 1.2). Thus, occupation of the central A subsite may be a prerequisite for a modulator to affect AMPA receptor deactivation. This finding is intriguing, as many of the newer designed modulators show structures optimized for occupation of these subsites (Grove et al., 2010, Jamieson et al., 2011, Timm et al., 2011, Harms et al., 2013).

Also an important consideration for modulator design is the difference between flip and flop recptor isoforms. As the flip/flop splice isofrom region alters "hinge" residues lining the modulator binding pocket (Sun et al., 2002, Jin et al., 2005, Ahmed et al., 2010, Timm et al., 2011), a certain compound can show different modulatory effects dependent on the receptor isoform to which it is applied. CX614, for example, shows a slight increase of GluA2 flip steady-state current with no observed effect on deactivation (Timm et al., 2011), while CTZ shows a more flip specific ability to block desensitiztion (Partin et al., 1996, Kessler et al., 2000, Timm et al., 2011). Given that reduced synaptic activity, such as

that seen in Alzheimer's disease (Chang et al., 2012), is sufficient to alter hippocampal flip/flop heteromerization in a regionally dependent manner (Penn et al., 2012), it may be beneficial to possess modulators capable of exerting positive effects independent of subunit isoforms.

1.5 Aims of this work

Presented here are several studies exploring AMPA receptor mechanisms of gating and modulation through a concerted analysis of structural and physiological information. Using this combined approach to study receptor kinetics, this research aims to uncover the molecular underpinnings of AMPA receptor gating mechanisms, including how positive allosteric modulators may influence these mechanisms dependent on subsite occupation. Additionally, this work investigates how alterations in the receptor distant to ligand binding might affect agonist dependent processes, thus exploring new potential sites for receptor modulation. Ultimately, better understanding the relationship between receptor structure and function, with a focus on structural correlates of its modulation, will facilitate the development of more beneficial drugs for treating cognitive disorders.

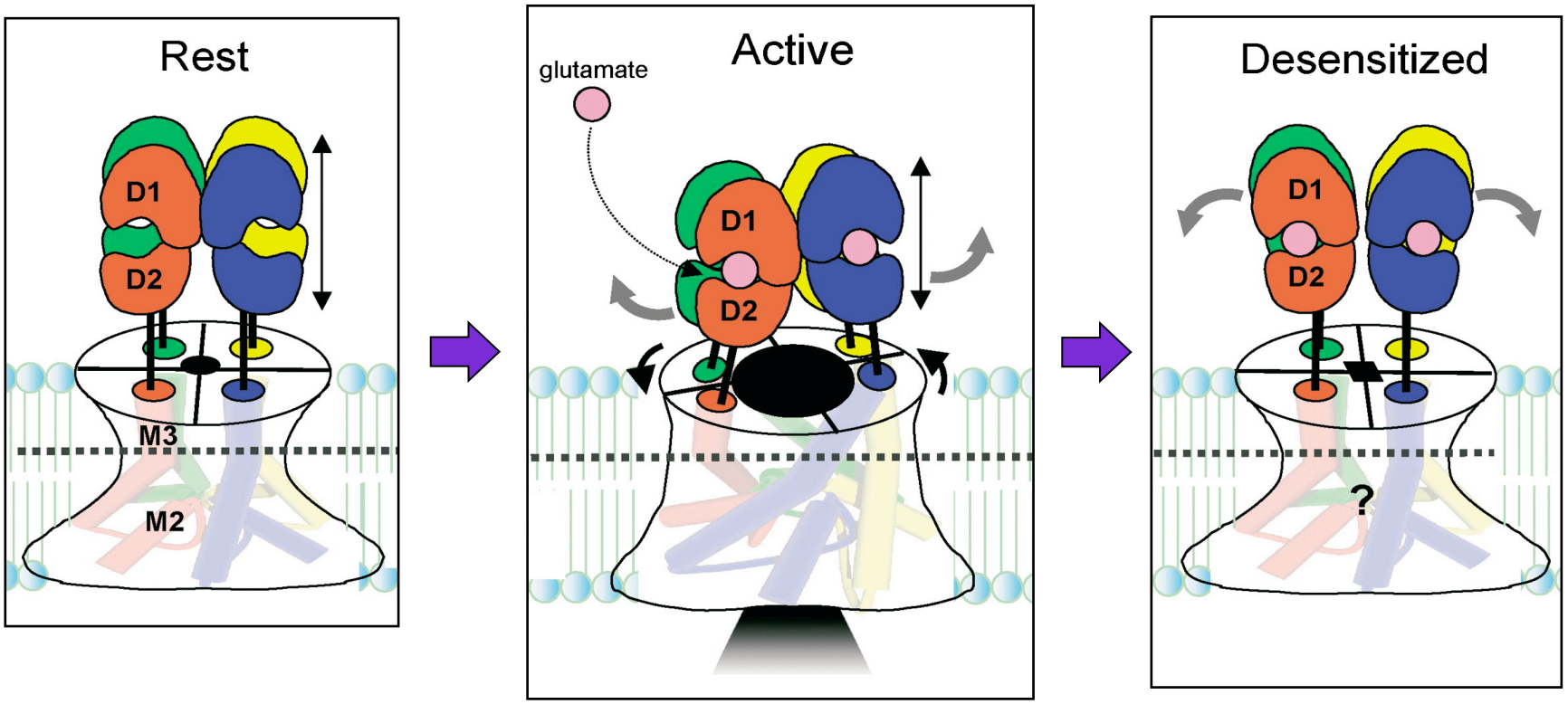

Figure 1.1: GluA2 gating is driven by agonist binding to the Ligand Binding Domain (LBD), causing conformational rearrangement of the LBD

Left) Cartoon showing the upper (D1) and lower (D2) lobes of the LBD for each subunit, connected by linker regions (black lines) to the membrane spanning helices that form the channel pore (black circle). **Center)** When glutamate (pink circle) binds, a conformational rearrangement occurs (grey arrows) to open the pore (large black circle) allowing current to flow (black gradient cone). **Right)** Desensitization occurs through a separate conformational rearrangement (grey arrows), with the interface between upper lobes breaking apart and the pore (black square) adopting an unknown conformation. (Figure taken from Stern-Bach, 2004)

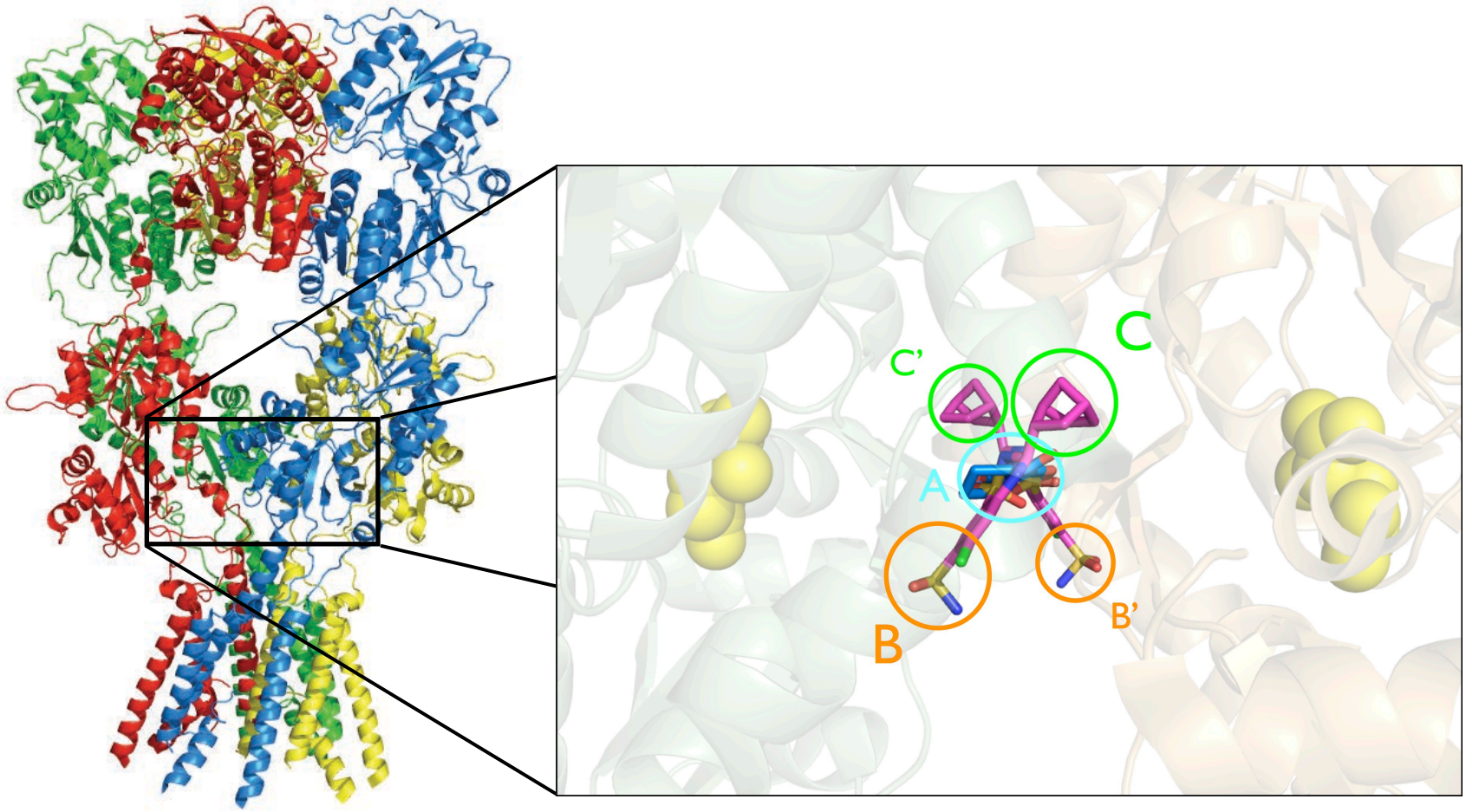

Figure 1.2: Modulators bind at a common pocket and occupy distinct subsites

Crystal structure from Sobolevsky et al. (2009) showing four subunits in different colors. Enlargement of Ligand Binding Domain (LBD, inset), shows two bound molecules of glutamate (yellow spheres). Modulators such as Cyclothiazide (magenta stick) and CX614 (blue Stick) bind in a pocket between LBD dimers to stabilize conformational rearrangements of the LBD interface. This pocket includes three distinct subsites: the central A subsite, the water-filled B subsites (B and B'), and the hydrophobic C subsites (C and C').

CHAPTER 2: FUNCTIONAL ANALYSIS OF A NOVEL POSITIVE ALLOSTERIC MODULATOR OF AMPA RECEPTORS DERIVED FROM A STRUCTURE-BASED DRUG DESIGN STRATEGY

This chapter discusses a positive allosteric modulator of GluA2, JAMI 1001 (in this chapter referred to as "JAMI 1001A"). JAMI 1001 was designed and furnished by a collaborator, Craig Jamieson, using structure-based drug design (SBDD) with a drug forward approach. This work is presented here as the manuscript published in a special issue of the journal, *Neuropharmacology*, titled "Cognitive Enhancers: molecules, mechanisms and minds". This special issue includes transcripts from the "22nd Neuropharmacology Conference," where I further presented this work and discussed it in the context of drug design. Though I did not write this manuscript, I did design the figures, perform all electrophysiology experiments, conduct statistical analysis on the resulting data, conduct structural analysis using PyMOL software and available crystal structure files, and manipulate a kinetic model to recapitulate the electrophysiology data.

2.1 INTRODUCTION

Glutamate is the primary excitatory neurotransmitter in the mammalian CNS. One of glutamate's primary target receptors, the AMPA family of ion channels, is responsible for mediating neural processes involved in learning and memory (reviewed in (Kessels and Malinow, 2009, Traynelis et al., 2010)). Furthermore, it has been shown that these processes, including synaptic plasticity and long-term potentiation (LTP), can be enhanced by modulatory drugs acting directly on AMPA receptors (Black, 2005, Ward and Harries, 2010). Because of such positive effects, AMPA receptors and their allosteric modulators represent key targets for treatment of cognitive disorders, ranging from Alzheimer's disease and Parkinson's disease to schizophrenia and ADHD (Morrow et al., 2006).

AMPA receptors are hetero-tetrameric membrane proteins, composed of various combinations of GluA1, 2, 3 and 4 subunits. These subunits have a large extracellular domain, a transmembrane domain that gates mono- and divalent ions, and a cytoplasmic domain that encodes post-translational modification and scaffolding sites (Traynelis et al., 2010). The extracellular region of the channel contains an N-terminal domain and a ligand binding core (LBC) in each subunit (reviewed in (Mayer, 2011). Both the N-terminal domain and LBC have strong intrasubunit associations such that the four subunits form a dimer of dimers in these regions (Sobolevsky et al., 2009). Both agonist and positive allosteric modulators bind within this LBC (Armstrong and Gouaux, 2000, Sun et al., 2002). The LBC is formed from an upper lobe, domain 1 (D1), and a lower lobe, domain 2 (D2), which are brought together when agonist binds within the cleft formed between the domains (referred to as a "clamshell"). D1 and D2 are connected by "hinge" residues that

are thought to impart stability upon the closed-cleft, agonist-bound conformation. Once agonist is bound, the channel will likely open and then may desensitize or close. Desensitization causes a structural rearrangement of the interface between the paired LBCs of different subunits. Alternatively, upon brief exposure to glutamate, the channel may close and deactivate, such that the LBC cleft reopens and glutamate dissociates.

Positive modulators bind to the LBC, within a water-accessible cleft that lies at the interface between two protomers, which is formed in part from the clamshell hinge residues that connect D1 and D2 (Sun et al., 2002, Jin et al., 2005, Ahmed et al., 2010, Timm et al., 2011). This allosteric modulatory site has been described as five overlapping subsites: the central subsite, A, lies across the axis of symmetry between the protomers and is formed by hinge residues (connecting D1 and D2 of one protomer), including Pro497, Ser497, and Ser729 (Ptak et al., 2009). Subsite B is an exposed, hydrophilic pocket formed by residues Tyr424, Phe495, Ser497, Lys763, and Ser729, whereas subsite C is a deep, hydrophobic pocket lined by residues Ile481, Lys493, and Leu751. Subsites B and C are self-contained within each protomer such that there are two B sites and two C sites per dimer, whereas there is only one, shared A site. It has been demonstrated that differential occupancy of these subsites by the various classes of positive modulator determines different mechanisms of action of these modulators. Amongst the classes of positive modulator compound that have been characterized include the benzothiadiazides (cyclothiazide), the benzamides (aniracetam and CX614), and the biarylsulfonamides (LY404187, CMPDA, CMPDB) (Sun et al., 2002, Jin et al., 2005, Fernandez et al., 2006, Timm et al., 2011).

In an effort to expedite the development of novel positive AMPA receptor modulators, a unique structure-based drug design (SBDD) approach in combination with a screening-led hit identification campaign has been used to discover compounds with positive modulatory effects and optimize them for use as potential therapeutics (Grove et al., 2010, Jamieson et al., 2010a, Jamieson et al., 2010b, Jamieson et al., 2011). The benefits of such a design strategy allow for the rapid identification of new chemotypes and their expedient optimization into relevant drug-like compounds. However, in addition to catalyzing the hit and lead identification trajectory, SBDD may offer further benefits for understanding drug and receptor mechanisms of action.

In this study, we confirm SBDD as an effective method for designing a targeted lead compound through the study of JAMI1001A ((2-(2-4-(hydroxymethyl)-3-(trifluoromethyl)-1H-pyrazol-1-yl)acetamindo)-4,5,6,7 tetrahydrobenzo[b]thiophene-3-carboxamide). Further, we reveal surprising biophysical properties of JAMI1001A that challenge the current dogma of the consequence on function of occupancy of specific subsites within the positive allosteric modulatory site.

2.2 MATERIALS AND METHODS

Compound Synthesis

JAMI1001 was synthesized according to the method delineated in our earlier publications (Jamieson et al., 2010a, Jamieson et al., 2010b). Briefly, (3-(trifluoromethyl)-1H-pyrazol-4-yl)meth- anol was treated with potassium tert-butoxide (1.2 eq) in DMF for 30 min before 2-(2- chloroacetamido)-4,5,6,7-tetrahydrobenzo[b]thiophene-3-carboxamide (1 eq) was added. The reaction mixture was heated to 60°C for 4 h before being concentrated to dryness and the residue purified by flash column chromatography, eluting with 40% ethyl acetate/hexane to furnish the target compound as a white solid.

X-ray crystallography

Crystals were grown as described by Armstrong et al. (Armstrong et al., 1998) and more latterly by Jamieson et al (Jamieson et al. 2010a). Co-crystals were prepared by soaking JAMI1001A (100 mM) with crystals for 24h prior to isolation and data collection. Coordinates and structure factors have been deposited in the Protein Data Bank for the complex of JAMI1001A with the AMPA LBC (4FAT.pdb).

AMPA receptor recombinant cDNAs

The flip and flop isoforms of rat GluA2 cDNAs were expressed in pRK, a CMV expression vector. cDNAs were a gift of Dr. Peter Seeburg (University of Heidelberg, Germany). “WT” GluA2 DNA was made from the original plasmids, into which the pore mutation ($R_{607}Q$) was made, using site-directed mutagenesis (QuikChange II XL Site-Directed Mutagenesis Kit,

Stratagene; La Jolla, CA). Mutant receptors conduct current robustly and have an inwardly rectifying current-voltage relationship, whereas receptors with arginine at position 607 express currents that are too small to measure with conventional patch-clamp electrophysiology (Hume et al., 1991, Verdoorn et al., 1991).

HEK293 cell culture and transient transfection

Passages 38-45 human embryonic kidney 293 (HEK-293) cells (CRL 1573; American Type Culture Collection; Manassas, VA) were cultured in 35mm polystyrene dishes (Becton-Dickinson and Company; Lincoln Park, NJ). Cells were transiently transfected using PolyJet reagent (SignaGen Laboratories; Gaithersburg, MD) with yellow-fluorescent-protein (YFP) tagged wild type GluA2 flip or wild type GluA2 flop AMPA receptor DNA (1 μg/dish). Media was changed 4-5 hours post transfection and NBQX was added to a final concentration of 10-20 mM to prevent toxicity.

Patch-clamp electrophysiology

Currents were recorded 1-2 days after transfection from cells expressing a moderate level of fluorescence from the YFP tag. Outside-out membrane patches were held under voltage-clamp at -60 mV using an Axopatch 200B amplifier (Molecular Devices; Union City, CA). Patchmaster software (version 2.43; HEKA Instruments Inc.; Bellmore, NY) controlled data acquisition and movement of a two barrel flowpipe perfusion system driven by a piezo-electric device (Burleigh Instruments; Fishers, NY). Micropipettes (TW150F; World Precision Instruments; Sarasota, FL) contained the following intracellular solution (in mM): 135 CsCl, 10 CsF, 10 HEPES, 5 Cs_4BAPTA, 1 $MgCl_2$, and 0.5 $CaCl_2$, pH 7.2. Patches were

perfused at 0.2 mL/min with solutions emitted from a two-barrel flow pipe made with theta tubing (BT150-10; Sutter Instruments; Novato, CA). One barrel contained control solution (in mM): 145 NaCl, 5.4 KCl, 5 HEPES, 1 $MgCl_2$, 1.8 $CaCl_2$, with 0.01 mg/mL phenol red, pH 7.3. The other barrel contained L-glutamate (10 mM) dissolved in the control solution. For drug studies, each barrel additionally contained either 100 μM cyclothiazide (CTZ), 100 μM CX614, or 100 μM JAMI1001A. CTZ and CX614 were dissolved in DMSO. JAMI1001A was dissolved in control solution. After attaining whole-cell voltage clamp, outside-out patches were pulled from cells, raised off the dish and positioned near the interface between the glutamate-free and glutamate-containing solutions of the flowpipe. Rapid solution exchanges of 1 or 500 ms between control and glutamate containing solutions were done to test for deactivation and desensitization, respectively. Solution exchange was measured for each patch by measurement of junction potentials after obliterating the patch at the end of the experiment. Solution exchange times were approximately 500 μs. Responses were digitized at 20 kHz, and stored on an iMac computer (Apple, Inc.; Cupertino, CA) using an ITC-16 interface (HEKA Instruments Inc.; Bellmore, NY) connected through a USB-16 adapter (HEKA Instruments Inc.; Bellmore, NY)).

Data analysis

IGOR Pro 6.2 (Wavemetrics; Oswego, OR) software was used for data analysis. Traces were averaged (4-10 traces per sweep) and a single exponential was fit to the trace. I_{Peak} was calculated using an average of three points. I_{SS}/I_{Peak} was calculated using an averaged steady state current (SS).

Kinetic simulations

Simulations of currents under voltage clamp to an AMPA receptor model were performed using code originally written by John Clements (Benveniste et al., 1990), revised and converted by M.B. to an Igor Pro XOP. Receptor state occupancies at each time point were determined numerically. The change in each state occupancy was calculated according to first order reaction rate kinetics for transitions into and out of each state, as detailed in Benveniste *et al.* (1990). This was done iteratively at least 20 times per time point. With the present model, flip and flop differences were largely replicated by simply changing the rate of onset of desensitization by 10-fold. Simulations, fitting and related analyses were run on a Macintosh MacBook Pro computer utilizing Igor Pro 6.2.

Molecular Visualization

Structural data files were obtained from the RCSB Protein Data Bank as .pdb files and opened using the The PyMol Molecular Graphics System (version 1.3, Schrödinger, LLC). The following were shown in cartoon representation and aligned manually: Chains A and C of the 3H6T.pdb file for cyclothiazide (Hald et al., 2009), Chains D and F of the 2AL4.pdb file for CX614 (Jin et al., 2005), and Chain A of JAMI1001A (4FAT). A mask was applied to the CX614 subunit of 2AL4 so only one confirmation of CX614 would be displayed. The 3O6H file was modified to portray the JAMI1001A structure by changing N5 color to red and masking C10 and C13 of object 025. Modulators shown in complex are against Chains D and F of the 2AL4.pdb file at 60% transparency.

2.3 RESULTS

2.3.1 Structure of JAMI1001A

JAMI1001A was derived from lead "**Compound 1**" as described in (Jamieson et al., 2011). JAMI1001A is a U-shaped molecule of 402 Da molecular weight (figure 2.1) that contains a hydrophobic trifluoromethyl group attached to the 3-position of a pyrazole ring (shown in green), and a hydrophobic tetrahydrobenzothiophene moiety (shown in blue). A hydrophilic carboxamide (red) extends from the 3-position of the tetrahydrobenzothiophene motif. The extended distal structures are connected by a linear acetamide chain that forms the bottom of the "U" shape. The structure of JAMI1001A differs from other positive allosteric modulators of AMPA receptors such as the benzamide or sulfonamide systems in its lack of central heterocyclic rings.

2.3.2 X-ray crystallography structure of JAMI1001A bound to the AMPA receptor GluA2 S1S2 domain

JAMI1001A lies at the dimer interface between two ligand-binding cores. The long axis of the molecule lies perpendicular to the axis of symmetry. The interactions between the compound and the GluA2 LBC are predominately mediated by hydrophobic contacts, with most of these contacts lying at the distal ends of the compound facilitated by the trifluoromethyl system on the pyrazole ring and the cycloalkane ring of the tetrahydrobenzothiophene, respectively. Specific interactions between the LBC and the ligand which can be discerned are made by a hydrogen bond between the pendant

hydroxyl at the 4-position of the pyrazole motif and the amide backbone of Pro494 as well as the side chain of Ser729.

A recent structural study suggests that relative occupancy of the modulator-binding pocket sub-domains influences the mechanisms of action of allosteric modulators (Ptak et al., 2009). For instance, the central subsite, A, lies across the axis of symmetry between the protomers and is occupied by the planar rings of CX614, and biarylsulfonamide compounds (Timm et al., 2011). Hinge residues within subsite A (connecting domain 1 and domain 2 of one protomer), particularly Pro497, Ser497, and Ser729 form hydrogen bonds with these compounds and are believed to contribute to stabilization of closed clamshell conformations (Jin et al., 2005). Subsite B, or B' on the opposing protomer, is an exposed, hydrophilic pocket formed by residues Tyr424, Phe495, Ser497, Lys763, and Ser729, and interacts with the sulfonamide groups of CTZ. The norbornenyl group of CTZ inserts into the hydrophobic pocket of subsite C, which is lined by residues Ile481, Lys493, and Leu751. The sulfonamide oxygens form hydrogen bonds with the side chain of S497 and through a water molecule with the carbonyl of K730.

The prototypical benzamide, CX614, which occupies only subsite A, efficaciously modulates channel deactivation and desensitization. Cyclothiazide, which occupies susbsites B, B', C and C', with only partial occupancy of subsite A, has little effect on channel deactivation, with a robust effect on channel desensitization (of the flip isoform). Because structural studies have indicated that occupancy of subsites B and C may impart more efficacious allosteric modulation (Ptak et al., 2009, Timm et al., 2011), it is interesting to

note that the central portion of JAMI1001A occupies subsite A, and the distal ends of the compound occupy subsites C and C'. Based on the structural model of the positive allosteric modulator binding site, one might predict that the critical interactions between the distal portions of JAMI1001A – the tetrahydrobenzothiophene domain that overlaps with the norbornenyl ring of cyclothiazide at subsite C, and the trifluoromethyl domain that overlaps with the sulfonamides at subsite C' - could potentially contribute to the strong modulation of both deactivation and desensitization.

2.3.3 JAMI1001A is an efficacious modulator of GluA2 deactivation and desensitization

Although previous studies had characterized some of the chemical and biological properties of the new chemotype (Jamieson et al., 2010a, Jamieson et al., 2010b), insight into its molecular mechanism of action requires higher resolution electrophysiological recordings of channel activity. Specifically, recording the response to a brief (1 ms) pulse of glutamate is thought to be a proxy for channel "deactivation", a process that entails channel closing, the opening of the cleft between the upper and lower domains of the ion channel that forms the agonist-binding "clamshell", and dissociation of glutamate from its binding site. This process of terminating a response to glutamate is predicated on a synaptic response in which glutamate is only briefly presented to postsynaptic AMPA receptors. Desensitization is the process by which the two ligand binding cores forming a dimer dramatically rearrange their interactions, disrupting non-bonded interactions to relieve strain induced by channel opening, thereby uncoupling the occupied agonist binding site from the channel pore in the lipid bilayer (Sun et al., 2002). This process is recapitulated by applying a prolonged (500 ms) pulse of glutamate to induce receptor desensitization. The

effects of JAMI1001A on channel deactivation and desensitization were assessed by measuring current reduction following 1 or 500 ms pulses of glutamate, in the absence and presence of modulator, were measured on outside-out membrane patches from HEK293 cells transiently expressing the flip and flop isoforms of GluA2.

As previously published, CTZ has little effect on channel deactivation of either the flip or flop isoforms of AMPA receptors (Arai et al., 1996, Partin et al., 1996, Mitchell and Fleck, 2007), whereas CX614 slows deactivation significantly of the flop but not the GluA2 flip isoform. JAMI1001A slows channel deactivation of both GluA2 isoforms by approximatley 1.5-fold (figures 2.3a and 2.4a). This deactivation modulation profile for JAMI1001A clearly differs from other known channel modulators in its lack of isoform selectivity. Because different populations of neurons express specific repertoires of subunits and splice isoforms (Geiger et al., 1995), resulting in neuron-specific efficacy of modulation (Xia and Arai, 2005), the physiological consequence of the lack of isoform specificity of the JAMI1001A compound may be quite important.

The lack of isoform selectivity of JAMI1001A was also apparent when measuring channel desensitization (figure 2.3b). The ratio of the steady-state current to the initial peak current is a measure of the efficacy of modulation, such that a ss/pk ratio of one would indicate a complete inability of the channel to desensitize during a prolong pulse of glutamate. JAMI1001A blocked desensitization more efficaciously than CX614, and to virtually the same extent in both the flip and flop isoforms (figures 2.3b and 2.4b).

2.3.4 Mechanism of action of JAMI1001A

In JAMI1001A, the absence of aromatic rings that occupy subsite A may have mechanistic implications. It has been hypothesized that the aromatic rings of aniracetam, CX614 and "CMPDA" or "B" (Jin et al., 2005, Timm et al., 2011) allow hydrophobic interactions that stabilize the hinges of the clamshell formed by the upper and lower lobes of the ligand binding core. In the present study, JAMI1001A has an acetatamide linker which could potentially interact with the channel in the same way and, therefore, may modulate channel deactivation. Macroscopic rates of channel deactivation (the decay of the current after a brief pulse of agonist) can be influenced by allosteric modulation of different conformational transitions. For example, the decay is slowed by agonists that have a higher affinity (Kessler and Arai, 2006), thereby slowing the off rate of agonist association (K_{off}). Alternatively, the rate of decay can be slowed by a slowing of the channel "gate" (a). Finally, the rate of decay can be changed by slowing the entry into the desensitized state (Partin et al., 1996, Mitchell and Fleck, 2007), although the impact on deactivation by this mechanism is very modest.

Computational modeling of conformational transitions is useful in assessing potential mechanisms of action of allosteric modulators. Recent studies on two novel allosteric modulators of channel deactivation and desensitization, CMPDA and CMPDB, led to the conclusion that the effects on channel deactivation arose from an independent mechanism rather than as a consequence of their actions on channel desensitization (Timm et al., 2011). Figure 2.5a and table 2.1 show an analogous, albeit simplified, gating scheme

that has been used in a computational simulation of electrophysiological currents (figure 2.5b).

In this model, the decays of deactivation and desensitization in the absence of modulator are 0.9 ms and 1.4 ms, respectively. Slowing $k'_{glu\ \mathrm{off}}$ by two-fold to simulate the effects of 10 μM JAMI1001A slows the rate of channel deactivation to 1.0 ms, less than JAMI1001A does experimentally, and has little effect on channel desensitization. Similarly, slowing the onset of channel desensitization by 500-fold results in "blocking" desensitization, but also slows channel deactivation only to 1.1 ms. Thus, adjusting either channel rate independently does not simulate the actual results shown in figure 2.3. However, adjusting both rates together, accurately replicates the physiological data (t_{Deact}=1.6 ms; t_{Des}=211 ms; SS/PK =0.6). These simulations indicate that two independent processes of modulation are required to replicate JAMI1001A data (figure 2.5b). Our data suggest that the hydrophobic contacts made by JAMI1001A on modulator pocket subsite A has an independent and efficacious impact on channel deactivation. One possibility is that the unique occupancy of subsite A *together* with subsite C accounts for the efficacious modulation of deactivation. This would have important consequences to future SBDD efforts in terms of designing new classes of modulator.

2.4 DISCUSSION

Here, we describe biophysical activity of a novel chemotype of AMPA receptor positive modulator. The compound was derived from a high throughput screen, followed by structure-based design leveraging the available biostructural data (Jamieson et al., 2010a, Jamieson et al., 2010b, Jamieson et al., 2011). The optimization trajectory was driven by *in vitro* developability characteristics such as potency, solubility, selectivity and microsomal stability, allied with knowledge of how the ligands interacted with the receptor. *In vitro* studies were complemented with *in vivo* assays such as oral bioavailability and stability as measured by pharmacokinetics. These studies led to *in vivo* electrophysiological assessment of efficacy, measured primarily by looking at evoked single unit recordings in the hippocampus of rats, which had received an intravenous dose of a test compound. Although the optimization strategy led to the development of a novel chemotype, little information on the precise biophysical mechanism was known. Accordingly, our studies reinforce the value of the overall approach in finding new drugs to treat dysfunction of AMPA receptors, which contributes to mental illness and cognitive decline.

The most significant finding of the present study is that JAMI1001A somewhat unexpectedly modulates both channel deactivation and desensitization (figures 2.3 and 2.4). Based on the overlap of the tetrahydrobenzothiophene domain of JAMI1001A with the norbornenyl group of cyclothiazide in the subsite C domain, and the absence of large hydrophobic substituents such as aromatic rings in subsite A of the allosteric binding pocket, it may have been predicted that JAMI1001A would impact desensitization with less

effect on channel deactivation. Based on the structure, one might predict that JAMI1001A would prevent the rearrangement of the dimer interface necessary for the onset of channel desensitization but not affect deactivation, similar to cyclothiazide (Sun et al., 2002). However, this is not the case. Rather, through hydrogen bonds with residues in subsite C , and with only minimal hydrophobic interactions in subsite A to "stabilize" the closed cleft conformation, JAMI1001A is as effective as previously described modulators such as CX614 in blocking desensitization and slowing deactivation. Importantly, however, JAMI1001A lacks the isoform selectivity of CX614 (figures 2.3 and 2.4). Thinking about targeting modulators to specific diseases, which involve unique brain regions expressing unique populations of receptors and splice isoforms with differing efficacy of modulation (Geiger et al., 1995, Xia and Arai, 2005), the ability to synthesize potential drugs that are efficacious on both splice isoforms may be a fundamentally important drug design goal.

Significant advances have been made in our understanding of the molecular basis through which positive allosteric modulators exert their biological effect on the AMPA receptor. These studies are complemented by an SBDD approach that provides a more extensive understanding of biophysical properties for novel compounds showing promising in vivo and in vitro properties, thereby possibly reducing the time from discovery to delivery as a therapeutic.

In conclusion, the synergistic combination of structural biology, receptor biophysics and modeling have led to a significant advance in our understanding of the specific mechanism of action of this novel class of AMPA receptor modulator. Detailed knowledge of how JAMI1001A and related compounds facilitate modulation of the receptor will

undoubtedly have a significant impact on the design of additional new molecular entities derived through further evolution of the existing assets.

Table 2.1: Rate constants used for kinetic simulations shown in Figure 2.5

Alternative nomenclature					
Transition number	Transition			Forward rate	Reverse rate
	Forward	Ligand	Reverse		
1	$2k_{glu\ on}$	Glu	$k_{glu\ off}$	15 $\mu M^{-1}\ s^{-1}$	1000 s^{-1}
2	$k_{glu\ on}$	Glu	$2k_{glu\ off}$	7.5 $\mu M^{-1}\ s^{-1}$	2000 s^{-1}
3	β	—	α	4000 s^{-1}	10,000 s^{-1}
4	δ	—	γ	500 s^{-1}	20 s^{-1}
5	2δ	—	γ	1000 s^{-1}	20 s^{-1}
6	$k_{glu\ on}$	Glu	$k_{glu\ off}$	7.5 $\mu M^{-1}\ s^{-1}$	1000 s^{-1}
7	$k_{jami\ on}$	JAMI	$k_{jami\ off}$	0.1 $\mu M^{-1}\ s^{-1}$	0.1 s^{-1}
8	$2k'_{glu\ on}$	Glu	$k'_{glu\ off}$	15 $\mu M^{-1}\ s^{-1}$	1000 s^{-1}
9	$k'_{glu\ on}$	Glu	$2k'_{glu\ off}$	7.5 $\mu M^{-1}\ s^{-1}$	2000 s^{-1}
10	β	—	α	4000 s^{-1}	10,000 s^{-1}
11	δ	—	γ	500 s^{-1}	20 s^{-1}
12	2δ	—	γ	1000 s^{-1}	20 s^{-1}
13	$k'_{glu\ on}$	Glu	$2k'_{glu\ off}$	7.5 $\mu M^{-1}\ s^{-1}$	1000 s^{-1}
14	$k_{jami\ on}$	JAMI	$k_{jami\ off}$	0.1 $\mu M^{-1}\ s^{-1}$	0.1 s^{-1}
15	$k_{jami\ on}$	JAMI	$k_{jami\ off}$	0.1 $\mu M^{-1}\ s^{-1}$	0.1 s^{-1}
16	$k_{jami\ on}$	JAMI	$k_{jami\ off}$	0.1 $\mu M^{-1}\ s^{-1}$	0.1 s^{-1}
17	$k_{jami\ on}$	JAMI	$k_{jami\ off}$	0.1 $\mu M^{-1}\ s^{-1}$	0.1 s^{-1}

GLU, 10 mM glutamate; JAMI, 10 µM JAMI1001A, β, $k_{glu\ on}$ and $k_{glu\ off}$, respective forward and reverse microscopic rate constants for glutamate; $k'_{glu\ on}$ and $k'_{glu\ off}$, respective forward and reverse rate constants for glutamate in the presence of JAMI1001A; β, $k_{jami\ on}$ and $k_{jami\ off}$, respective forward and reverse microscopic rate constants for JAMI1001A binding; channel opening; α, channel closing rate; β, channel opening rate; δ, rate of onset of receptor desensitization; γ, rate of recovery from channel desensitization. (courtesy Morris Benveniste)

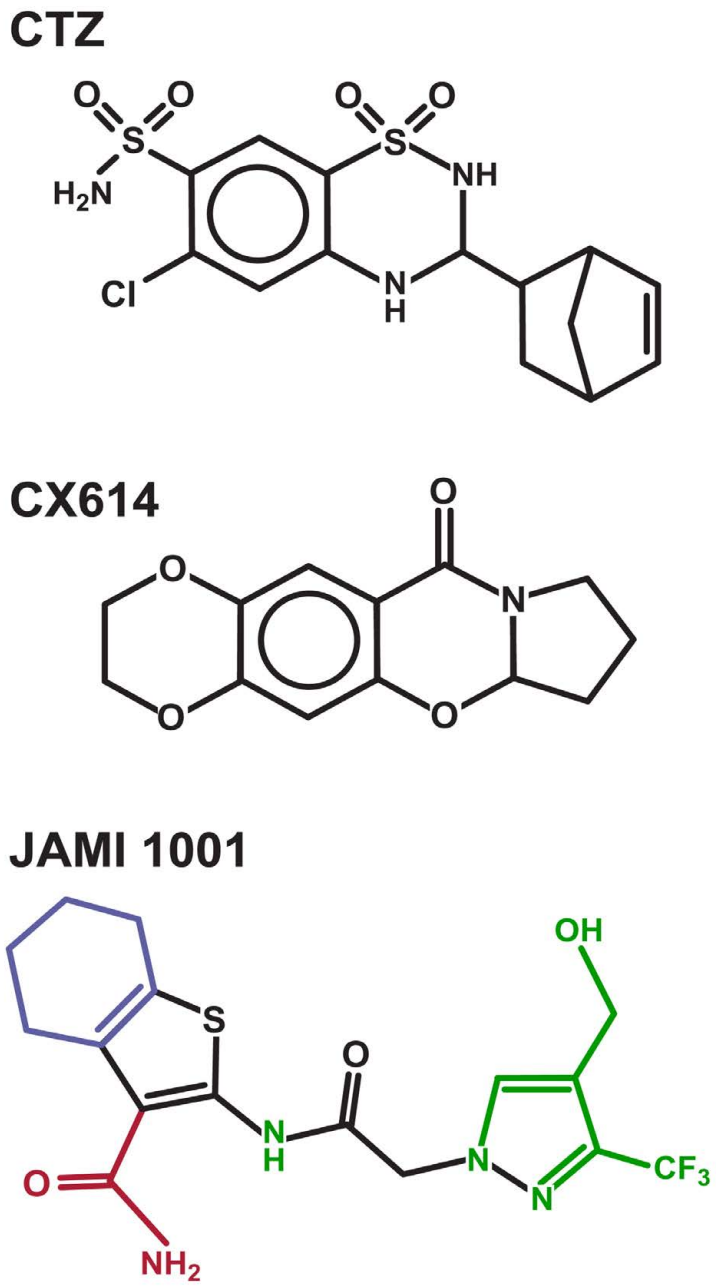

Figure 2.1: Chemical structures of three positive allosteric modulators of AMPA (a-amino-3-hydroxy-5-methyl-4-isoxazole-propionic acid) receptors

CTZ, cyclothiazide (2,4-benzothiadiazine-3-bicyclo[2.2.1]hept-5-en-2-yl-6-chloro-4-dihydro-2h-1); CX614 (2H,3H,6aH-pyrrolidino(2,1-3',2')1,3-oxazino(6',5'-5,4)benzo(e)1,4-dioxan-10-one), a prototypical benzamide compound; and JAMI1001A (2-(2-(4-(hydroxymethyl)-3-(trifluoromethyl)-1*H*-pyrazol-1-yl)acetamido)-4,5,6,7-tetrahydrobenzo[**b**]thiophene-3-carboxamide), a new chemotype tested in this paper. Moieties discussed in the Results include: a trifluoromethyl group attached to a pyrazole ring (shown in green), a tetrahydrobenzothiophene moiety (shown in blue), and a carboxamide (red) which extends from the tetrahydrobenzothiophene. The extended distal structures are connected by a linear acetamide chain. (structures re-drawn by John Gieser)

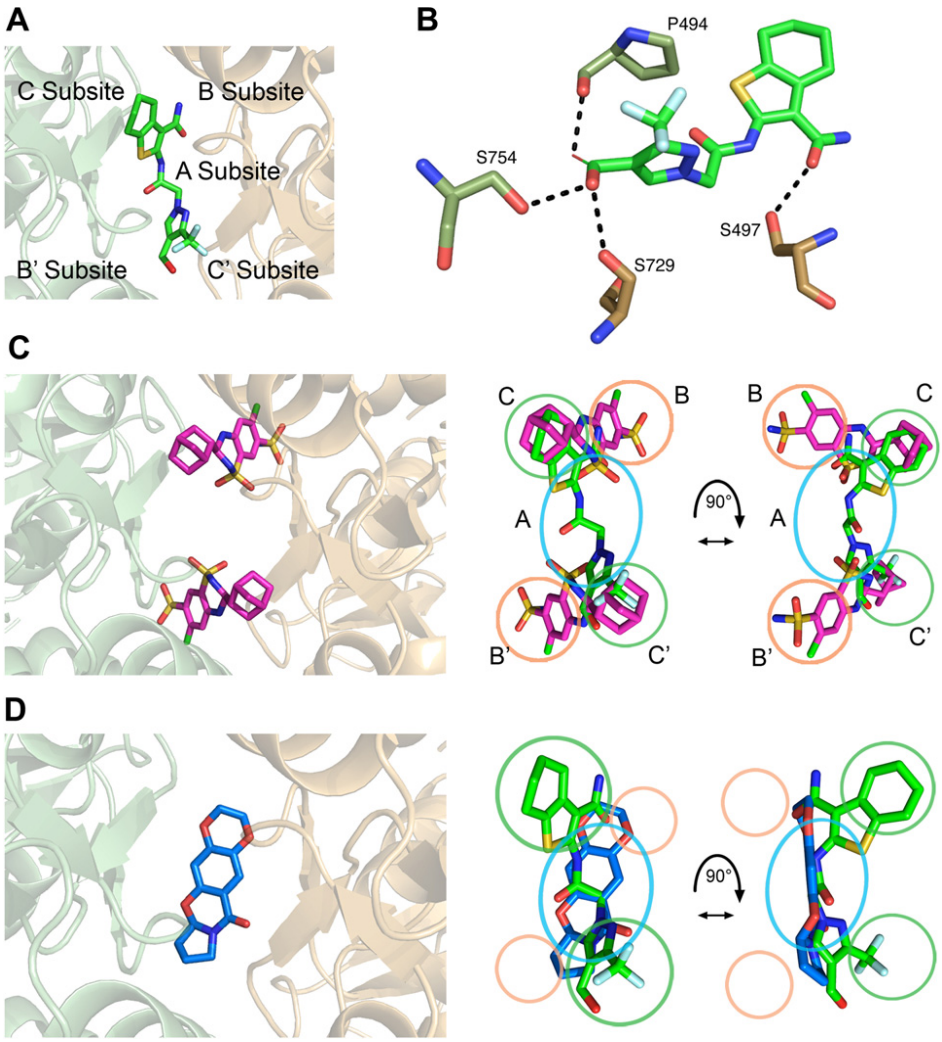

Figure 2.2: Structural comparison between JAMI1001A and CTZ or CX614

A) A single molecule of JAMI1001A lies at the interface between two AMPA receptor protomers, straddling the axis of symmetry. B, Contact map of JAMI1001A showing polar interactions with GluA2 (dotted black lines). The pendant hydroxyl of the pyrazole crystallizes in two orientations: one (shown as stick) interacts with Ser729 and the isoform-specific Ser754, the other (shown as line) with the main chain of Pro494. An additional interaction is found between the side chain hydroxyl of Ser497 with the carboxamide of JAMI1001A. C, Two molecules of CTZ lie at the dimer interface, either side of the axis of symmetry (left panel). There is significant overlap between moieties at the distal ends of JAMI1001A and CTZ, particularly in subsite C (green circles, right panels). D, A single molecule of CX614 lies at the interface, straddling the axis of symmetry (left panel). There is significant overlap between the planar rings of CX614 and the central, alkyl moiety of JAMI1001A, which occupies subsite A (blue ellipses; right panels). This figure was generated with pdb files from the RCSB Protein Data Bank using The PyMol Molecular Graphics System (version 1.3, Schrödinger, LLC). The following are shown in cartoon representation, aligned manually: Chains A and C of the 3H6T.pdb file for cyclothiazide (Hald et al., 2009), Chains D and F of the 2AL4.pdb file for CX614 (Jin et al., 2005), and Chain A of JAMI1001A (4FAT.pdb). A mask was applied to the CX614 subunit of 2AL4 so only one conformation of CX614 would be displayed. Modulators shown in complex are against Chains D and F of the 2AL4.pdb file at 60% transparency.

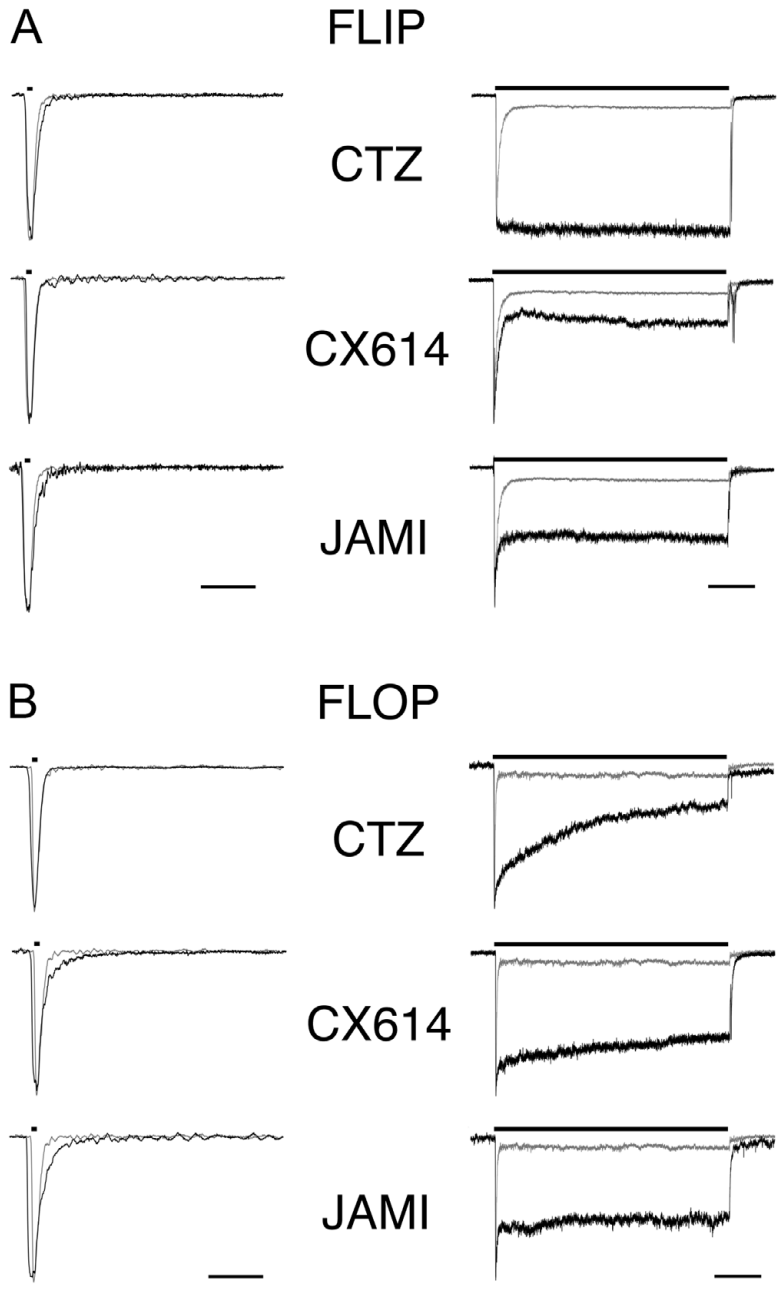

Figure 2.3: JAMI1001A modulates AMPA receptor deactivation and desensitization

A) Modulation of a 1 ms pulse of 10 mM glutamate (deactivation, left) and of a 500 ms pulse of glutamate (desensitization, right) of the flip isoform of GluA2 by 100 µM CTZ, 100 µM CX614, and 100 µM JAMI1001 in outside-out patches of transiently transfected HEK293 cells. Control (No Drug) responses are shown in light gray; modulated responses in black. **B)** Identical parameters measured for the flop isoform of GluA2.

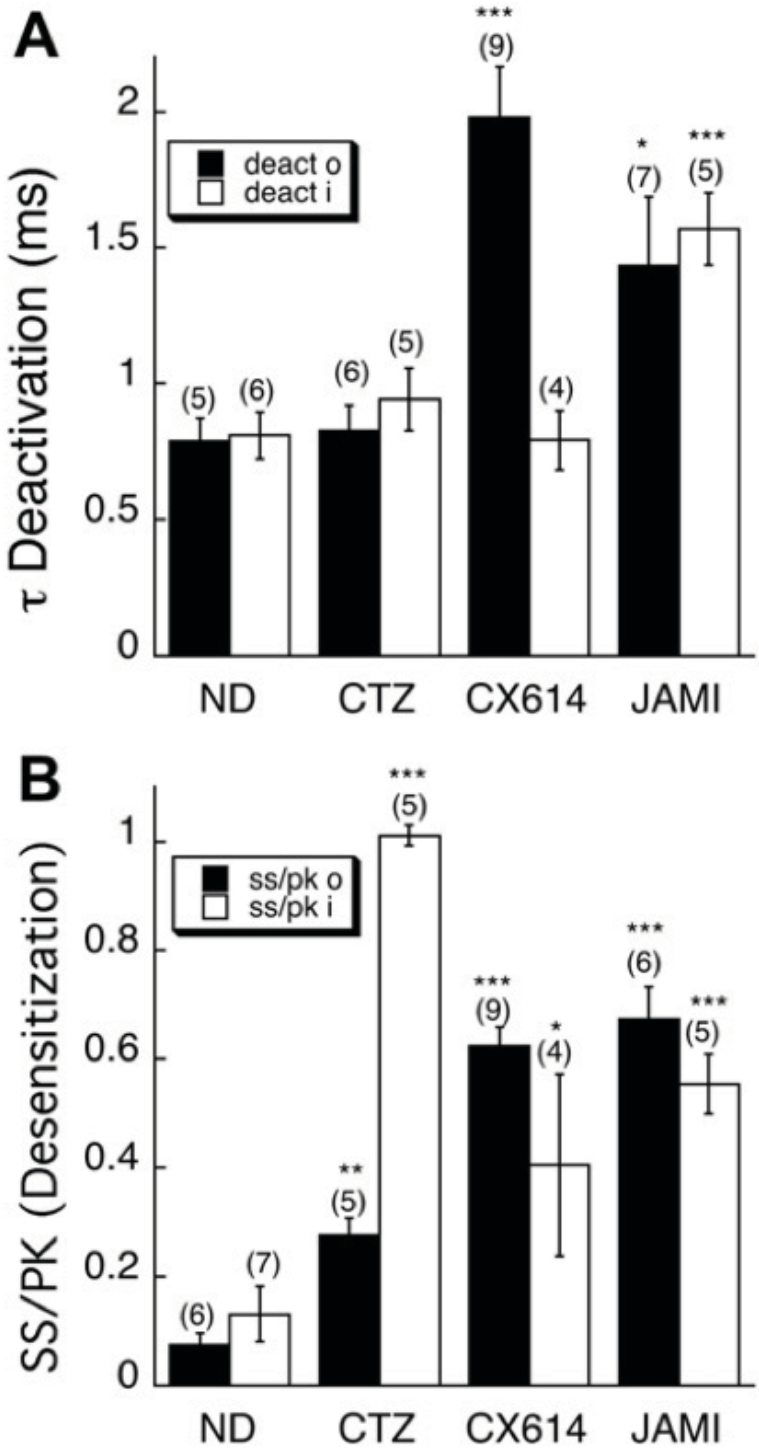

Figure 2.4: JAMI1001A significantly modulates AMPA receptor deactivation

A) Mean data for a 1 ms pulse of glutamate demonstrates that JAMI1001 significantly modulates the kinetics of channel deactivation for both splice isoforms of GluA2. **B)** Mean data for 500 ms pulses of glutamate demonstrate that JAMI1001A significantly modulates the equilibrium desensitization for both splice isoforms of GluA2. n values are indicated in parentheses. A paired student's t-test demonstrates significance, such that *p<.05, **p<.01, ***p<.001. (graphs generated by Kathy Partin)

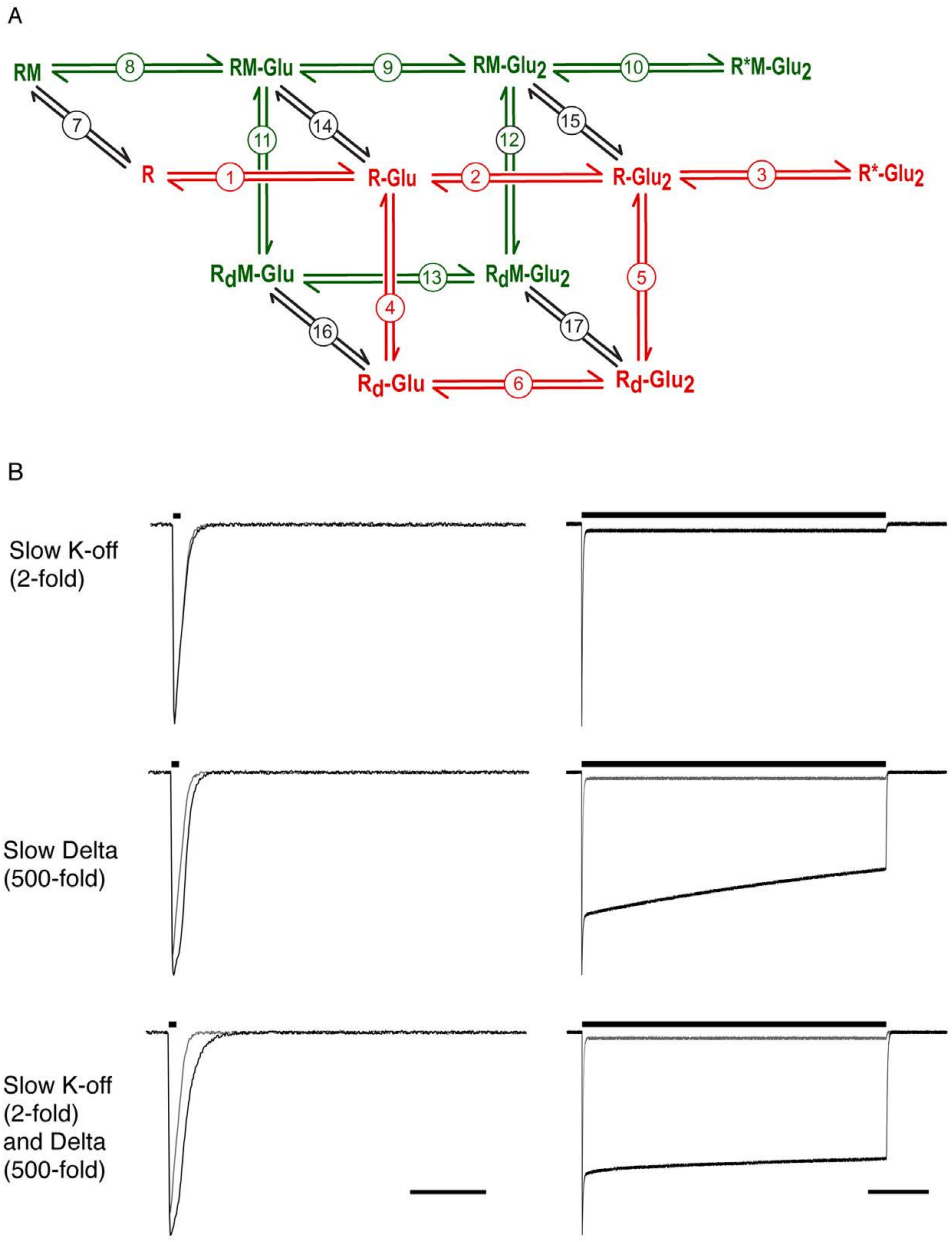

Figure 2.5: Kinetic model of mechanism of action of JAMI1001A

A) A simplified gating scheme was used to test likely mechanism(s) of action of JAMI1001A. The model shows gating conformations in the absence (red) and presence (green) of an allosteric modulator. R, receptor; R_{des}, desensitized receptor; Glu and Glu_2, one and two molecules of glutamate, respectively; M, modulator; *, open channel. Transitions are indicated by number and rates are given in table 2.1. **B)** Simulated responses to 1 ms or 500 ms of 10 mM glutamate, with no drug (gray) or in the presence of 10 mM JAMI1001A (black), demonstrate that electrophysiological data can be well-recapitulated by slowing the rate of agonist dissociation for deactivation, together with the rate of onset of desensitization or the rate of recovery from desensitization, but not by changing a single rate constant. Thus, JAMI1001A appears to modulate both deactivation ($k'_{glu\ off}$) and desensitization (δ/γ). (schematic by John Gieser)

CHAPTER 3: THE CHARGE-INVERTING R628E MUTANT IN THE LINKER REGION OF GLUA2 ALTERS AGONIST BINDING AND GATING KINETICS INDEPENDENTLY OF ALLOSTERIC MODULATORS

This chapter is a manuscript I have prepared for submission to *The Journal of Neuroscience* as a scientific publication detailing the arginine 628 to glutamate (R628E) mutation and its effects on GluA2 mechanisms. This manuscript is still being revised with input from all authors, whose contributions are denoted in the figure legends. In addition to writing the text, my contributions to this work include: performing electrophysiological experiments on wildtype and mutant receptors, statistical analysis of the resulting data, performing structural analysis in the PyMOL software package, manipulating a kinetic model to recapitulate electrophysiological and binding data (with assistance from the designer, Morris Benveniste), and designing and preparing most figures and tables.

3.1 INTRODUCTION

AMPA receptors mediate fast excitatory transmission involved in learning, memory, and synaptic plasticity. These tetrameric receptors exist as combinations of four individual subunits (GluA1-4) responsible for different biochemical and biophysical profiles of an intact receptor (Traynelis et al., 2010). In addition, RNA editing and alternative splicing can occur in each of these subunits. In GluA2, for example, the kinetically slower, "flip" ("i") isoform and a faster, "flop" ("o") isoform are differentiated by 9 specific residues over a 33 amino acid long sequence comprising the flip/flop domain (Partin and Mayer, 1996, Swanson et al., 1997, Koike et al., 2000). This region defines a flexible hinge connecting the upper and lower sections of the ligand binding domain (LBD), where agonist binds and gates the channel through still unknown mechanisms (Stern-Bach et al., 1994, Traynelis et al., 2010).

Studies using targeted receptor mutations have played a major role in describing GluA2 physiological processes. Notably, the threonine 686 to alanine (T686A) mutation, located within the ligand-binding cleft, identified a cross-cleft bond that occurs during glutamate binding and contributes to receptor desensitization (Robert et al., 2005). Other mutant studies have investigated the inter-dimer interactions between ligand binding clefts that result in receptor desensitization (Jin et al., 2003, Plested and Mayer, 2009); with the actions exerted by these receptor mutants further rationalized by X-ray crystallography (Jin et al., 2003, Zhang et al., 2008, Plested and Mayer, 2009).

However, while these mutant studies have described agonist-driven changes of receptor conformation both structurally and physiologically, other such studies have not been explained in as much detail. In particular, the GluA2 arginine 628 to glutamate mutant

(R628E) has been shown to alter receptor desensitization through an unknown mechanism that potentially involves electrostatic interactions (Yelshansky et al., 2004). Also, unlike the aforementioned mutants, X-ray crystallography has verified R628 to be distant from the LBD, residing along a linker region (the M3-S2 linker) connecting the LBD to the transmembrane domains that make up the channel pore (Sobolevsky et al., 2009).

With its position in the receptor outside of the LBD, we aimed to further describe how the R628E mutant exerts its effects on AMPA receptor function. Using the full-length AMPA receptor crystal structure, we analyzed the structural arrangement and electrostatic interactions in this region, discovering a distinctly different conformation than previously expected. To further investigate the role of R628E on receptor kinetics, we used electrophysiology to measure receptor deactivation, desensitization and effect of modulators on R628E mutant receptors for both flip and flop isoforms of GluA2. These results were supported by ligand binding assays on wildtype and R628E mutant GluA2 using [^{3}H]fluorowilliardiine to assess mutant induced alteration of agonist binding. Finally, to help inform our interpretations of the data, we replicated our physiological findings using a kinetic model. Our results suggest that R628 and the M3-S2 linker play an important role in glutamate binding and ligand-gated GluA2 kinetics. Further, our model identifies specific changes in receptor kinetics caused by the R628E mutant, suggesting a potential mechanism through which the mutant exerts its observed physiological effects. The findings of this study present a new target for AMPA receptor positive allosteric modulators. Additionally, our findings suggest that modulators acting at this new target site can supplement presently available modulators to exert an additive or compensatory effect.

3.2 METHODS

DNA constructs

Rat wildtype (WT) GluA2 flip (i) and flop (o) cDNA encoding plasmids were gifts of Dr. Peter Seeburg (University of Heidelberg, Heidelberg, Germany). WT plasmids as referred to here were modified to include the R607Q mutation, as described previously (Timm et al., 2011), to enhance currents for observation using electrophysiology. Arginine 628 to glutamate (R628E) flip and flop mutants were made from the respective WT plasmid using the Quickchange II Site-Directed Mutagenesis Kit (Agilent Technologies, Santa Clara, CA) using primers sourced from Integrated DNA Technologies (Coralville, IA).

Transient-transfections for electrophysiology

Passages 38-45 human embryonic kidney 293 (HEK293) cells (CRL 1573; American Type Culture Collection; Manassas, VA) were cultured in 35 mm poly-styrene dishes (Becton-Dickinson and Company; Lincoln Park, NJ). Cells were transiently transfected using PolyJet reagent (SignaGen Laboratories; Gaithersburg, MD) with yellow-fluorescent-protein (YFP) fused in-frame to the C-terminus of wild type GluA2 flip, wild type GluA2 flop, GluA2 R628E flip, or GluA2 R628E AMPA receptor DNA (1 mg/dish). Media was changed 4-5 h post-transfection and NBQX was added to a final concentration of 10-20 mM to prevent toxicity.

Patch-clamp electrophysiology

Currents were recorded 24-60 hours after transfection from cells expressing a moderate level of fluorescence from the YFP tag. Outside-out membrane patches were held under voltage-clamp at -60 mV using an Axopatch 200B amplifier (Molecular Devices; Union City,

CA). Patchmaster software (version 2.43; HEKA Instruments Inc.; Bellmore, NY) controlled data acquisition and movement of a two barrel flowpipe perfusion system driven by a piezo-electric device (Burleigh Instruments; Fishers, NY). Micropipettes (TW150F; 2e5 MU; World Precision Instruments; Sarasota, FL) contained the following intracellular solution (in mM): 135 CsCl, 10 CsF, 10 HEPES, 5 Cs_4BAPTA, 1 $MgCl_2$, and 0.5 $CaCl_2$, pH 7.2. Patches were perfused at 0.2 mL/min with solutions emitted from a two-barrel flowpipe made with theta tubing (BT150-10; Sutter Instruments; Novato, CA). One barrel contained control solution (in mM): 145 NaCl, 5.4 KCl, 5 HEPES, 1 $MgCl_2$, 1.8 $CaCl_2$, with 0.01 mg/mL phenol red, pH 7.3. The other barrel contained L-glutamate (10 mM) dissolved in the control solution. For modulator studies, each barrel additionally contained either 100 μM cyclothiazide (CTZ; Tocris Bioscience; Bristol, UK), or 100 μM CX614 (Cortex Pharmaceuticals, Inc; Irvine, CA) dissolved in DMSO. After attaining whole-cell voltage clamp, outside-out patches were pulled from cells, raised off the dish and positioned near the interface between the glutamate-free and glutamate-containing solutions emitting from the flowpipe. Agonist applications were achieved by stepping into and out of the glutamate containing solution for either 1 or 500 ms to test for deactivation and desensitization, respectively. Solution exchange was measured for each patch by measurement of junction potentials after obliterating the patch at the end of the experiment. Open-tip solution exchange times were between 150 and 200 μS. Responses were digitized at 20 kHz, and stored on an iMac computer (Apple, Inc.; Cupertino, CA) using an ITC-16 interface (HEKA Instruments Inc.; Bellmore, NY) connected through a USB-16 adapter (HEKA Instruments Inc.; Bellmore, NY).

Confocal imaging

For confocal microscopy, transfections were performed as described above using 35mm poly-d-lysine coated dishes with cutouts and glass coverslips (). Transfected cells were fixed with 4% paraformaldehyde in 0.1 M phosphate buffer (pH 7.2-7.4) for 1-3 hours and then washed with 0.1 M phosphate buffer prior to imaging. Confocal analyses were done using a Zeiss LSM 510 Meta with a Plan-Achromat 63X/1.4 NA oil DIC objective. An argon laser was used to excite EYFP (excitation maximum 514 nm) and EYFP emission was measured with a LP 530 filter. Images were collected using the LSM software, then exported as .tif files.

Ligand-binding assays

Agonist-binding was measured at 0°C on membranes harvested 24-48h after transfection using 1-400 nM FW* (^{3}H-fluorowillardiine). Binding in presence of modulator was measured using a fixed, 5nM FW* concentration and varying concentrations of drug, at 0 and 25°C. Binding at each drug concentration was normalized to that without drug and averaged across experiments. Mean data was plotted in Prism 6 software (Graphpad Software, Inc., La Jolla, CA) with normalized binding on the y–axis over modulator concentration on the x-axis, and then fitted with a sigmoidal curve (3-point logistic equation with $n_{Hill} = 1$).

Computational modeling and simulations

Modeling simulations were conducted with IGOR Pro 6.22 software (Wavemetrics, Lake Oswego, OR) using a custom XOP file derived from code originally written by MB and John Clements (Benveniste et al., 1990), as described previously (Harms et al., 2013). Briefly,

receptor state occupancies were mathematically calculated from pre-defined transition rates into and out of each receptor state. Current simulations in presence and absence of modulator differed only by the concentration of modulator predefined for that simulation. Simulations of glutamate binding were conducted by assigning all agonist-bound states as conductive states. Agonist binding in presence of modulator was normalized to the [0] modulator concentration condition.

Data analysis and statistics

Digitized current recordings were imported to Igor Pro 6.22 software using custom macros designed by MB. Traces of receptor deactivation and desensitization were averaged over 4-10 sweeps and tau was calculated by fitting an exponential to the averaged trace in the form: $x=y_0+A\text{^}[-(x-x_0)/\tau]$. Paired-pulse recordings were analyzed individually and plotted as the ratio of Peak2/Peak1 on the y-axis over the interpulse-interval on the x-axis and tau recovery calculated using the predefined exponential fit. Statistical means and standard errors were calculated from raw data imported into Prism 6 software and analyzed for significant effects using ANOVA with multiple comparisons.

3.3 RESULTS

3.3.1 The R628 sidechain in one dimer of the closed state receptor forms an inter-subunit molecular interaction with the adjacent R628 sidechain

Sobolevsky's x-ray crystal structure (figure 3.1a) revealed the GluA2 receptor to have separate areas of 2-fold and 4-fold symmetry (Sobolevsky et al., 2009). Using the 3KG2.pdb file and PyMOL for structural analysis, we looked more closely at the linker regions encompassing R628. Of interest, this intact crystal structure representing a putative closed state revealed that the R628 residue resides within the 2-fold to 4-fold symmetry transition region (figure 3.1b). Essential for this transition is an asymmetry of the pore-forming, membrane-spanning M3 helices, with the A (green) and C (blue) subunits of the tetramer having a longer helical coil than the B (yellow) and D (red) subunits (figure 3.1b). This asymmetry results in a less ordered structure of the B and D subunits, consequently aligning the A/B and C/D R628 residues with their guanidino groups opposite each other (figure 3.1c). This alignment is further appreciated by looking down through the pore occluding methionine-629 residues from an extracellular viewpoint (figure 3.1d). Here, the 4-fold symmetry of the trans-membrane regions is seen as a central square, with the proline-632 residues having a 2-fold, trapezoid arrangement. Once again, looking through the upper, B/D R628 subunits (translucent), we can see how the arginine guanidino groups interact with backbone oxygens to form a "latch" adjacent to the pore occluding methionine residues. We believe this arginine "latch," which would be disrupted by a charge inverting mutation to glutamate (R628E), plays an essential role in stabilizing certain conformational states of the receptor. As such, we sought to re-evaluate the role this residue could be

playing in receptor gating, with a specific focus on how information is transmitted from the ligand binding core to the channel pore.

3.3.2 The R628E mutation alters kinetics of GluA2

Our first approach was to understand the functional consequence of the mutation on receptor activation. To characterize the effect of the R628E mutant on gating, we used ultra-fast perfusion exchange to record wildtype and mutant receptor responses to glutamate in outside-out patches pulled from transiently-transfected HEK 293 cells. In response to a 1 ms pulse of glutamate to simulate receptor deactivation (figure 3.1a), the R628E mutant decayed significantly slower than wild-type in both flip and flop receptor isoforms [τ_{deact} R628E flip: 3.5 ± 0.55 ms (n=12) p< .001 vs WT flip: 0.81± 0.09 ms (n=6), R628E flop: 3.3 ± 0.37 ms (n=11) p< .01 vs WT flop: 0.79 ± 0.07 ms (n=5), figure 3.2c]. While wild-type receptor traces were easily fit to a single exponential time constant, R628E mutant receptor decay showed fast and slow components; and thus two exponentials provided a better fit. This change manifested most commonly as a small but appreciable slow component (table 3.1), and thus contributes to the general slowing of mutant receptor kinetics. However, in most cases, both fast and slow components of the mutant were individually slower than wildtype (table 3.1).

In addition to slowed deactivation, we also saw kinetic changes when using a more prolonged, 500 ms pulse of glutamate (figure 3.2b). A more robust steady-state current was observed with both flip [ss/peak R628E: 0.69 ± 0.03 (n=11) p<.001 vs WT: 0.13 ± 0.05 (n=7)] and flop [ss/peak R628E: 0.78 ± 0.04 (n=12) p<.001 vs WT: 0.07 ± 0.02 (n=6)] receptor isoforms (figure 3.2e). In addition to increasing the steady-state current, the

R628E mutant also slowed desensitization for the flop isoform of GluA2 [τ_{des} R628E: 21.1 ± 2.19 (n=9) p< .001 vs WT: 1.6 ± 0.09 ms (n=6), figure 3.2d]. Interestingly, the flip isoform did not show this extent of change, and only slowed slightly, but not significantly [τ_{des} R628E: 12.7 ± 2.82 ms (n=4) p=.51 vs WT: 8.8 ± 0.62 ms (n=7), figure 3.2d). Although our results are modestly different than those reported in Yelshansky *et al.* (2004), the differences may be explained by our use of an ultrafast perfusion technique.

The dramatic impact on ss/pk current during prolonged glutamate exposure could arise either due to a slowed onset of macroscopic desensitization or a slowed recovery from desensitization (Robert and Howe, 2003). To assess the impact of the mutation on recovery from desensitization, we used a paired-pulse protocol. Following a 200 ms desensitizing prepulse of 10 mM glutamate, a second 10 mM application of glutamate was applied at increasing interpulse intervals (figure 3.2g). The ratio of the second current peak to the prepulse response was plotted and fitted to an exponential (figure 3.2h), revealing an isoform dependent effect of the R628E mutant on recovery [τ_{rec}: R628E flip: 32.63 ± 5.34 ms (n=3) p< 0.05 vs WT flip: 50.83 ± 7.34 (n=4), R628E flop: 29.48 ± 2.15 ms (n=4) p=0.17 vs 33.28 ± 0.72 ms (n=4), figure 3.2f). Similar to our finding on the timecourse of receptor desensitization, our result is modestly different than Yelshansky *et al.* (2004), who found similar recovery rates between WT flip and flop, but did not measure recovery of R628E flip.

These data confirm that R628, plays an important role in channel desensitization kinetics, as reported previously (Yelshansky et al., 2004); but also significantly slows the onset of receptor deactivation, a previously unappreciated finding.

3.3.3 The R628E mutation alters receptor trafficking

In recording from patches to generate the data for figure 3.2, we experienced greater difficulty obtaining current recordings from HEK293 cells transfected with R628E than from wildtype controls. Since receptor expression at the membrane surface is essential for observing currents in patch-clamp electrophysiology, we explored the implications of the R628E mutation on receptor trafficking. We transiently-transfected HEK 293 cells with YFP-tagged wildtype or R628E mutant receptors and assessed their subcellular fluorescence distribution over time using confocal microscopy (figure 3.3). Wild-type (flip) receptors displayed distinct "rings" of fluorescence along the outer membrane as early as 24 hours post-transfection, which remained stable at 48 hours, consistent with the findings of other groups (Matsubara et al., 1996, Nusser, 2000) as referenced in (Meyer et al., 2009). In contrast, cells transfected with R628E receptors developed areas of dense fluorescence ("aggresomes")(Corboy et al., 2005, Bedoukian et al., 2006), which became more numerous as time progressed and accompanied a decrease in banding at the membrane surface (figure 3.3). These results signify that the R628E mutant causes a perturbation in receptor trafficking, and provide at least a partial explanation for the difficulty in recording functional data for the mutant receptor.

3.3.4 Allosteric modulation of R628E is conserved

The fact that the R628E mutation altered both receptor deactivation and desensitization is reminiscent of the actions of positive allosteric modulators that bind at the dimer interface of the ligand binding core (Partin et al., 1996, Sun et al., 2002, Xia et al., 2005, Hald et al., 2009, Timm et al., 2011, Harms et al., 2013), but is also similar to the

allosteric modulation of receptor gating that transmembrane accessory receptor proteins such as stargazin allow (Bedoukian et al., 2006, Kato et al., 2008, Gill et al., 2012). We therefore hypothesized that assessing the efficacy of positive allosteric modulators on gating of the R628E mutation might provide insight into the molecular mechanism through which the mutation perturbed gating compared to wild type receptor. To this end we measured the effects of allosteric modulators on R628E mutant receptors. For this investigation, we chose the modulators cyclothiazide (CTZ), a commonly used benzothiadiazide; and the pyrrolidinone, CX614. These drugs were chosen due to their contrasting isoform and deactivation/desensitization efficacies. CTZ has been shown to be a flip selective modulator of GluA2 desensitization, with little effect on deactivation kinetics (Partin et al., 1996, Kessler et al., 2000, Jin et al., 2005, Ptak et al., 2009), while CX614 is more selective for GluA2 flop, modulating both deactivation and desensitization of that isoform (Jin et al., 2005, Harms et al., 2013).

Recording glutamate-gated currents on flip receptors in the presence of modulator (figure 3.4a), we observed no appreciable change on deactivation with either modulator, for both wild-type [τ_{deact} CTZ: 0.941 ± 0.11 ms (n=5) p=.98, CX614: 0.79 ± 0.11 ms (n=4) p>.99 vs ND: 0.81 ± 0.09 ms (n=6)] and mutant receptors [τ_{deact} CTZ: 4.10 ± 0.59 ms (n=4) p=.72, CX614: 4.26 ± 1.06 ms (n=3) p=.65 vs ND: 3.53 ± 0.55 ms (n=12), figure 3.4b]. This was not the case for desensitization, however, as recordings in the presence of CTZ appeared to be non-desensitizing for both wildtype [ss/peak = 1.01± 0.02 (n=5) p<.001 vs ND: 0.13 ± 0.05 (n=7)] and R628E mutants [ss/peak = 1.01± 0.04 (n=4) p<.01 vs ND: 0.69 ± 0.03 (n=11)] (figure 3.4c). Lastly, the effect of CX614 on R628E flip receptors showed nearly complete loss of desensitization [ss/peak=0.96 ± 0.02 (n=4)], and though

significantly more robust, even showed a slight re-sensitization as seen with CX614 application on flip wildtype receptors, [ss/peak= 0.40 ± 0.17 (n=4), p< 0.05, figure 3.4a,c]. While this pattern is similar to the effects of CX614 on wildtype flip receptors, what is somewhat surprising is the extent to which CX614 modulated the steady-state current of the mutant receptor, as compared to the extent of CX614 modulation of wild-type flip. Thus, there may be a synergistic effect of CX614 on R628E flip desensitization.

Testing modulators on flop isoforms (figure 3.5a) showed, much like the flip isoforms, a maintained effect of modulator with the mutant receptor. CTZ, having little ability to modulate wildtype flop deactivation [τ_{deact} CX614: 0.83 ± 0.09 ms (n=6) p> 0.99 vs ND: 0.79 ± 0.07 ms (n=5)] shows similar difficulty in modulating deactivation of R628E flop receptors [τ_{deact} CX614: 2.77 ± 0.76 ms p=0.56 vs ND: 3.29 ± 0.37 ms, figure 3.5b]. CX614, on the other hand, is an efficacious modulator of flop deactivation for wildtype receptors [τ_{deact} CX614: 1.98 ± 0.18 ms (n=9), p<0.05]. Likewise, onset of deactivation is slowed significantly (τ_{deact} CX614: 6.8 ± 0.40, p<0.001, figure 3.5b, bold) when recording from R628E flop in the presence of CX614, demonstrating the R628E mutation does not adversely affect CX614 modulation. This trend continues for recordings of R628E desensitization in presence of modulator. Although CTZ and CX614 seemingly block desensitization of the mutant receptor [ss/peak CTZ: 0.98 ± 0.01 (n=4), p<0.01; CX614: 0.96 ± 0.03 (n=4), p<0.01 vs ND: 0.78 ± 0.04 (n=12)], it should be noted that such an effect might be expected if mutant and modulator have an additive effect. While this block of desensitization is not seen for wildtype flop receptors, a similar change is observed [ss/peak CTZ: 0.28 ± 0.03 (n=6), p<0.01; CX614: 0.62 ± 0.04 (n=9), p<0.001 vs ND: 0.07 ± 0.02 (n=6)]. Thus, the already minimal desensitizing component of flop R628E allows for complete block of

desensitization by even partial modulators.

That positive allosteric modulators, which bind to the dimer interface of the ligand-binding core, and the R628E mutation, have additive rather than antagonistic or occluding effects on slowing of channel deactivation and desensitization, may suggest that there is a "parallel" rather than "serial" allosteric modulation "pathway" to the pore. This could be confirmed by looking at the effects of the mutation on ligand binding in the presence and absence of modulator, as CTZ and CX614 show opposite effects on ligand binding in wildtype receptors (Kessler and Arai, 2006).

3.3.5 Radiolabelled binding assays show altered agonist affinity of GluA2

We therefore conducted binding assays on transiently-transfected HEK 293 cells using [^{3}H]flurowillardiine ([^{3}H]FW) as an agonist to determine if the mutation altered the pattern of ligand binding (enhanced or reduced ligand-binding) imposed on the receptor due to CTZ or CX614. As documented previously (Kessler and Arai, 2006), wild-type GluA2 demonstrates distinct high and low affinity binding sites, and is best described by two hyperbolic fits: [Flip Hi/Low: Kd= 17.30± 2.24/325.8± 76.70, Bmax= 0.91± 0.067/2.52± 0.14 (26.59% Hi); Flop Hi/Low: Kd= 13.74± 2.78/163.7± 33.54, Bmax= 0.46± 0.10/1.47± 0.06 (23.87% Hi); figure 3.6a open circles]. Surprisingly, assay data for both isoforms of GluA2 R628E was best fit by a single exponential demonstrating relatively high affinity [Flip: Kd= 27.79± 1.68, Bmax= 2.827± 0.04; Flop: Kd= 66.8± 8.35, Bmax= 1.69± 0.067; figure 3.6a, dark circles]. Thus, these data suggest that the R628E mutation enhances apparent affinity for agonist, despite the fact that the mutation is not located near the ligand binding core of the receptor.

To pursue this finding, we tested the effects of modulator on agonist binding for both isoforms of wildtype and R628E receptors (figure 3.6b-c). These studies were conducted using a constant concentration of [^{3}H]FW, and normalized to modulator-free values. For flip receptor isoforms, neither drug displayed much of an effect on [^{3}H]FW binding (figure 3.6b-c and table 3.3) compared with wild type receptors. Wildtype flop receptors told a much different story, however, with the effects of both CTZ (reducing ligand binding) and CX614 (enhancing ligand binding) being quite dramatic (table 3.3). Interestingly, the effect of the mutation attenuated the CTZ-induced loss of binding, whereas the mutation enhanced the CX614-induced increase in agonist binding, thus effectively increasing apparent binding with both modulators.

Having kinetic data for gating transitions and binding data in hand, we hypothesized that computational modeling aimed at recapitulating these data might suggest a molecular mechanism for the actions of the R628E mutation on receptor gating.

3.3.6 Replicating physiological data using a kinetic rate model of R628E

Given the complexity of the R628E data, we modified a previously published kinetic model (Partin et al., 1996, Harms et al., 2013) to simulate R628E kinetics (figure 3.7a). This model consists of 12 individual receptor states: six of these states (black) represent conformations of the receptor (R) as it binds agonist (R-Glu) in duplicate (R-Glu_2) leading to channel opening (R*-Glu_2) or desensitization (R_d-Glu, R_d-Glu_2) in the absence of modulator. The other six states (light grey) represent these receptor conformations with modulator bound. Forward and reverse transitions between these receptor states can be identified in table 3.2 using associated number overlays.

Using our electrophysiology data as an initial guide, we first set out to recapitulate currents observed in the presence of modulator using a flop based model, chosen due to the more profound effects of modulator on R628E flop receptors (figures 3.2, 3.5-3.6). We found that the only change necessary to recapitulate WT flop currents in presence of CTZ was to slow the rate for onset of desensitization in presence of modulator (δ) by 100-fold (table 3.2). Modulation of kinetics caused by CX614 was more involved, requiring changes to δ (500-fold slower), recovery from desensitization (γ, 15-fold slower) and agonist dissociation (k-off, 20-fold slower), as shown in table 3.2.

Having identified modulator parameters, we then attempted to recapitulated R628E flop receptor currents in absence and presence of modulator. Since the mutation changes endogenous rate receptor kinetics in absence of modulator, we chose to alter transition rates 1-6 (figure 3.7a). Using electrophysiology (figure 3.2) as a guide, we were able to identify two separate strategies for recapitulating R628E flop currents. The first of these strategies required slowing channel closure (α) 10-fold and δ close to 20-fold. While these rate changes were able to recapitulate kinetics of receptor deactivation and desensitization, a 5-fold increase of current amplitudes, which is not seen in our electrophysiology data (table 3.1), was also observed for the model. The other model strategy to recapitulate electrophysiology data involved slowing k-off 40-fold and δ 100-fold. Unlike the other strategy of changing α, the k-off strategy replicated R628E kinetics while preserving wildtype (and observed R628E) current amplitudes. However, since our electrophysiology recordings were made from macroscopic patches containing an unknown number of channels, we considered both strategies to be plausible.

Finally, we combined our mutant and modulator models to recapitulate currents of R628E in presence of drug. While we could not simply apply rate changes observed with the modulator models to the R628E model, by adjusting rates in presence of modulator in an additive manner, as observed with electrophysiological currents (figure 3.5), we were able to replicate our electrophysiology data.

3.3.7 Application of binding data to a kinetic model suggests the R628E mutant alters receptor kinetics through changes to agonist binding and dissociation

Having established rate change strategies capable of replicating R628E and modulator currents, we aimed to identify a single modulation pathway of R628E by extending the model to replicate our ligand binding data (figure 3.8). As discovered in binding assays, R628E flop receptors show higher apparent agonist affinity reflected by a single K_D (24.48± 1.13), whereas WT receptors show apparent high ($K_{D\ High}$=13.74± 2.78) and low ($K_{D\ Low}$=163.70± 33.54) affinity binding components, with lower apparent affinity overall (127.90± 26.20, figure 3.6 and table 3.3). To gain a better understanding of how our model reflects changes in agonist binding, we manipulated the model using a step-by-step approach and observed the resulting effects on modeled glutamate binding. We found that changing α alone in our model failed to cause any appreciable change in binding with (CTZ: Min=5.70%, CX614: Max=169.66%) or without ($K_{D\ High}$=22.26 ± 1.18, $K_{D\ Low}$=151.73 ± 15.04, $K_{D\ Weighted}$=72.64 ± 6.58) modulator compared to modeled WT conditions ($K_{D\ High}$=22.25 ± 1.18, $K_{D\ Low}$=153.08 ± 15.16, $K_{D\ Weighted}$=73.10 ± 6.61; CTZ: Min=6.62%, CX614: Max=169.66%). Changing α and δ together, as suggested by one of our strategies, resulted in lower apparent affinity ($K_{D\ Weighted}$=260.31 ± 3.41), however it was best fit by a single

exponential. While using this same strategy we observed close to the desired extent of binding change with CTZ (Min= 50.18%), the modeled effect of CX614 was drastic, increasing more than 6-fold greater than what is observed in binding assays (1050.85%, figure 3.8 and table 3.3).

Failing to observe the desired effects by changing α in our model, we next looked at how our other strategy, changing k-off and δ, affected agonist binding. By changing k-off alone, we observed an increase in agonist affinity in the absence of any modulator, with a single exponential fit reflecting a K_D of 1.19 ± 0.12. Though this result was higher affinity than observed with electrophysiology, the additional change of δ brought the model more in accordance with our binding assays, having an apparent K_D of 13.71 ± 0.68 obtained from a single exponential fit (figure 3.8 and table 3.3). For binding in presence of modulator, slowing k-off alone had a minimal effect on binding in presence of CTZ (Min= 7.41%) but caused a shift in the opposite direction of what was expected for CX614 (Min=18.86%). Again, the additional change of slowing δ in the model was sufficient to revive the CX614 induced increase in agonist binding (Max=179.21%), and attenuated CTZ induced binding loss (Min=86.09%) to a similar extent as that observed in binding assays (table 3.3).

3.4 DISCUSSION

Studies of GluA2 ligand-binding domain mutants have provided a great deal of insight into AMPA receptor agonist binding and gating mechanisms. Although an essential element to these investigations has been structural data gained from the isolated S1S2 ligand binding domain, there remain other mutations outside of this region that alter receptor kinetics. Here, we have re-evaluated one of these mutations, the arginine 628 to glutamate mutant (R628E) first described by Yelshanky et al. (2004), using more recently available structural data of an intact, homozygous GluA2 receptor (Sobolevsky et al., 2009).

3.4.1 Charge inverting mutation of R628->E disrupts inter-subunit electrostatic interactions that favor the open-cleft conformation

The unique orientation of R628 residues within the tetramer differs in several ways from that anticipated when the R628E mutant was first published. While the majority of the receptor transmembrane region has 4-fold symmetry about the tetramer, this symmetry is broken near the site of R628 as one pair of subunits breaks secondary helical structure and takes on a less ordered, extended conformation, bringing the R628 residues into alignment (figure 3.1). Although electrostatic interactions along an extended conformation were originally predicted for this region (Yelshansky et al., 2004), the subunit asymmetry and subsequent alignment of R628 could not be deduced without the now available structural information. Our newfound understanding of R628 alignment in the antagonist bound conformation suggests new implications of the R628E mutant. The resulting charge inversion might result in a receptor that energetically favors the ligand-

bound, closed-cleft confirmation in order to relieve electrostatic strain near the channel pore. Indeed, energy diagrams of our modeled data, as described below, reflect this energetically favored closed-cleft conformation.

An alternative explanation proposed by Dong and Zhou (2011) is that the R628E mutation creates an unfavorable electrostatic interaction with negatively charged lipids in the cell membrane upon entering the desensitized state. While a similar interaction may explain the slowed onset of deactivation we observe (figure 3.2), such an interaction would be best explained as a manipulation of alpha, which poorly explains changes to apparent binding (figure 3.6) as shown by our model (figure 3.8) and discussed below. However, we cannot rule out electrostatic interactions with the membrane as the cause for observed effects of R628E on receptor desensitization, although it seems unnecessarily complex for such independent mechanisms to describe a single mutant's effects on deactivation and desensitization, respectively.

3.4.2 The R628E mutant alters fast kinetics of gating and onset of desensitization

Though previous work (Yelshansky et al., 2004) characterized the effects of the R628E mutant on receptor desensitization, we sought to gain a better understanding of receptor mechanisms by studying the fast kinetics of R628E receptor deactivation (figure 3.2). Here we found R628E receptors have a slowed time-course of deactivation. However, what causes slow deactivation in the mutant isn't clear. Though it is possible that electrostatic interference caused by R628E near the channel pore might slow channel closing and consequent receptor deactivation, our models of such an interaction (figure 3.7, 3.8) do not accurately convey observed binding data (figure 3.6). Rather, in a

manner opposite that of LBD mutations such as T686A (Robert et al., 2005, Zhang et al., 2008), the R628E mutant may slow LBD opening, similar to what was modeled for the *Lurcher* mutant (Klein and Howe, 2004). Interestingly, the time-constants of R628E exponential decay were best fit by a two-exponential line of fit that seemed to result from a small amplitude slow component (figure 3.2). While our simplified model does not ideally portray this slow component, we can more accurately fit the curve by independently slowing cleft-opening in a more complex variant of this model that has been used previously (Timm et al., 2011).

3.4.3 Allosteric modulation of GluA2 is preserved for the R628E mutant

Many allosteric modulators, including CTZ and CX614, bind to a common pocket between LBD dimers (Ptak et al., 2009) through which they exert their modulatory effects. We chose to probe the R628E mutant using CTZ and CX614, as it is proposed they favor the open state through different mechanisms of action; with CTZ slowing the onset of desensitization while CX614 slows receptor deactivation (Timm et al., 2011). Though given its location, we did not expect the R628E mutant to physically occlude modulator binding, there was still a possibility that unknown structural alterations reulting from the mutant could prevent modulation by these compounds. Here we show that modulation of receptor kinetics is qualitatively preserved for both CTZ and CX614 (figures 3.4, 3.5). It is interesting to note that we consistently saw an additive effect of modulators on the R628E mutant, suggesting that the mutant and modulators alter GluA2 kinetics through different, non-interferring mechanisms. This is an exciting finding in the spirit of drug research, as it identifies the AMPAR outer vestibule as a potential target for the design of future

modulatory drugs. Further, these results suggest that compounds acting at the outer vestibule can be co-administered with currently established modulators to enhance observed effects. Additionally, it may also be possible to design non-competitive antagonists with a compensatory effect at this site, similiar to the GYKI compounds (Donevan and Rogawski, 1993, Arai et al., 2000).

3.4.4 R628E mutant receptors show loss of a low affinity binding component

A surprising finding given the loaction R628E mutation is that it causes an increase in apparent agonist affinity (figure 3.6), as has been shown previously with glutamate concentration-response curves (Yelshansky et al., 2004). Here, we sought to evaluate R628E induced changes to agonist affinity by directly measuring agonist binding using tritiated fluorowilliardiine ([^{3}H]FW). As described elsewhere (Kessler and Arai, 2006), binding assays using [^{3}H]FW, though a partial agonist, show similiar binidng charachteristics to the full agonist [^{3}H]AMPA, including apparent high and low affinity binding components (Kessler et al., 2008). Here (figure 3.6) we see these seperate components of apparent high and low affinity binding manifest as two-exponential fits to the [^{3}H]FW binding assay data. Curiously, repeating these [^{3}H]FW binding experiments on R628E mutant GluA2 receptors yields data best fit by a single exponential representing high affinity binding, thus suggesting the loss of the low apparent affinity binding component.

It is interesting to consider this loss of a binding component when integrated with the structural data (figure 3.1). It has been proposed that glutamate dissociation rates may differ for individual subunits within a receptor (Robert and Howe, 2003). Since GluA2

subunits are assymetric (Sobolevsky et al., 2009), it is possible that apparent high and low affinity binding components result from structural differences between these assymetric subunits. Thus, given the location of R628 at the symmetry transition, the R628E mutant may greatly influence GluA2 structure in this area, resulting in the loss of specific structural differences between subunits responsible for the observed binding affinity differences. Alternatively, the loss of an observed low affinity component could be due to differences between assay and electrophysiological conditions. Though patch clamp electrophysiology is limited to studying receptors expressed on the cell membrane surface, binding assays used here include all receptors in the membrane. It has been proposed that apparent high and low receptor affinities are a consequence of this difference in receptor expression, with a higher percentage of low affinity receptors occuring over time as receptors are trafficked away from the membrane surface (Kessler and Arai, 2006). If this were the case, the near 100% high affinity observed through binding assays would suggest almost all receptors are expressed on the membrane surface. However, our confocal data shows disturbed receptor trafficking (figure 3.3), and we do not see greatly increased current amplitdues for R628E receptor patches (table 3.1).

3.4.5 The flop isoform of R628E shows greater sensitivity for modulator enduced changes to agonist binding

Another peculiar observation for the binding data is that flop receptor isoform mutants show greater sensitivity to modulator induced binding changes than flip isoform mutants (figure 3.6). This is rather unexpected, as there seems to be little difference between isoforms for binding without modulator. Furthermore, isoform speficity of

modulator does not seem to be involved, as R628E flop receptors showed greater binding change even with the more flip specific modulator, cyclothiazide (Partin et al., 1996, Kessler et al., 2000). One potential explanation, as gained from the electrophyisiological data, is that the R628E mutant only slows desensitization onset significantly for flop receptors (figure 3.2). If this slow onset of desensitization results from stabilization of nondesensitizaed states, we would expect the flop isoform mutant to show greater observed binding effects with modulators. Similarly, onset of desenstiization for wildtype flip GluA2 is already significantly slower than flop, suggesting more stable non-desenstized states and thus less drastic modulator enduced changes for flip isoform R628E receptors.

3.4.6 R628E data can be recapitulated in a model by slowing k-off and delta

Since our electrophysiology data represents receptor activity on a macroscopic level, we used a previously published model (Harms et al., 2013) to make inferences into how R628E mutation modifies GluA2 kinetics. Using electrophysiology (figures 3.2, 3.4-3.5) as a guide, we found two distinct rate-change strategies capable of modeling measured GluA2 kinetics (figure 3.7), both of which require slowing the desensitization on-rate but differ by the transition rate modified to recapitulate R628E's slower onset of deactivation. One strategy for slowing deactivation rate is to slow the agonist dissociation rate, k-off, which in the present model reflects both cleft-opening and agonist dissociation. Though cleft opening and agonist dissociation are modeled as seperate rates elsewhere (Robert et al., 2005), including a more comprehensive variant of the model used here (Timm et al., 2011), combining these transitions simplifies the model and more easily allows for integration of allosteric modulators (figure 3.7). The other strategy capable of slowing

macroscopic deactivation is to slow the channel off rate (α). While we initially expected the later pathway would best describe the mutant given the proximity of R628E to the channel pore (figure 3.1), when we attempted to recapitulate agonist binding data with the model the opposite held true (figure 3.8). This finding reinforces our observation that the R628E mutant alters agonist binding, and is further reflected by energy diagrams for various manipulations to the model (figure 3.8). These diagrams suggest that slowing k-off and δ together is sufficient to better stabilize the closed-cleft, ligand bound preopen and open states without affecting energy characteristics of the desensitized state. Thus, the agonist bound and open states would be favored and the desensitized state less favored due to the apparent energetic "peaks" that must be overcome starting from a more stable ligand bound closed-cleft state.

Here, we have extended that interactions in the AMPA receptor external vestibule have a profound effect on AMPA recpeptor gating kinetics, including agonist binding, through mechanisms independent of current allosteric modulators. As such, we propose the external vestibule is a viable target for advances in drug research, and reaffirm the importance of targeted mutagenesis for glutamate receptor research.

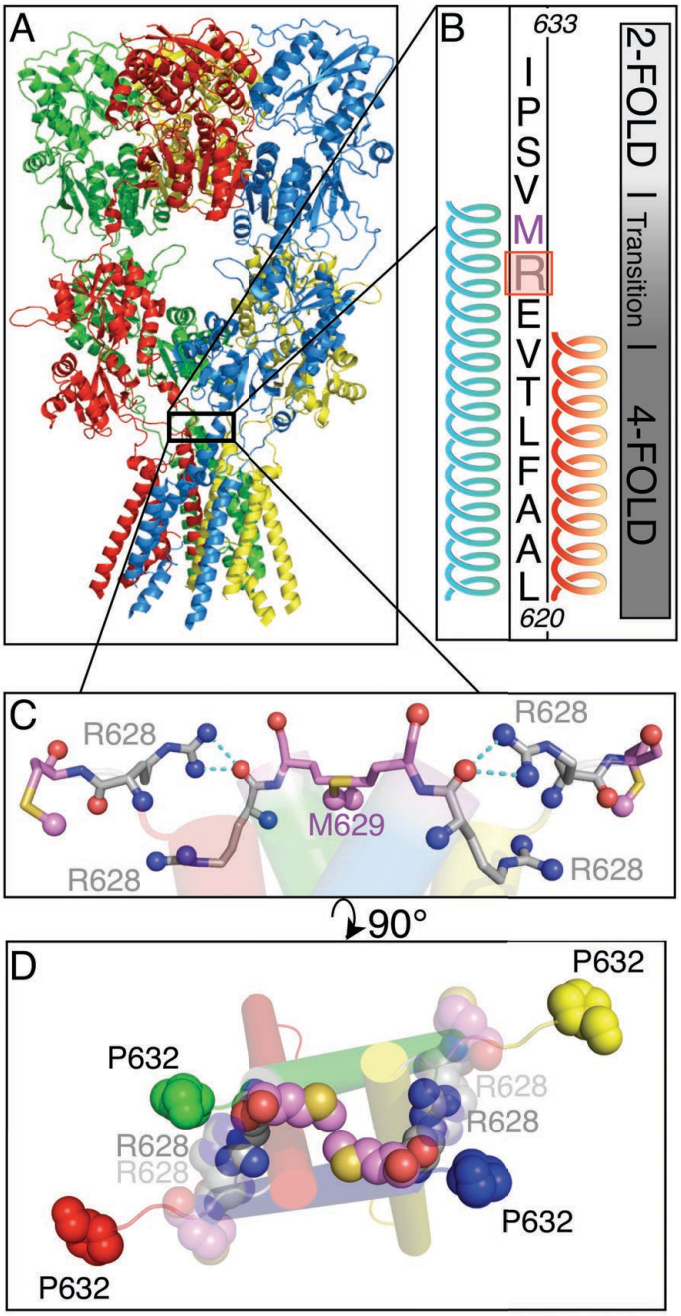

Figure 3.1: R628 lies at a transition in receptor symmetry and forms the "latch" in the closed-receptor-state

A) GluA2 crystal structure from Sobolevsky et al. (2009) showing receptor subunits by color (A: green, B: yellow, C: blue, D: red). **B)** GluA2 amino-acid sequence from L620 in M3 (bottom) to I633 in the linker region (top). Subunits A and C feature an extended M3 helix, creating a 4-fold to 2-fold symmetry transition over a region inclusive of R628 (highlighted by red) and M629 (magenta). **C)** The symmetry transition positions the R628 sidechain nitrile group of subunits B and D within hydrogen bonding distance to the backbone of subunits C and A, respectively. **D)** R628 of subunits B and D (translucent) form a latch with R628 from subunits A and C (opaque), which include M629, the most constrictive area over the pore (Sobolevsky et al., 2009) (pink spheres).

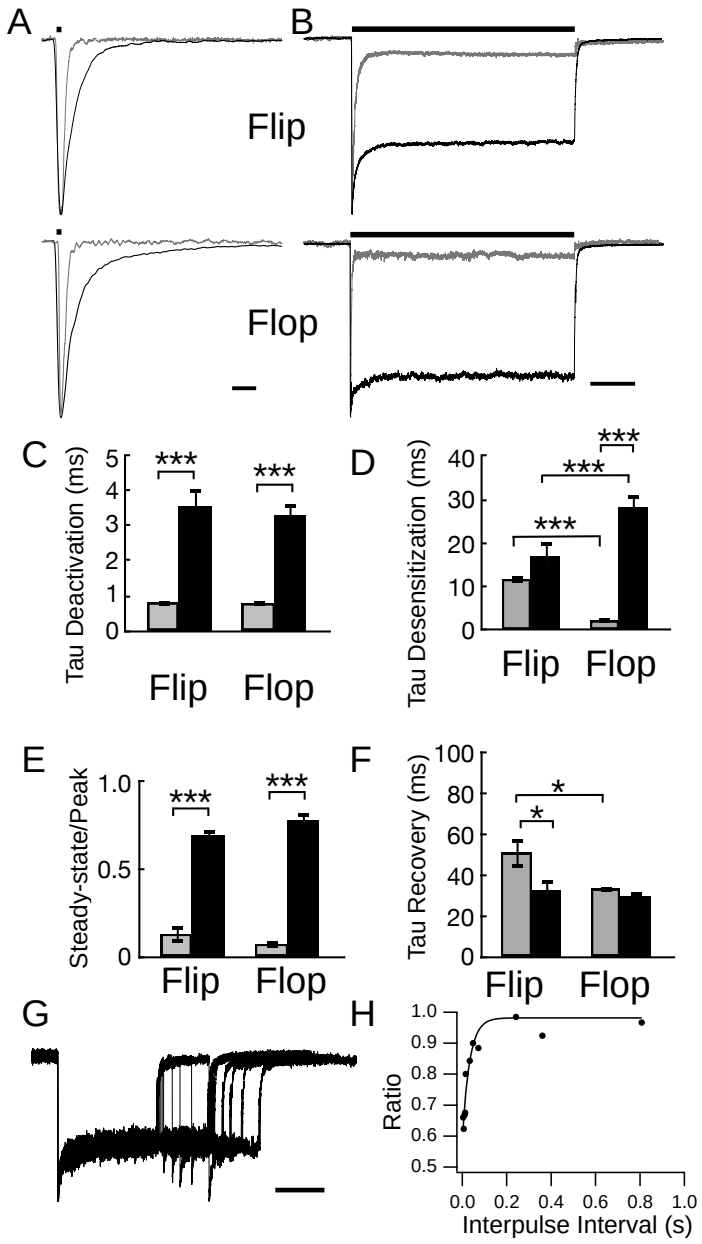

Figure 3.2: Electrophysiological recordings of R628E currents show altered receptor kinetics compared to wildtype GluA2

A,B) Representative current traces of outside-out patches pulled from HEK293 cells transfected with homomeric GluA2 flip (upper traces) or GluA2 flop (lower traces). R628E mutant (black) normalized to wildtype (grey) responses to a 10 mM pulse of glutamate (bar above trace) for 1 ms (a, deactivation) or 500 ms (b, desensitization). Scale bars: 5 ms for deactivation, 100 ms for desensitization. **C-F)** Comparison of mean data between WT (grey) and R628E (black) shows the R628E mutant to have significantly slowed onset of deactivation (c) and increased steady-state current (e) for both flip and flop isoforms of GluA2. Only the flop isoform of R628E showed significantly slower desensitization (d), whereas only the flip isoform had significantly faster recovery. R628E deactivation data shows the weighted mean of 2 exponentials. *p<.05, ***p< .001. **g,h)** Representative paired-pulse recovery sweep for R628Eo (g), and corresponding plot of second-peak to first-peak ratio with increasing intervals (h).

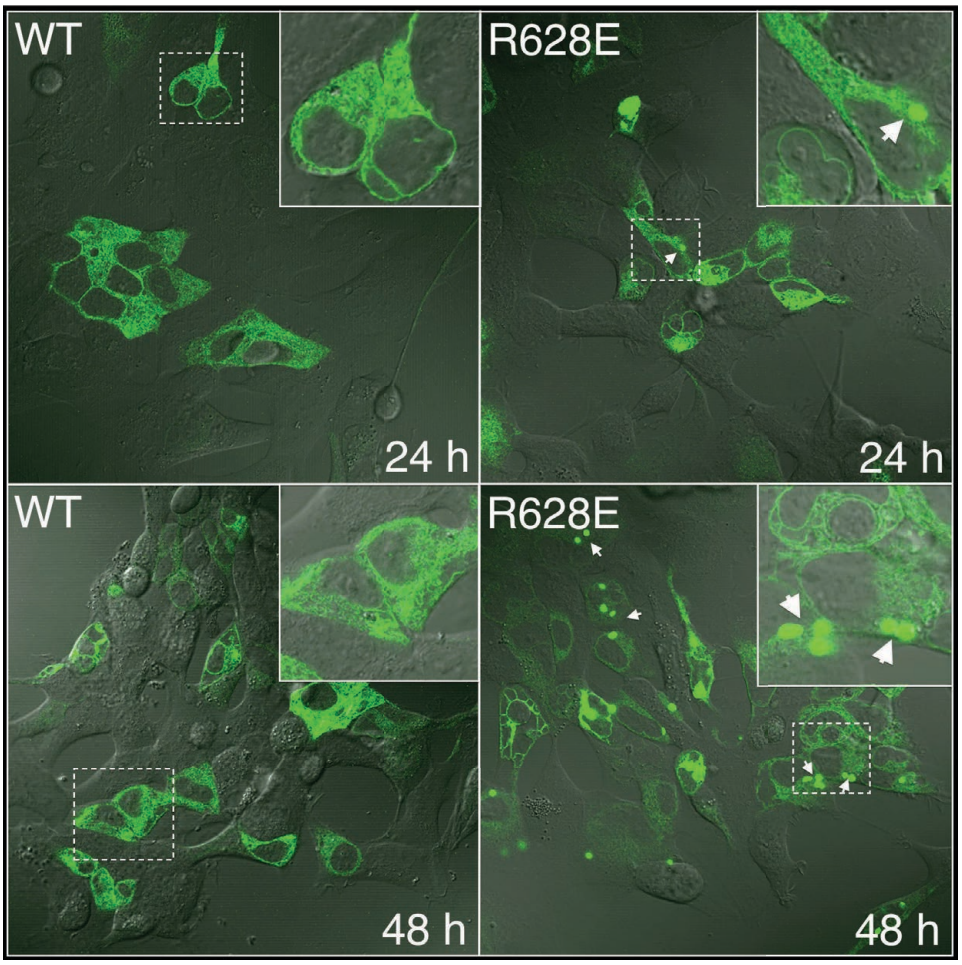

Figure 3.3: The R628E mutant shows impaired trafficking and formation of aggresomes

Confocal images of HEK 293 cells transiently-transfected with YFP tagged wildtype (WT) flip (left) or YFP tagged R628E flip (right) constructs. Top row: images taken 24 hours after cell transfection; bottom row: images taken 48 hours post-transfection. Inset in upper right corner of each panel shows magnification of the area drawn by dotted white box. Note the increased number of aggresomes (white arrows) in HEK cells transfected with the R628E construct, indicative of disrupted channel trafficking. (images courtesy Leslie Stone)

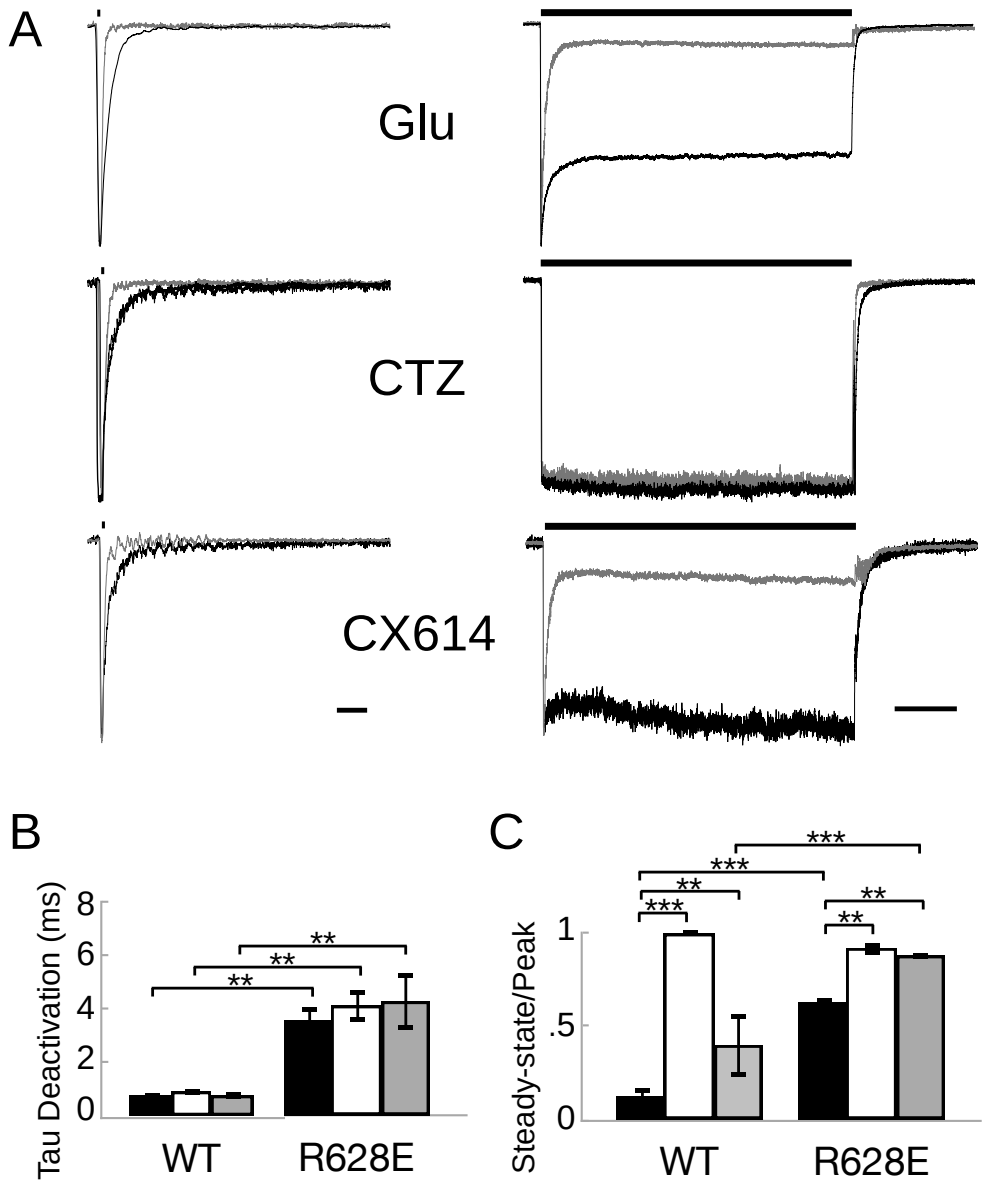

Figure 3.4: The R628E mutant does not occlude effects of modulator for the flip isoform of GluA2

A) Representative current traces of outside-out patches pulled from HEK293 cells transfected with homomeric GluA2 flip. R628E mutant (black) normalized to wildtype (grey) responses to a 10 mM pulse of glutamate (bar above trace) for 1 ms (left, deactivation) or 500 ms (right, desensitization). Currents recorded with glutamate only (Glu) or in continuous presence of 100 µM CTZ or 100 µM CX614 Scale bars: 10 ms for deactivation, 100 ms for desensitization. **B,C)** Mean data for tau deactivation (b) and steady-state/peak ratio (c) for flip isoform wildtype (WT) and R628E currents as shown above (black, glutamate only; white, with 100 µM CTZ; grey, with 100 µM CX614). *p< .05, ** p< .01, ***p< .001

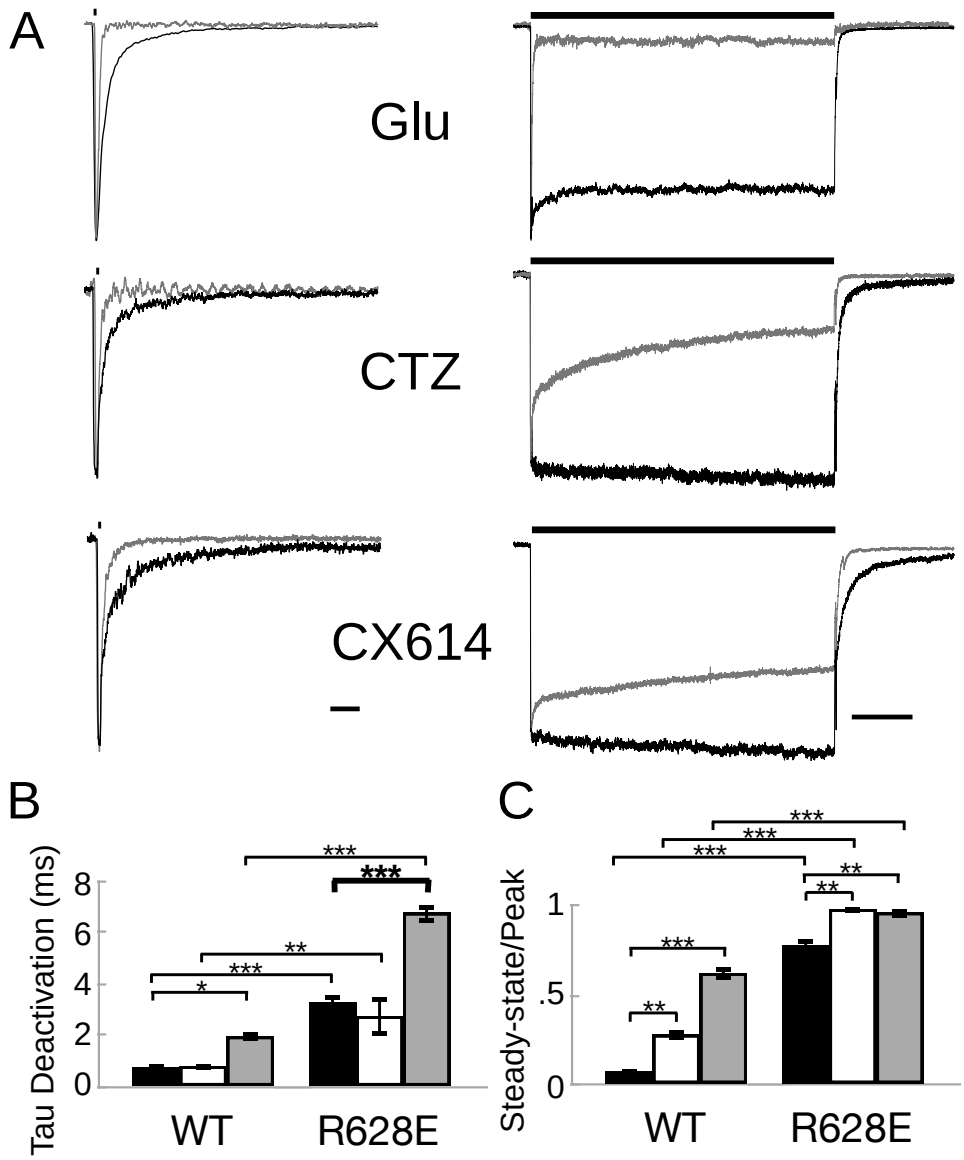

Figure 3.5: The R628E mutant does not occlude effects of modulator for the flop isoform of GluA2

A) Representative current traces of outside-out patches pulled from HEK293 cells transfected with homomeric GluA2 flop. R628E mutant (black) normalized to wildtype (grey) responses to a 10 mM pulse of glutamate (bar above trace) for 1 ms (left, deactivation) or 500 ms (right, desensitization). Currents recorded with glutamate only (Glu) or in continuous presence of 100 µM CTZ or 100 µM CX614 Scale bars: 10 ms for deactivation, 100 ms for desensitization. **B,C)** Mean data for tau deactivation (b) and steady-state/peak ratio (c) for flip isoform wildtype (WT) and R628E currents as shown above (black, glutamate only; white, with 100 µM CTZ; grey, with 100 µM CX614). *p< .05, ** p< .01, ***p< .001

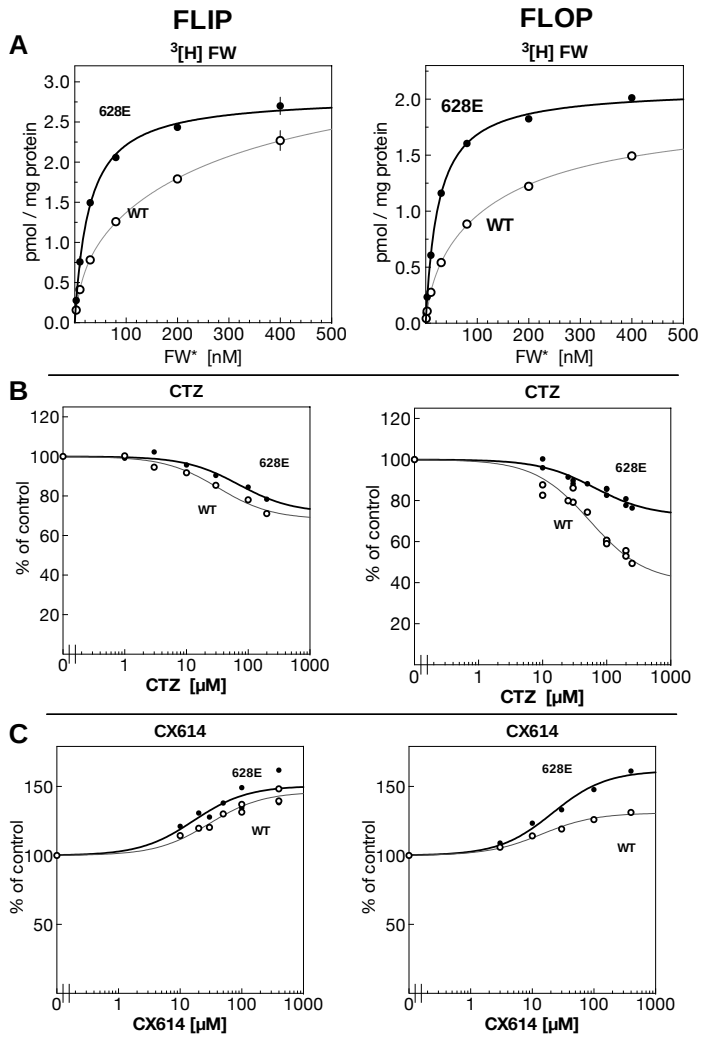

Figure 3.6: The R628E mutant shows altered agonist affinity, with an isoform specific effect in presence of modulator

A) Saturation binding curves for [^{3}H]FW binding to wildtype (WT, open circles, grey line) and R628E receptors (closed circles, black line). Binding was measured at 1-400 nM radioligand at 0°C. The data are shown as averages and s.e.m. from two experiments in which WT and mutant receptors were tested in tandem (absence of error bars indicates that the error was smaller than symbol size). The data points were fitted with the sum of two hyperbolic functions (Prism 6, Graphpad Software, Inc., La Jolla, CA) or with a single hyperbolic function if statistically preferred. K_D and B_{max} values are described in the text. These data show that both flip (left) and flop (right) R628E receptors exhibit a shift towards higher agonist affinity and towards having a single high-affinity component. **B,C)** The effect of CTZ (cyclothiazide; b) and CX614 (c) was measured using a fixed, 5 nM [^{3}H]FW concentration and varying concentrations of drug. Binding at each drug concentration was normalized to that without drug and averaged across experiments. Mean data was plotted on the y–axis against the modulator concentration on the x-axis, and then fitted with a sigmoidal curve (3-point logistic equation with $n_{Hill} = 1$). In the flop isoform (right panels), the CTZ induced reduction in [^{3}H]FW binding was greatly attenuated in R628E (-27% compared to -60% in WT). Conversely, the CX614 induced increase in [^{3}H]FW binding was significantly enhanced in R628E receptors (+62% compared to +30% in WT). In the flip isoform (left panels), these changes in the effectiveness of CTZ and CX614 were much smaller. (data courtesy Markus Kessler)

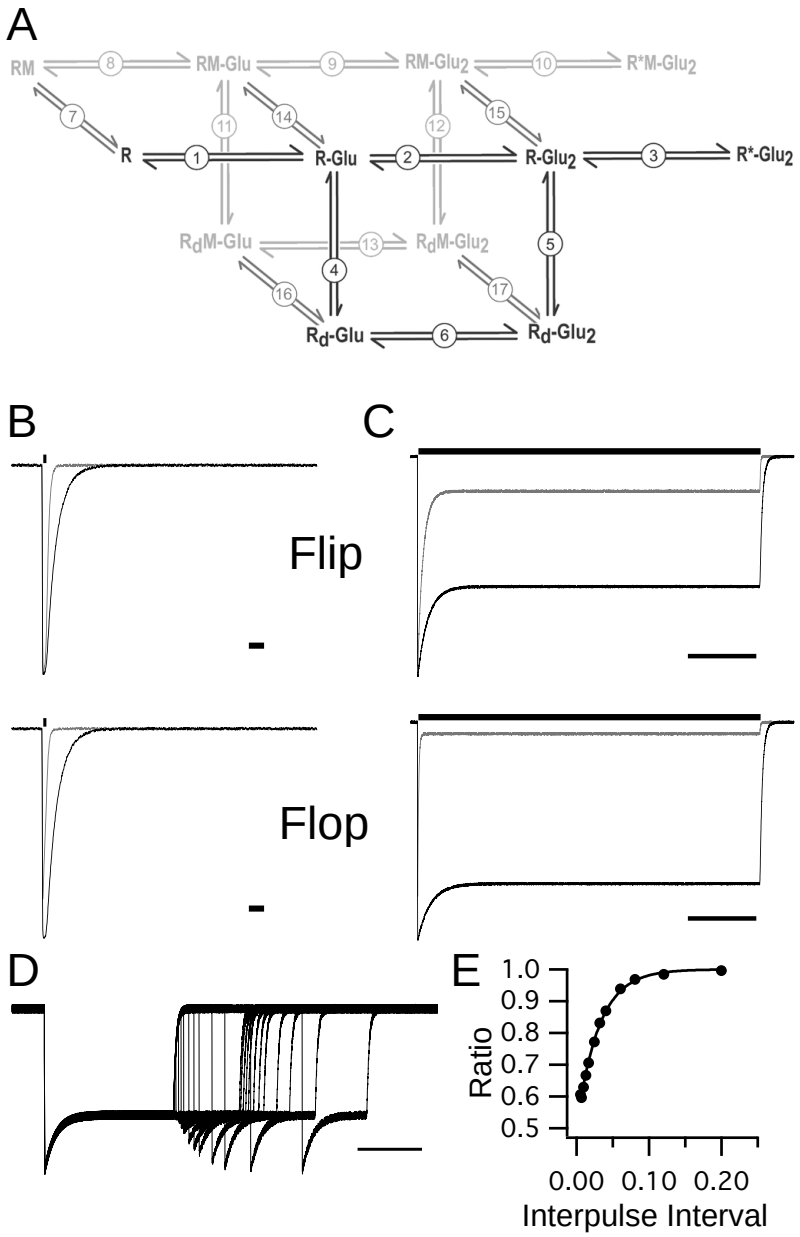

Figure 3.7: R628E physiological data can be replicated by a mathematical model

A) Model schematic showing receptor states in black. Glutamate binds (R-Glu) to a receptor at rest (R) in duplicate (R-Glu_2) to cause channel opening (R*-Glu_2). Alternatively, receptors can enter desensitized states (R_d-Glu, R_d-Glu_2). Identical states are seen for receptor in presence of modulator (light grey), with modulator binding transitions (grey). **B,C)** Simulations of flip (upper) and flop (lower) deactivation (c) and desensitization (d) using wildtype (WT, grey) and R628E (black) transition parameters. (black bar= 10 mM glutamate; scale bars = 5ms deactivation, 100ms desensitization). **D)** Simulated paired-pulse recovery of R628Eo using an initial 200ms desensitizing pulse of 10mM glutamate. (scale bar = 100ms). **E)** Plot of data generated in (d). A single exponential was fit to the resulting values (see methods) with a tau recovery of 29.3 ms. (model design by Morris Benveniste, schematic drawn by John Gieser)

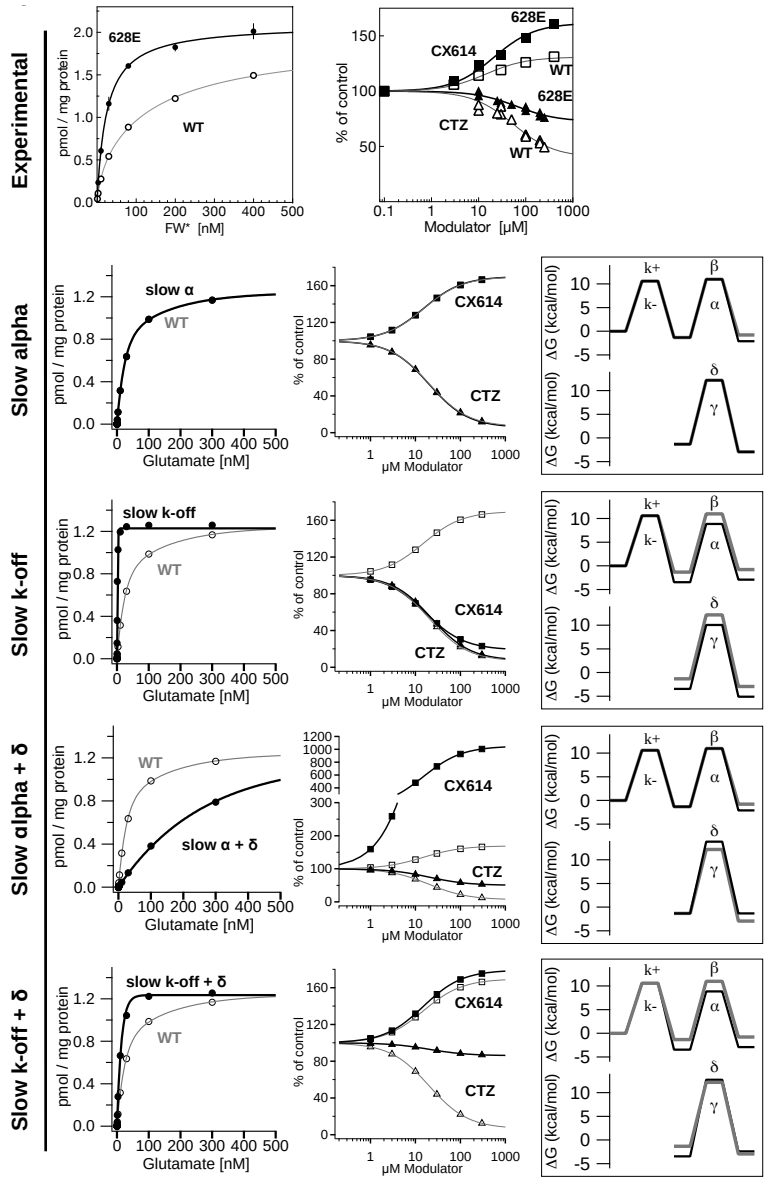

Figure 3.8: Experimental binding data is best modeled by changing both k-off and delta

The experimental data for wildtype (WT, open markers, grey lines of fit) and R628E (filled markers, black lines of fit) receptors is shown for [^{3}H]Flurowilliardiine (FW*) binding. Concentration dependent agonist binding (left panel) shows higher apparent affinity with R628E receptors, and is best fit by a single exponential reflecting loss of a low affinity binding site seen in WT, which is best fit by two exponentials reflecting high and low affinity binding sites as described previously (2008, 2006). Modulator dependent changes in agonist binding (right panel) shows a respective decrease and increase of agonist binding in presence of CTZ and CX614, with R628E receptors showing an overall increase in binding for both modulators. Various manipulations to the model (other panels, filled markers and black lines) differentially alter output, from no change at all for changing alpha alone to closely recapitulating R628E by changing k-off and delta together. An energy state diagram is also shown (far right panels), displaying the predicted effect of each manipulation on receptor state stability as predicted by Gibb's free energy (ΔG). Troughs from left to right of upper trace represent: the unbound receptor, the receptor with LBD closed on agonist, and the receptor with open channel. The lower trace represents the transition between receptor with LBD closed on agonist and the desensitized state.

Table 3.1: Mean data recorded for WT and R628E GluA2 deactivation and desensitization

	Deactivation		Desensitization	
WT Flip	Tau	0.81 ± 0.09 ms	τDes	8.78 ± 0.62 ms
			Steady-state	13.26 ± 3.38 pA
			Peak	151.03 ± 30.44 pA
	Peak Amplitude	111.85 ± 19.86 pA	SS/peak	0.13 ± 0.05
WT Flop	Tau	0.79 ± 0.07 ms	τDes	1.64 ± 0.09 ms
			Steady-state	7.91 ± 2.28 pA
			Peak	99.86 ± 32.71 pA
	Peak Amplitude	93.57 ± 41.14 pA	SS/peak	0.07 ± 0.02
R628E Flip	τFast	1.31 ± 0.25 ms	τDes	12.7 ± 2.82 ms
	τSlow	12.04 ± 2.04 ms	Steady-state	129.50 ± 32.38 pA
	% Fast	76.01 ± 4.10%	Peak	191.70 ± 55.83 pA
	Weighted τ	**3.53 ± 0.55 ms**	SS/peak	0.69 ± 0.03
	Peak Amplitude	106.60 ± 13.74 pA		
R628E Flop	τFast	1.28 ± 0.16 ms	τDes	21.10 ± 2.19 ms
	τSlow	15.33 ± 3.89 ms	Steady-state	114.09 ± 25.41 pA
	% Fast	80.30 ± 3.80%	Peak	146.80 ± 33.65 pA
	Weighted τ	**3.29 ± 0.37 ms**	SS/peak	0.81 ± 0.05
	Peak Amplitude	123.21 ± 26.13 pA		

Homomeric WT and R628E GluA2 flip and flop isoform receptor currents were recorded from outside-out patches of transiently transfected HEK293 cells. Deactivation and desensitization were respectively simulated by 1 ms and 500 ms applications of 10 mM glutamate. Currents from R628E receptors were best fit by two exponentials (τFast, τSlow) which were weighted (Weighted τ) by percent amplitude (% Fast). The mutant receptors also showed greater steady-state/peak ratios (SS/peak). Peak amplitudes did not differ significantly for either condition. (see also, figure 3.2)

Table 3.2: Transition rates and fold-change from WT for a kinetic model of R628E mutant and modulator conditions

Trans	Rate	WT			R628E (k-off)		
		ND	CTZ	CX614	ND	CTZ	CX614
1	On	15					
	Off	8000			40-fold	40-fold	40-fold
2	On	7.5					
	Off	16000					
3	On	4000					
	Off	10000					
4	On	500			100-fold	100-fold	100-fold
	Off	30					
5	On	1000					
	Off	30					
6	On	7.5					
	Off	1000					
7 (*)	On	1	1	1	1	1	1
	Off	1	20	15	1	20	15
8 (1*)	On	15					
	Off	8000		20-fold		**40-fold**	**40-fold**
9 (2*)	On	7.5					
	Off	16000					
10 (3*)	On	4000					
	Off	10000					
11 (4*)	On	500	100-fold	500-fold		**5000-fold**	**5000-fold**
	Off	30		15-fold			15-fold
12 (5*)	On	1000					
	Off	30					
13 (6*)	On	7.5					
	Off	1000					

Rates used for kinetic model (figure 3.7). On and off rates for a WT flop model are shown for the no drug (ND) condition. Transitions that use a shared rate are denoted by shade. Transition 7 represents modulator binding. Transitions 8-13 represent the modulator bound condition (*) of transitions 1-6. Table indicates fold-slowing from WT, no drug, condition to replicate electrophysiological data in presence and absence of modulator for WT and R628E recordings. Numbers shown in bold indicate an additive change of modulator on the mutant.

Table 3.3: Alterations to agonist binding by a kinetic model of R628E

Model Data	Glutamate Binding		Binding w/ Modulator		
WT	K_D High	22.25 ± 1.18	**CTZ**	Min	6.62405
	K_D Low	153.08 ± 15.16		EC_{50}	20.0619
	% High	61.13	**CX614**	Max	169.658
	Weighted K_D	**73.10 ± 6.61**		EC_{50}	14.9654
Slow Alpha	K_D High	22.26 ± 1.18	**CTZ**	Min	5.69774
	K_D Low	151.73 ± 15.04		EC_{50}	20.0625
	% High	61.09	**CX614**	Top	170.035
	Weighted K_D	**72.64 ± 6.58**		EC_{50}	14.9652
Slow K-off	K_D High	1.19 ± 0.12	**CTZ**	Min	7.41027
	K_D Low	n/a		EC_{50}	22.4627
	% High	100	**CX614**	Min	18.8569
	Weighted K_D	**1.19 ± 0.12**		EC_{50}	16.6187
Slow Alpha + Delta	K_D High	260.31 ± 3.41	**CTZ**	Min	50.1795
	K_D Low	n/a		EC_{50}	20.0037
	% High	100	**CX614**	Max	1050.85
	Weighted K_D	**260.31 ± 3.41**		EC_{50}	14.9465
Slow K-off + Delta	K_D High	13.713	**CTZ**	Min	86.0915
	K_D Low	n/a		EC_{50}	20.0244
	% High	100	**CX614**	Max	179.207
	Weighted K_D	**13.71 ± 0.68**		EC_{50}	14.8958
Experimental Data	**^{3}[H]Flurowilliardiine Binding**		**Binding w/ Modulator**		
R628E Flop	K_D High	24.48	**CTZ**	Min	72.55
	K_D Low	n/a		EC_{50}	64.68
	% High	100	**CX614**	Max	161.5
	Weighted K_D	**24.48 ± 1.13**		EC_{50}	21.35
WT Flop	K_D High	13.74 ± 2.78	**CTZ**	Min	40.21
	K_D Low	163.7 ± 33.54		EC_{50}	54.83
	% High	23.87	**CX614**	Max	130.9
	Weighted K_D	**127.90 ± 26.20**		EC_{50}	14.22

Using a step-by-step approach, we extended our model parameters (table 3.2) to investigate how specific rate changes affect agonist binding. High and low affinity K_D values are presented where appropriate. Weighted K_D standard error is presented as the weighted error of high and low affinity components. Note that model simulations use glutamate as an agonist, where as experimental binding assays used [^{3}H]flurowilliardiine. Modulatory conditions resulting in decreased binding (<100% normalized) are expressed as the minimum (Min) percentage; with conditions increasing binding (>100% normalized) expressed as the maximal (Max) value.

4. ADDITIONAL WORK

Along with the two aforementioned papers, I have collected additional data with potential implications for future publication. While these collections of data are not complete works on their own, I believe they nonetheless complement other information presented herein. These works include a series of compounds derived from the JAMI 1001 compound (the NC compounds, chapter 4.1), a study I conceived and designed using cysteine mutations to study intra-receptor interactions (chapter 4.2), and a fusion of chapters 2 and 3 with JAMI 1001 being applied to R628E mutant receptors (chapter 4.3).

4.1 PHYSIOLOGY OF JAMI DERIVATIVES: THE NC COMPOUNDS

4.1.1 Introduction to NC compounds

The first collection of data is in many ways a continuation of chapter 2, the published work on JAMI 1001. To recall, my initial involvement with the JAMI project was to perform electrophysiology on a novel class of modulator designed with drug-ability in mind. As a continuation of the JAMI project, our collaborator who furnished the drug, Craig Jamieson, synthesized further compounds by using JAMI 1001 as a template and altering specific moieties (outlined in figure 4.1.1). Using similar methods as described in chapter 2 (Greger et al., 2002), I recorded current responses, in the presence or absence of modulator, to applications of 10 mM glutamate on excised patches of WT flip and flop GluA2 expressed in HEK293 cells. However, rather than 100 μM concentrations of modulator as used for JAMI 1001, only a 30 μM concentration of each NC compound was included in each perfusion barrel due to limited availability.

Chemical structures of the modulators are shown in figure 4.1.1. A shared feature of JAMI 1001 with the NC compounds is a pyrazole moiety with attached trifluromethyl substituent. Though structural information of NC compounds bound to the ligand binding pocket is not available at this time, this substituent is expected to occupy the C or C' subsite, dependent on orientation (Appendix 1). Apart from the preserved pyrazole and trifluromethyl group, the remainder of NC compound makeup is mostly modified from JAMI 1001. Rather than an extended alkyl chain, NC compounds show a backbone with more closed ring structure, either attached directly to the pyrazole (NC1-013), or by a short

linker (NC2-006, NC2-022). To some extent, this imparts a more "CX614-like" appearance to the NC compounds.

4.1.2 Physiological results of NC compounds

Results are outlined in table 4.1.1 and figure 4.1.2, with JAMI 1001 results included for purpose of comparison. No significant effects of the NC compounds on WT flip deactivation were found. Although NC1-013 seems to slow tau deactivation, this result was mostly attributed to a single slow recording that showed no difference with or without modulator on the same membrane patch. For flop receptors, a significant effect was found for NC2-006, slowing mean tau deactivation over 2.5 fold and to a greater extent than JAMI 1001. NC2-022 also looked to slow flop deactivation, with $p<.05$ when compared to WT flop using a student's t-test. However, this finding did not hold when assessed using two-way ANOVA with Fisher's LSD. Thus, only NC2-006 slowed deactivation of GluA2, doing so in a flop specific manner.

Looking at tau desensitization, a pattern similar to tau deactivation is seen, with no observed effects of the NC compounds on flip GluA2. Interestingly, although JAMI 1001 did not change tau desensitization from WT rates for either isoform, the NC compounds did show significant effects; with NC-006 and NC-022 slowing tau desensitization for flop by nearly one and two orders of magnitude, respectively (9-fold and 80-fold, table 4.1.1). Noticeably, however, the steady-state of NC2-022 progresses towards WT levels by the end of the 500ms glutamate pulse, with NC2-006 the only NC compound to show an effect on steady-state to peak ratio. Surprisingly, this effect was also observed for NC2-006 on flip

receptors, despite showing no other effects on flip receptors. Still, with only two-recordings to show (although little variation), these results should be taken with some reservations.

4.1.3 Discussion of NC compound results and integration with structural models

The NC compounds evolved from the JAMI 1001 compound featured in chapter 2, all synthesized by a collaborator on that paper, Craig Jamieson. Upon first receiving the compounds, I had the initial impression that they looked like hybrids of CX614 with JAMI. While this is not the case, the NC compounds do show more of a fused ring backbone than JAMI 1001, much like that of CX614. Due to this, I initially suspected the NC compounds would show some CX614-like properties, including preference for the flop isoform and potentially greater influence on deactivation.

It has been documented elsewhere that the fused structure of CX614 imparts greater rigidity leading to higher potency (Arai et al., 2000). Interestingly, what looks to be the most "rigid" NC compound, NC1-013, showed no effects on either receptor isoform. The most logical explanation for this outcome is that JAMI 1001 and its NC progeny are larger compounds designed to occupy hydrophobic subsites (C and C') while spanning the central region (A subsite). However, space-filling models of the modulator-binding pocket (Appendix 1) show a slight hump or "saddle" near the middle, which modulators must bend around. CTZ binds with two molecules on either side of this saddle, occupying the B/B' and C/C' subsites. CX614 is likely small and flat enough to position along the A subsite without interference from the saddle. JAMI 1001, with its extended alkyl chain, can rotate and bend more freely around this saddle, allowing it to occupy the C and C' subsites. While the carbon linker between the pyrazole and fused rings of NC2-006 and NC2-022 likely allows

for these structures to bend around the saddle region, the subtraction of this linker as seen with NC1-013 likely prevents sufficient binding to have a modulatory effect. Thus, with no binding of modulator, no observed physiological effects of modulator application.

While NC1-013 likely doesn't bind, the observed physiological effects of the other NC compounds suggest at least a partial ability to bind in the modulator-binding pocket. Additionally, these compounds show isoform specific effects not observed with JAMI 1001. As such, it is interesting to note that models predict JAMI 1001 to bind in approximately the same conformation regardless of modulator, whereas NC2-006 is predicted to show different conformations dependent on a flip or flop receptor binding pocket (Appendix 1). Thus, isoform specific effects of NC-006, and to some extent NC-022, are probably due to isoform dependent binding conformations. Additionally, replacement of the carbonyl substituent of NC-006 with a sulfonyl group in NC2-022 imparts additional steric bulk, potentially resulting in less favorable binding and thus less modulatory ability. Such increased steric bulk would further discourage binding to the flip receptor isoform, where the isoform specific serine residue pokes into the binding pocket (Appendix 1).

4.1.4 Conclusions of NC compound work

In part, these findings and models support the suggestions mentioned in chapter 2 and elsewhere (Ptak et al., 2009, Timm et al., 2011), that binding subsite occupation regulates modulator function. While it may still be premature to draw further conclusions from modeled structural information, some interesting patterns are starting to emerge. Not surprisingly, it appears that a modulator's efficacy largely depends on its ability to bind to the modulator-binding pocket. Somewhat more interesting is that JAMI 1001 is predicted

to bind in the same conformation to both flip and flop receptor isoforms. Also interesting is that isoform specific effects of modulator may be a consequence of steric interference preventing modulator binding, rather than changes to specific binding partners due to flip/flop differences. Extending predictions even further, there is additional evidence that modulator rigidity enhances efficacy, permitted it does not impair or impede modulator binding. Ultimately, the continued study of modulator structure and physiological effects in concert will continue to tease out structural correlates of allosteric modulation at this site.

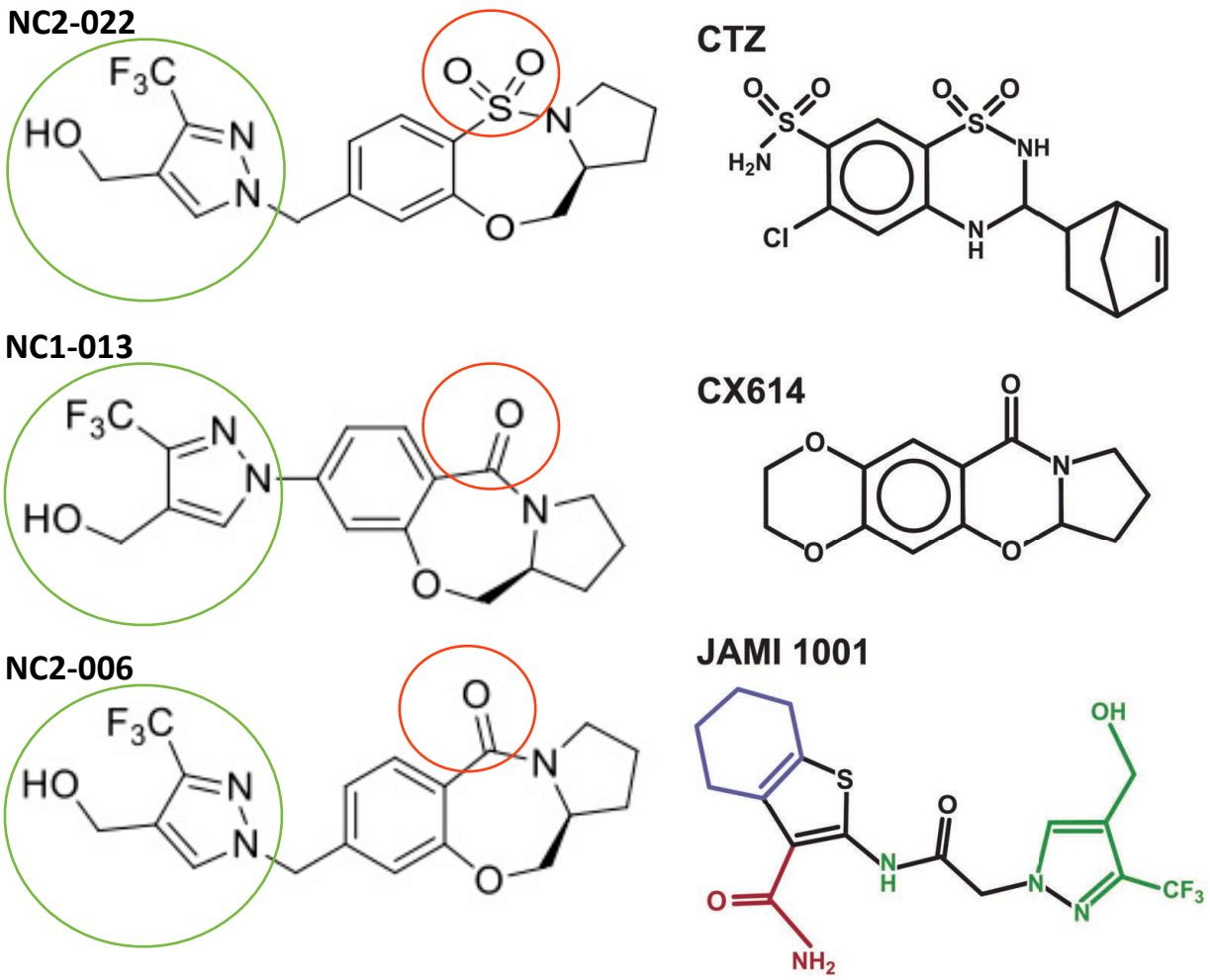

Figure 4.1.1: Chemical structures of three new potential allosteric modulators (NC compounds) in comparison with compounds used in chapter 2

Similar to JAMI 1001, the NC compounds feature a pyrazole moiety with attached trifluromethyl substituent (circled in green, and green on JAMI 1001). The amide substituent of JAMI 1001 (red) is varied with NC compounds (circled in red). The NC compounds also show additional closed ring structures in place of an extended alkyl chain seen with JAMI 1001. Also note the shortened linker of NC1-013 compared to NC2-006 and NC2-022. (Structures for NC compounds courtesy Craig Jamieson, other compounds redrawn by John Gieser).

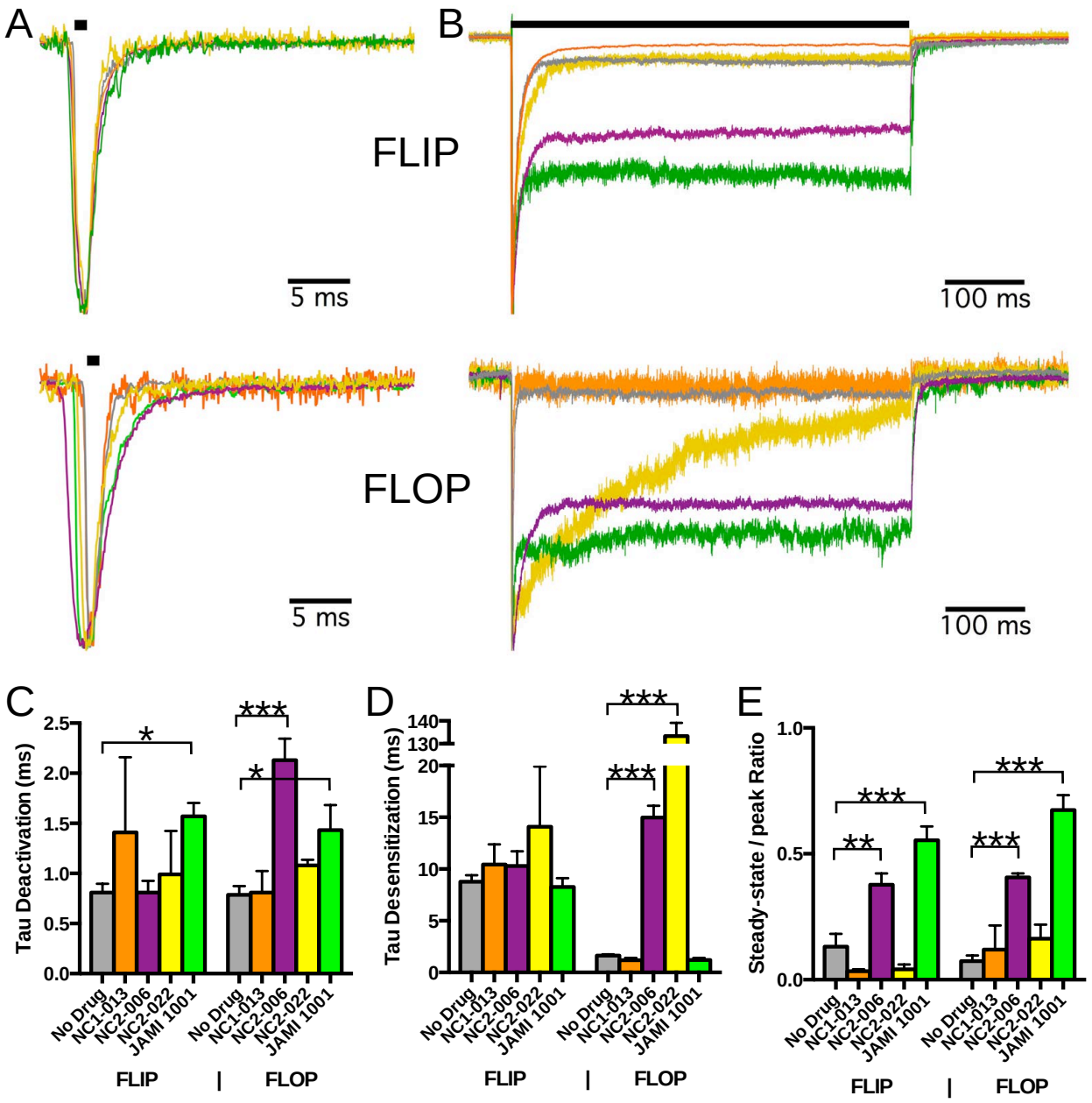

Figure 4.1.2: Effects of NC compounds on GluA2

A) Current responses to 1 ms deactivating glutamate pulses on flip (upper) and flop (lower) GluA2 in presence or absence of modulator. Trace color indicates drug condition in co-ordinance with graphs below. **B)** Current responses to 500 ms desensitizing glutamate pulses on flip (upper) and flop (lower) GluA2 in presence or absence of modulator. **C-E)** Graphical representations showing Tau Deactivation (c), Tau Desensitization (d) and Steady-state to peak ratio (e). *p<.05, **p<.01, ***p<.001, as assessed using two-way anova with Fisher's LSD.

Table 4.1.1: Mean NC compound data

	Deactivation			Desensitization			SS/Peak		
	Mean	SEM	N	Mean	SEM	N	Mean	SEM	N
FLIP									
No Drug	0.81	0.087	6	8.78	0.624	7	0.131	0.051	7
NC1-013	1.41	0.750	3	10.44	1.935	3	0.034	0.007	3
NC2-006	0.81	0.117	2	10.30	1.416	2	0.377	0.045	2
NC2-022	0.99	0.435	3	14.08	5.820	3	0.041	0.019	3
JAMI 1001	1.57	0.134	5	8.26	0.861	5	0.554	0.055	5
FLOP									
No Drug	0.79	0.086	5	1.64	0.113	6	0.074	0.022	6
NC1-013	0.81	0.214	3	1.18	0.232	3	0.120	0.095	3
NC2-006	2.13	0.215	6	14.97	1.145	6	0.406	0.016	6
NC2-022	1.08	0.057	3	133.35	5.745	3	0.163	0.056	3
JAMI 1001	1.43	0.254	7	1.20	0.201	5	0.674	0.059	5

Mean tau deactivation, tau desensitization, and SS/Peak ratio data for NC drug compounds in comparison with no drug and JAMI 1001 for flip and flop receptor isoforms. SEM = Standard error of mean, N indicates number of recordings for each condition. See also figure 4.1.2.

4.2 INVESTIGATING FLIP/FLOP INTERACTIONS WITH R628 USING TARGETED CYSTEINES

4.2.1 Introduction

The second collection of data is in many ways an extension of chapter 3 regarding the R628E mutation. Evident early on in data collection, I noticed a discrepancy between flip and flop isoforms for tau desensitization (figure 3.2d). Conveniently, it was around this time that the intact GluA2 crystal structure was first published (Sobolevsky et al., 2009). Using this structure, along with PyMOL software (The PyMOL Molecular Graphics System Version 1.3, Schrödinger, LLC.), I performed some quick investigations looking into R628 interactions with isoform specific residues, with a special focus on the KDSG/GGGD (flip/flop respectively) region. My first priority was generating a b-factor overlay to observe flexibility of regional structure (figure 4.2.1). I was pleased to find that the KDSG/GGGD containing helix is a highly dynamic structure, suggesting it may potentially move into closer proximity with R628. On this premise, and upon closer examination of the 3KG2.pdb crystal structure file in PyMOL, I devised an experiment (outlined in figure 4.2.2) to probe for an interaction between the R628 residue and the residue 779, which is glycine in the flip isoform, but aspartate for flop receptors. As two cysteine residues in close proximity can form spontaneous disulfide bonds, by making targeted cysteine mutations at these residues I could test for a potential interaction between these sites.

4.2.2 Methods

Methods were similar to those described for testing the R628E mutant. To aid testing of cysteine mutations, a 4-barrel flowpipe was used to allow for separate barrels containing oxidizing and reducing agents. These agents either facilitate cysteine crosslinking (oxidizing) or cause breaking of the disulfide bond (reducing). Copper (II) Phenanthroline at 1 mM concentration was used as an oxidizing agent, while 1 mM – 10 mM dithiothreitol (DTT, Sigma-Aldrich), 1 mM 2-Mercaptoethanol (BME, Sigma-Aldrich) and 750 μM Tris(2-carboxyethyl)phosphine hydrochloride (TCEP, Sigma-Aldrich) were all attempted as reducing agents. Copper (II) Phenanthroline (CuPhen) was made up from stock concentrations of (1,10) phenanthroline (Sigma-Aldrich) and Copper (II) Chloride (Sigma-Aldrich) dissolved in DMSO. DTT was added from a 1 M stock dissolved in DMSO. BME was added in its liquid form directly to EC-α solution. TCEP was made into a 75 mM stock in water, then added to EC-α to a final concentration of 750 μM. Cysteine mutations were made by Amanda Dudek and Vanessa Selwyn in a similar manner as described previously for R628E (Chapter 3). R628C flip and flop were mutated from the GluA2Q-YFP flip and flop construct, respectively. G779C (flip) and D779C (flop) mutants were also generated using the GluA2Q-YFP flip and flop construct, respectively. The double mutant (often referred to as i2x or o2x for flip and flop, respectively) was created using verified R628C flip or flop as a template for i2x and o2x, respectively. Final sequences of all receptor constructs were verified by CSU proteomics and metabolomics facility.

4.2.3 The dual flip mutant shows a synergistic effect of individual mutants

Though preliminary findings, data for the cysteine mutants is shown in figure 4.2.3. Currents for the R628C mutant were small in amplitude and decayed faster than WT flip (Tau desensitization= 4.91 ± 0.396 ms). Meanwhile, currents for G779C (flip) mutants showed no change from WT flip currents (Tau desensitization = 8.02 ± 0.036 ms). However, neither of these individual manipulations seems to account for the observed effect of the double mutant, which showed nearly complete block of desensitization. Additionally, this double mutant showed a slowing of deactivation onset, with a weighted tau of 12.11 ms resulting from fast and slow components (Tau fast = 0.897 ± 0.029 ms, 74%; Tau slow = 44.3 ± 1.03 ms, 26%), much like R628E. However, no change was observed for any oxidizing or reducing agent, suggesting they either do not have access to the mutated cysteines, or that these observed effects may not be due to disulfide bond formation.

4.2.4 Discussion of cysteine mutant studies

These experiments were conducted to investigate a potential interaction between the R628 residue and other receptor residues that show flip/flop differences. Cysteine mutations were made in attempts to form spontaneous disulfide bonds between residues in these regions. However, application of an oxidizing agent (CuPhen) or any of the reducing agents mentioned on double mutant receptors did not cause a change from glutamate alone, suggesting no disulfide bond was formed.

Despite this result, the recordings shown here still suggest an interaction between residues 628 and 779, with the combined mutation showing far greater effect than either individual mutant. As there are many complications that may be preventing bond

formation, it is possible that steric interference of the cysteine residues can cause the observed effect without forming a spontaneous disulfide bond. For example, disulfide bond formation is favored when residues interact at 90-degree angles. Another factor to consider is that substituted cysteines have shorter overall length compared to residues like arginine and glutamate, the two residues featured at the 628 position in chapter 3. Further, it is predicted that effects observed with R628E are due at least in part to electrostatic changes resulting from the mutation. Thus, between the shorter length and loss of Coulombic forces, it remains possible that the cysteines do not come into close enough proximity for spontaneous bond formation. Alternatively, electrostatic interference may also be preventing the cysteine residues from coming within close enough proximity for bond formation.

Another curiosity is how R628C residues in the double mutant interact compared to R628C residues in the R628C single mutant. While structural evidence indicates that R628 residues lie within close proximity and interact with those of adjacent subunits, this interaction occurs between the primary amines of arginine with oxygen atoms on the adjacent subunit backbone (figure 3.1). Thus, it is difficult to predict if R628C residues can form spontaneous disulfide bonds. Additionally, though prior studies suggest R628 to be a solvent accessible residue (Sobolevsky et al., 2009), there would be little room between R628C residues for reducing agents to function in a reducing role, further complicating the assessment of these bonds. As such, while I was not able to observe a direct bond between these sites, further exploration with the flop isoform remains of great future interest.

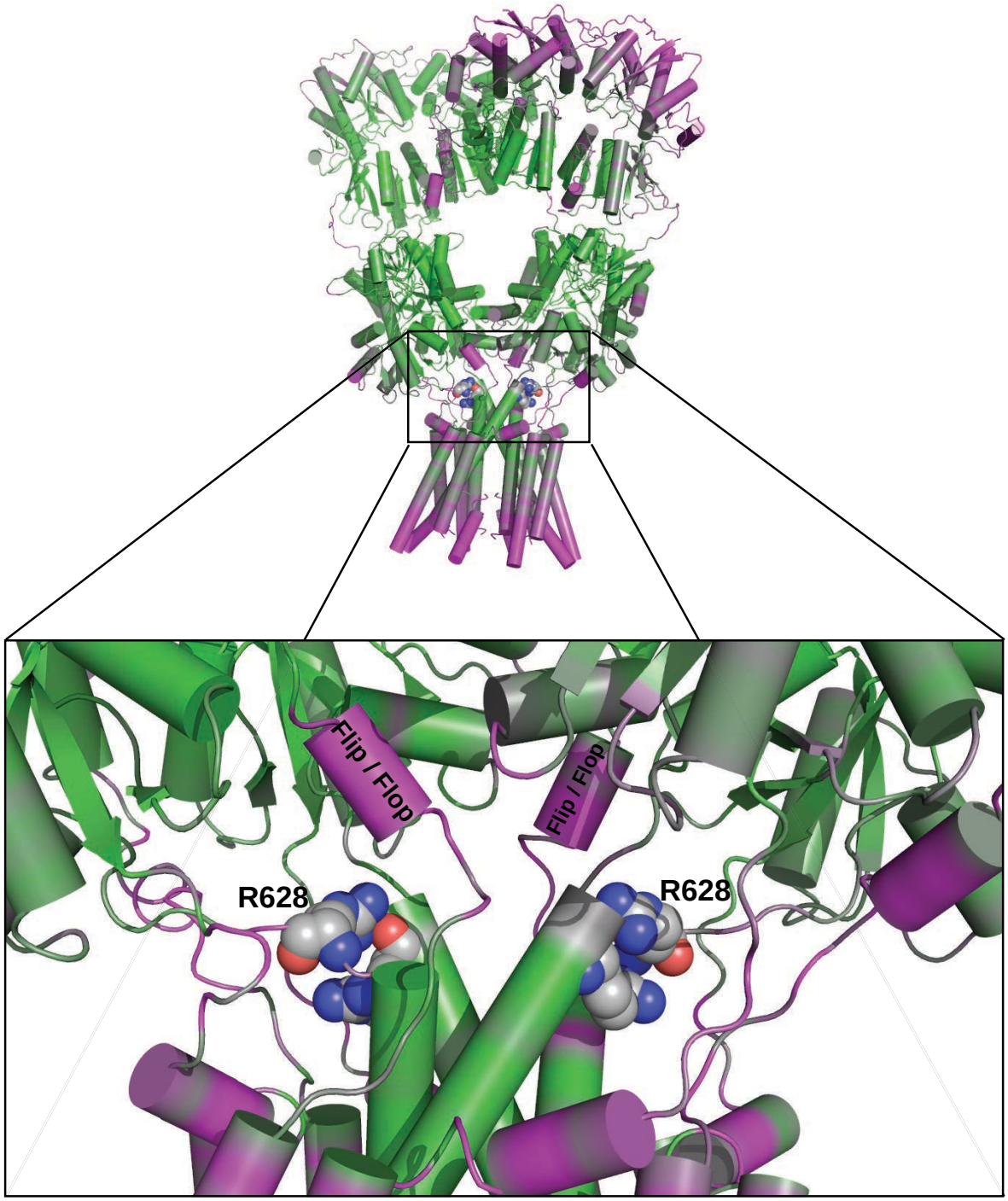

Figure 4.2.1: Proximity of R628 with pre-M4 flip/flop editing region

Cartoon (helices shown as cylinders) of GluA2 crystal structure (3KG2.pdb) with overlay showing relative b- factor. Inset shows region surrounding R628 residues (shown as spheres in CPK colors). Regions in green have more static properties, with magenta colored areas being more dynamic. Note the dynamic helices above R628 residues, which include the isoform edited KDSG / GGGD (flip / flop) region (residues 776-779).

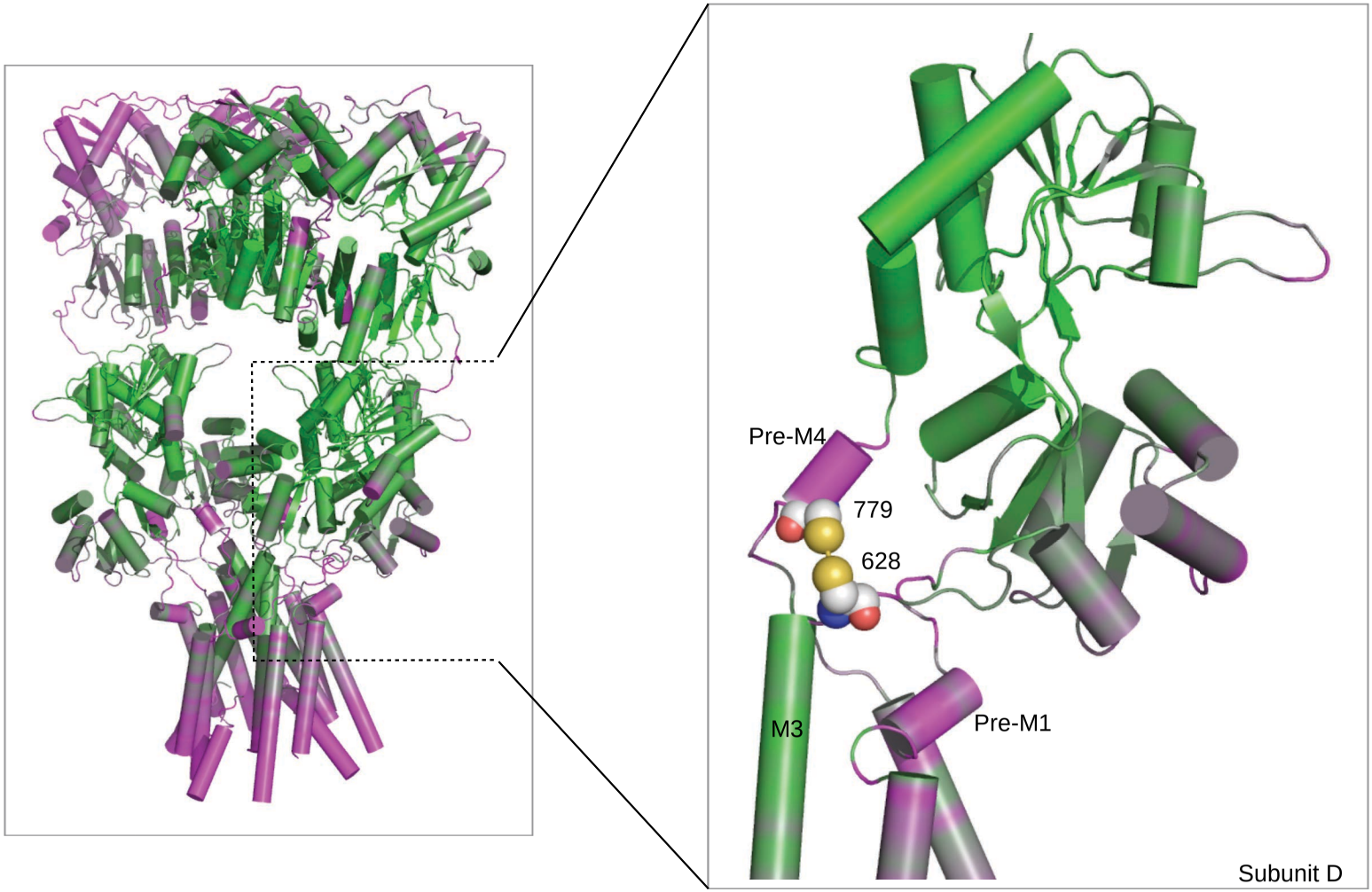

Figure 4.2.2: Structural diagram of chapter 4.2 design strategy

b-factor overlay on AMPA receptor (left panel) expands out to show subunit D only at right panel. Question being asked: Is the dynamic Pre-M4 helix, altered by flip/flop, in close enough proximity to R628 to make a disulfide bond if both are mutated to cysteine?

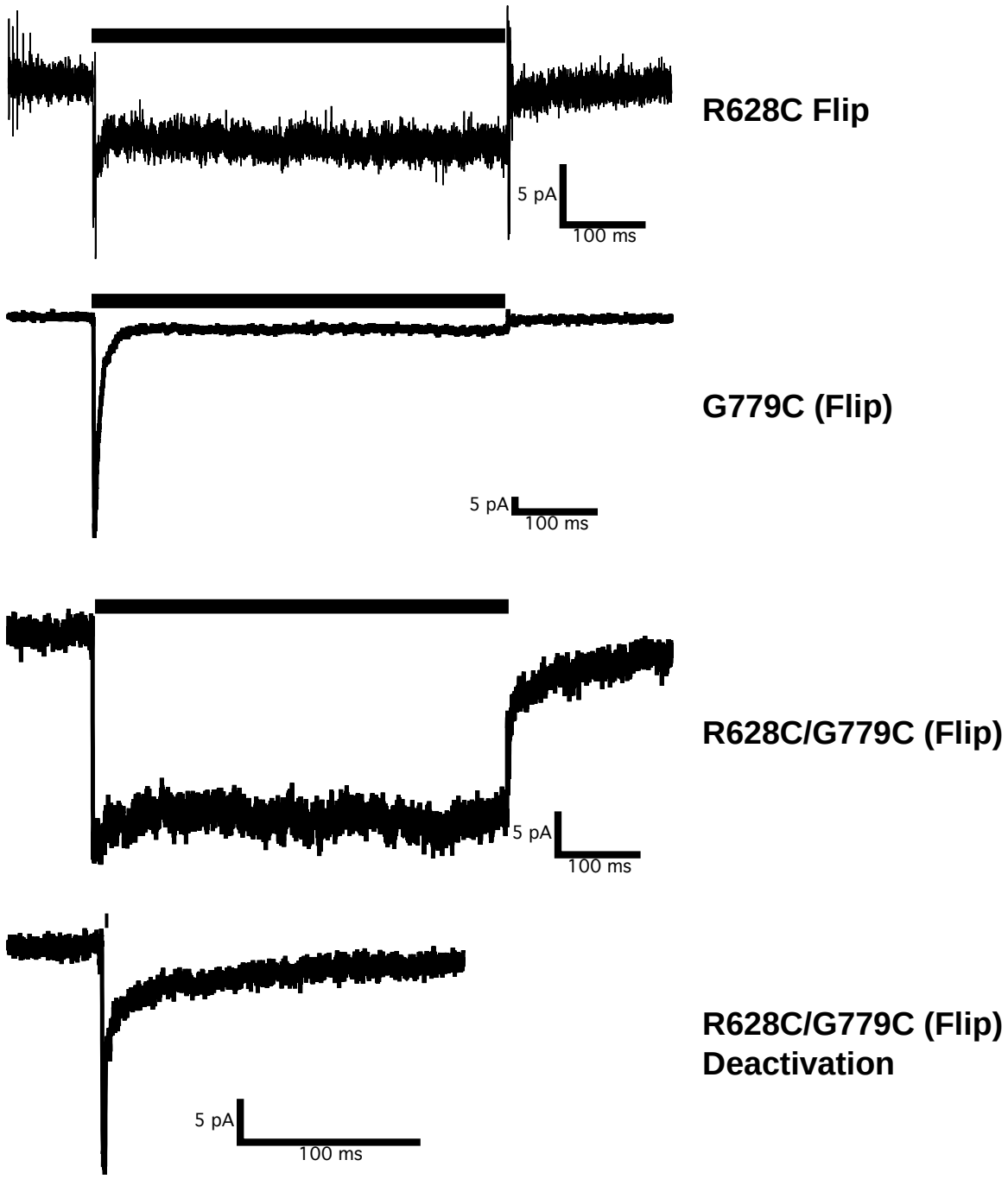

Fig 4.2.3: Double mutation of R628 and G779 residues to cysteine shows a synergistic effect of individual mutants

Desensitization recordings of outside-out patches pulled from HEK 293 cells expressing GluA2 with R628C mutation (top trace), G779C mutation (second tracefrom top) or both mutants together (second trace from bottom). The double mutant shows more than an additive effect of either mutant on its own. Recordings of deactivation for the double mutant are also shown (bottom trace).

4.3 R628E WITH JAMI 1001

4.3.1 Introduction

This last collection of data ties together chapters 2 and 3; that is, the application of JAMI on R628E mutant GluA2 receptors. Though I was in the middle of the R628E project at the time, when provided with a novel modulator for testing, I jumped on the opportunity. Thus, a year of overlapping experiments commenced, and on occasion I would have both prepared JAMI solutions and readied R628E transfected HEK293 cells. With nothing to lose, I took a look at R628E responses to 10 mM glutamate in presence of 100 μM JAMI 1001.

4.3.2 Methods for JAMI use on R628E

Methods were identical to those mentioned for electrophysiology in chapter 3, with the exception of drug used. JAMI 1001 was dissolved directly into EC-α to a final concentration of 100 μM and stored in a -20°C freezer until needed. Glutamate was added to one of the perfusion barrels from a 1M stock dissolved in EC-α to a final concentration of 10 mM.

4.3.3 Results

Since the other modulators applied to R628E traces (CTZ and CX614) showed an additive modulatory effect, it was not a surprise to see the same such observations for application of JAMI 1001 on R628E flip and flop receptors (figure 4.3.1). On homomeric R628E flip receptors, JAMI 1001 trended to slowing tau deactivation even further, from 3.5

± 0.55 to 5.9 ± 0.84 ms, seen from two components (Tau Fast = 0.74 ± 0.21 ms, 59.7%; Tau Slow= 9.30 ± 0.91 ms, 40.3%). Flop R628E receptors also showed an additive slowing for tau deactivation, from 3.3 ± 0.37 ms to 4.9 ± 0.66 ms, again stemming from two components (Tau Fast = 0.41 ± 0.06 ms, 53.0%; Tau Slow = 9.86 ± 1.08 ms, 47.0%). Similar to the other modulators applied to R628E flip and flop receptors, desensitization was completely blocked by JAMI 1001.

To look more closely at the fast and slow components of deactivation, I performed additional analysis on the JAMI and CX614 data with R628E receptors (figure 4.3.2). Interestingly, neither modulator caused a significant change on either the fast or slow component of tau deactivation for either isoform. Rather, observed slowing of deactivation was the result of a shift in weighting, with a greater percentage of the overall current being attributed to the slow component in presence of modulator. In presence of JAMI 1001, receptors shifted to a 40/60 percent split of fast/slow component contributions, compared to a 76/24 percent split with no drug (figure 4.3.2). This change was not seen for CX614 however, which shows no effect on flip deactivation. Similarly, flop receptors showed a shift from an 80/20 percent fast/slow split for R628E flop without drug, to 61/39 percent split for CX614 and 53/47 percent split for JAMI 1001.

4.3.4 Discussion and future directions of JAMI 1001 on R628E

The most interesting finding with JAMI 1001 on R628E receptors comes from the closer analysis of fast and slow components of deactivation. However, this finding is still difficult to interpret. Both JAMI 1001 and R628E are predicted by modeling to act through a slowing of k-off and δ (figures 2.5 and 3.8). Further, application of JAMI parameters to an

R628E flop model, as used in chapter 3, reproduces electrophysiological data seen for modulator on R628E flop. As such, the favored slow component may represent an additive effect of modulator and mutant on slowing k-off. However, why we see this manifest as increased weighting of the slow component and not an increased slowing of either component is not clear. Looking at the energy diagram for R628E models (figure 3.8), in addition to favoring the closed-channel, ligand-bound state, the open channel state also appears to be more favorable than WT, with less of a "peak" required to get between them. Acting through the same mechanisms, though at a different site, JAMI 1001 may even further stabilize these states; resulting in a greater open probability of receptors which is observed as an increased amplitude of the slow component. This may be a result of increased affinity, either for agonist or modulator. Additional information, such as agonist binding data, may be of further benefit for understanding this interaction.

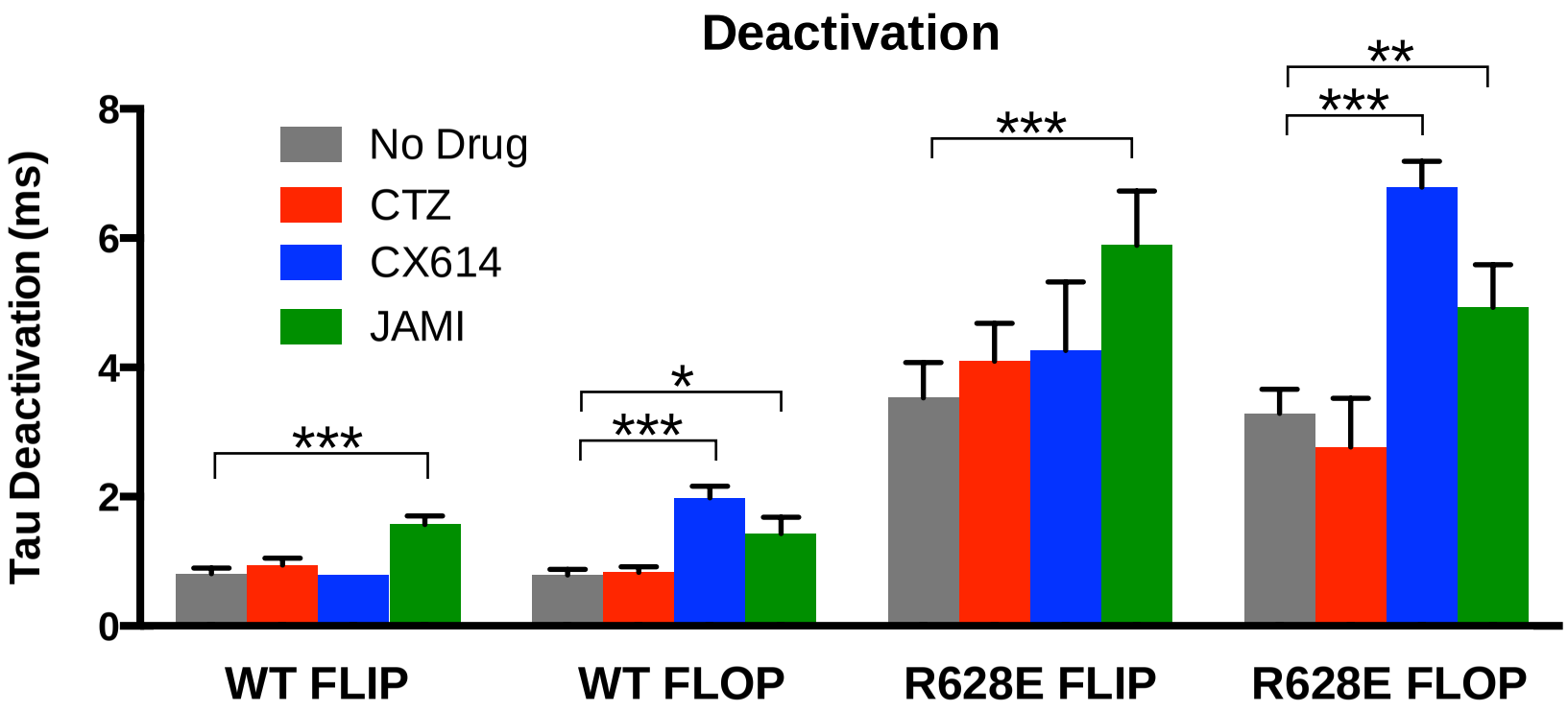

Figure 4.3.1: Mean deactivation data shows JAMI 1001 efficacy on R628E mutant receptors

In addition to modulating wildtype (WT) receptor currents, JAMI 1001 is efficacious on R628E mutant receptors. Deactivation of WT currents was best fit by a single exponential. R628E currents showed fast and slow deactivation components, with the amplitude weighted average depicted. *p < .05, **p < .01, ***p < .001

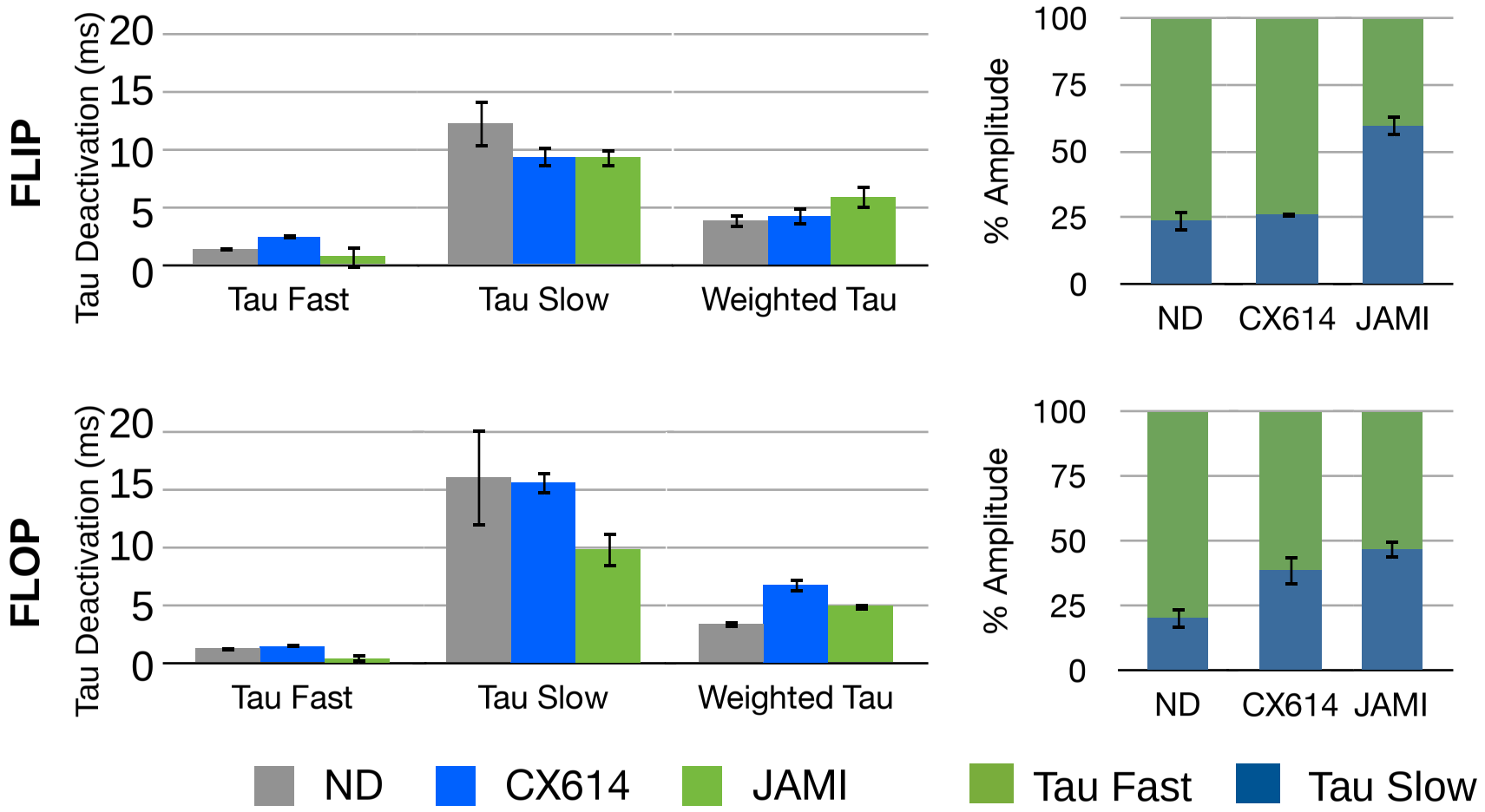

Figure 4.3.2: Fast and Slow components of R628E deactivation

Comparison between the fast and slow components of R628E receptor deactivation shows an interesting effect of modulator. For flip deactivation (top), JAMI 1001 slows overall Tau deactivation without slowing either the fast or slow component, but rather the contribution of each to the weighted Tau. This is also seen for flop receptors with JAMI 1001, and to a lesser extent, CX614.

5. Discussion

5.1 Summary of presented work

The ongoing quest to design better positive allosteric modulators for AMPA receptors continues to be beneficial, not only to the design of drugs themselves but to the understanding of receptor mechanisms. As pharmaceutical companies compete to design better drugs, they have started to use methods such as lead optimization and structure-based drug design (SBDD) to provide additional and useful structural information pertaining to modulatory mechanisms. Here, this structural information is incorporated with physiological analysis in attempts to identify the molecular mechanisms by which modulators induce physiological changes. In addition, GluA2 kinetics have been assessed through the reverse process, as with the case of R628E, where modulators are used to better inform mechanistic interpretations of a structural change to the receptor. Additionally, the application of a kinetic model is repeatedly used to integrate experimental data and suggest potential mechanistic pathways through which modulation occurs.

5.2 Effects of modulator rigidity on isoform specificity

Many AMPA receptor positive allosteric modulators show isoform specific effects (Partin et al., 1996, Kessler et al., 2000, Ptak et al., 2009, Ahmed et al., 2010, Timm et al., 2011). Here (Chapter 2) we present a novel allosteric modulator, JAMI 1001 that is efficacious on both flip and flop homomeric GluA2 receptors.

Alternative splicing leading to flip/flop isoform differences results in differential expression of either a serine (flip) or asparagine (flop) near the hinge of the GluA2 ligand

binding core and lining the allosteric modulator binding pocket between ligand binding dimers (Sun et al., 2002, Jin et al., 2005, Ahmed et al., 2010, Timm et al., 2011). While x-ray crystallography studies of the GluA2 ligand binding core show the flop arginine to be oriented up and out of the way of the ligand binding pocket, the flip isoform serine residue appears to partially obstruct the binding pocket (Appendix 1). Thus, this allosteric modulator binding site differs between flip and flop isoforms. Additionally, surface diagrams of the binding pocket reflect a central "saddle," suggesting a complex terrain in which allosteric modulators must bind.

Allosteric modulators exert their effects through stabilization of ligand binding domain dimers. As such, it makes sense that a more structurally rigid modulator might better stabilize the dimer interface, much in the same way a more structurally rigid car chassis underlies more stable vehicle handling. However, with that rigidity comes a tradeoff. As a structurally stiff car may ride harshly over bumps in the road, a structurally stiff modulator will have similar difficulty conforming to geographical variations of the binding pocket. Thus, while more rigid and/or bulky modulators may bind more tightly and show greater efficacy, flip/flop differences in the pocket can force these modulators to change binding conformation, or prevent binding altogether, resulting in isoform specific differences of modulator affinity and efficacy. JAMI 1001 has a more pliable alkyl chain, allowing it to better conform to surface changes in the binding pocket and tightly bind in a consistent orientation independent of receptor isoform.

5.3 Clues that modulator efficacy is mediated by subsite occupation and rigidity

It has been suggested that structural rigidity of a modulator is linked to its ability to modulate deactivation (Arai et al., 2000). Several studies appear to be consistent with this proposal, suggesting CX614 slows flop receptor deactivation to a greater extent than aniracetam (Jin et al., 2005), CMPDB more than CMPDA on flip receptors (Timm et al., 2011), and NC-006 more than JAMI 1001 on flop GluA2 (Chapter 4.1). While it should be mentioned that rigidity is only inferred; additionally, in each of these studies the more efficacious modulator also had more steric bulk and made additional protein interactions. Thus, while structural rigidity of a modulator may be related to its effect on deactivation, other factors such as size and specific interactions must also be considered.

Another factor appearing to be related to modulator efficacy is subsite occupancy. A consistent observation with modulators that affect GluA2 deactivation (Jin et al., 2005, Timm et al., 2011 , and studies presented here) is the occupation of the A subsite as defined by Ptak et al. (2009), and confirmed by x-ray crystallography. This is more easily seen in comparison with CTZ, which occupies the B and C subsites with little if any innervation into the A subsite, and does not affect deactivation of GluA2 (Timm et al., 2011 and studies here). Similarly, modulators showing the greatest effect on steady-state current reflect structural moieties that most fully occupy the C and C' subsites. Further, the hydrophobic properties of the C subsites suggest this relationship is not reliant on specific electrostatic interactions such as hydrogen bonds. Thus, while this is a small subset of data and there is still much more work to be done, particular patterns are beginning to emerge that show extent of occupancy of a particular subsite is proportional to observed modulatory effects.

5.4 Modulation of GluA2 at other sites

The R628E mutation in the AMPA receptor outer vestibule shows slowed kinetics of deactivation and desensitization as well as an increased steady-state current relationship (here, and Yelshansky et al., 2004). Additionally, it is shown here that these effects of the mutant are acting independently of other allosteric modulators that bind at the orthosteric site (figures 3.5 and 4.3.1). Thus, modulation by R628E must occur through some independent mechanism. An additional and interesting observation about the R628E mutant was the difficulty obtaining patches or currents from HEK cells co-transfected with R628E receptor DNA and the AMPA transmembrane accessory protein, γ-2 (stargazin), which has been shown to increase trafficking and alter kinetics by our lab (Bedoukian et al., 2006, Harms, unpublished data), and others (Tomita et al., 2005). This was observed as an apparent inability for γ-2 and R628E GluA2, as visualized by respective CFP and YFP insertions, to form "rings" of fluorescence in the same HEK293 cell. As such, it is possible that stargazin mediated modulation of GluA2 kinetics is somehow regulated by interactions with this site, and thus somehow occluded by the R628E mutation. Of note, a similar inability of stargazin to mediate trafficking and kinetics of receptors carrying the nearby *lurcher* mutation on the M3 alpha-helix (A622T, Klein and Howe, 2004) has been previously documented (Tomita et al., 2007). Thus, loss of stargazin mediated effects on these mutants suggests this region may be important for receptor trafficking as well; and though alternatively it remains possible that alterations to trafficking may be linked to changes of receptor kinetics, it also remains possible that a drug acting at this sight may be capable of modulating both properties. Therefore, the AMPA receptor external vestibule should be a site of interest for design of both positive and negative allosteric modulators.

5.5 R628E electrostatic interactions that stabilize the closed-cleft, non-desensitized state

Based on results of our modeling (figures 3.7, 3.8), the R628E mutant appears to stabilize the agonist-bound, closed-cleft, non-desensitized state. Looking closely at the crystal structure near R628 (figure 3.1), it is clear that mutating R628 to a residue of opposing charge will potentially result in electrostatic repulsion of negatively charged residues. As the GluA2 structure shown here was crystallized in a putative closed state resulting from bound antagonist, these repulsive forces would likely cause the receptor to favor the agonist bound state. This expected destabilization of the closed receptor position is expected to have a two-fold effect on gating: first, entry into the desensitized state (δ), is slower; and second, the combined process of cleft-opening and agonist dissociation (k-off), which is believed to first require channel closing (Robert and Howe, 2003, Robert et al., 2005), is also slowed, resulting in higher apparent affinity. This slowing of k-off resulting in higher apparent affinity is particularly unusual as explained by our model, which considers the rate of channel closure to be mediated by alpha (α). However, with the subunit asymmetry observed in GluA2 (figure 3.1 and Sobolevsky et al., 2009), R628 has a unique position at the transition of LBD-TMD linker and pore regions. Given this unique position, R628 appears to be a key residue in communicating cleft-closure from agonist binding to channel pore opening, as shown by the consequences of the R628E mutation.

5.6 Additional interactions of R628E suggesting isoform specific differences in modulation

A peculiar observation regarding R628E kinetics is the difference between flip and flop receptor desensitization rates (figure 3.2) and apparent affinity in presence of modulators (figure 3.6). Looking at receptor structure revealed a potential for interaction between R628E and the KDSG (flip)/GGGD (flop) isoform differentiated helix (pre-m4 helix). As can be inferred from amino-acid composition, the pre-m4 helix is interesting based on charge differences, and to a lesser extent, expected rigidity. Using targeted cysteine mutations, an attempt was made to force disulfide bridges between these areas to produce evidence of an interaction (outlined in chapter 4.2 and figure 4.2.2). Although neither disulfide bond formation nor reduction/oxidation effects were observed, a synergistic effect of double disulfide mutation was observed. This effect nearly completely blocked desensitization and slowed deactivation nearly 15-fold compared to WT. Meanwhile, single mutations either had no effect (G779C of the pre-m4 helix) or more minor effects (R628C, figure 4.2.3), suggesting a potential interaction between the two cysteines despite the absence of a disulfide bond. However, it should be mentioned that this study remains preliminary in nature, featuring low n's and yet to assess flop-based isoforms of these mutants. Additionally, previous studies have shown that pre-m4 helix differences are unrelated to differences in flip and flop desensitization kinetics (Quirk et al., 2004). Still, if nothing else, these results and b-factor analysis of the receptor (figure 4.2.1) suggest that the pre-m4 helix can move toward R628 during gating.

5.7 Unforeseeable structural changes resulting in modulation

An additional, potential explanation (that was not discussed in chapter 4.2) for the disulfide bond discrepancy is that structural changes resulting from mutation may assist an interaction between these two regions. As x-ray crystallography only takes "snapshots" of a particular receptor state and time, it becomes difficult to assess just how the mutation may affect overall receptor structure. While drastic changes in receptor conformation are unexpected, small-scale translations in certain dynamic structures, such as the pre-m4 helix, are possible. Additionally, these small changes may correspond to formation or breaking of additional inter- and intra-subunit connections affecting receptor state stability. Further, specific placement of these interactions may have profound effects on receptor kinetics. For an example of this, consider a pair of slip-joint pliers; with the plier "jaws" representing the agonist binding "clamshell" and the plier handles representing links to other parts of the receptor (such as the pore). Even though sliding the joint from one position to the other is a rather short distance (a few millimeters), this small repositioning of the joint (or hinge) can result in a several centimeter shift of the handles in order to open the plier jaws to the same extent. Thus, slight structural alterations close to the hinge can have a profound effect on receptor kinetics. Unsurprisingly, allosteric modulators binding to the orthosteric site and flip/flop residues altering receptor kinetics are located at or interact with the LBD hinges (Partin et al., 1995, Partin et al., 1996, Quirk et al., 2004). Consistent with this finding, newly presented evidence suggests that sites of interaction, and not linker length or tension, are responsible for kinetic changes occurring in NMDA receptors (Kazi et al., 2013).

5.8 Conclusions and considerations for future work

The work presented here analyses how the structure of receptors and positive allosteric modulators influences physiological effects of modulation. However, it is important to keep in mind that x-ray crystal structures used here to assess structural interactions are only "snapshots." Further, the studies detailed here involve a single, edited isoform (GluA2Q) of AMPA receptors. As such, it is important to consider how heteromeric tetramers differ in assembly, structure, and effect of modulation when evaluating this information. Similarly, these differences need to be considered in design of modulatory drugs as well. Still, much of the information presented here appears valuable in principle; and includes demonstrating patterns of modulator occupancy and effect, as well as exploring new receptor regions to consider for future drug design. Ultimately, it appears that structural correlates of modulator function can be discovered through sufficient research, facilitating the design of better AMPA receptor modulatory drugs.

REFERENCES

Ahmed AH, Ptak CP, Oswald RE (2010) Molecular mechanism of flop selectivity and subsite recognition for an AMPA receptor allosteric modulator: structures of GluA2 and GluA3 in complexes with PEPA. Biochemistry 49:2843-2850.

Arai A, Kessler M, Ambros-Ingerson J, Quan A, Yigeter E, Rogers G, Lynch G (1996) Effects of a centrally active benzoylpyrrolidine drug on AMPA receptor kinetics. Neuroscience 75:573-585.

Arai A, Kessler M, Rogers G, Lynch G (2000) Effects of the potent ampakine CX614 on hippocampal and recombinant AMPA receptors: interactions with cyclothiazide and GYKI 52466. Molecular Pharmacology 58:802-813.

Arai AC, Xia YF, Suzuki E (2004) Modulation of AMPA receptor kinetics differentially influences synaptic plasticity in the hippocampus. Neuroscience 123:1011-1024.

Armstrong N, Gouaux E (2000) Mechanisms for activation and antagonism of an AMPA-sensitive glutamate receptor: crystal structures of the GluR2 ligand binding core. Neuron 28:165-181.

Armstrong N, Mayer ML, Gouaux E (2003) Tuning activation of the AMPA-sensitive GluR2 ion channel by genetic adjustment of agonist-induced conformational changes. Proceedings of the National Academy of Sciences of the United States of America 100:5736-5741.

Armstrong N, Sun Y, Chen GQ, Gouaux E (1998) Structure of a glutamate-receptor ligand-binding core in complex with kainate. Nature 395:913-917.

Auer DP, Putz B, Kraft E, Lipinski B, Schill J, Holsboer F (2000) Reduced glutamate in the anterior cingulate cortex in depression: an in vivo proton magnetic resonance spectroscopy study. Biological psychiatry 47:305-313.

Ayalon G, Segev E, Elgavish S, Stern-Bach Y (2005) Two regions in the N-terminal domain of ionotropic glutamate receptor 3 form the subunit oligomerization interfaces that control subtype-specific receptor assembly. J Biol Chem 280:15053-15060.

Bedoukian MA, Weeks AM, Partin KM (2006) Different domains of the AMPA receptor direct stargazin-mediated trafficking and stargazin-mediated modulation of kinetics. J Biol Chem.

Benveniste M, Clements J, Vyklicky L, Mayer ML (1990) A kinetic analysis of the modulation of N-methyl-D-aspartic acid receptors by glycine in mouse cultured hippocampal neurones. Journal of Physiology (London) 428:333-357.

Berman RM, Cappiello A, Anand A, Oren DA, Heninger GR, Charney DS, Krystal JH (2000) Antidepressant effects of ketamine in depressed patients. Biological psychiatry 47:351-354.

Bialer M, Johannessen SI, Levy RH, Perucca E, Tomson T, White HS (2013) Progress report on new antiepileptic drugs: A summary of the Eleventh Eilat Conference (EILAT XI). Epilepsy research 103:2-30.

Black MD (2005) Therapeutic potential of positive AMPA modulators and their relationship to AMPA receptor subunits. A review of preclinical data. Psychopharmacology (Berl) 179:154-163.

Chang PK, Verbich D, McKinney RA (2012) AMPA receptors as drug targets in neurological disease--advantages, caveats, and future outlook. The European journal of neuroscience 35:1908-1916.

Corboy MJ, Thomas PJ, Wigley WC (2005) Aggresome formation. Methods in Molecular Biology 301:305-327.

Donevan SD, Rogawski MA (1993) GYKI 52466, a 2,3-benzodiazepine, is a highly selective, noncompetitive antagonist of AMPA/kainate receptor responses. Neuron 10:51-59.

Dong H, Zhou HX (2011) Atomistic mechanism for the activation and desensitization of an AMPA-subtype glutamate receptor. Nature communications 2:354.

Fernandez MC, Castano A, Dominguez E, Escribano A, Jiang D, Jimenez A, Hong E, Hornback WJ, Nisenbaum ES, Rankl N, Tromiczak E, Vaught G, Zarrinmayeh H, Zimmerman DM (2006) A novel class of AMPA receptor allosteric modulators. Part 1: design, synthesis, and SAR of 3-aryl-4-cyano-5-substituted-heteroaryl-2-carboxylic acid derivatives. Bioorganic & medicinal chemistry letters 16:5057-5061.

Geiger JRP, Melcher T, Koh DS, Sakmann B, Seeburg PH, Jonas P, Monyer H (1995) Relative abundance of subunit mRNAs determines gating and Ca^{2+} permeability of AMPA receptors in principle neurons and interneurons in rat CNS. Neuron 15:193-204.

Gill MB, Kato AS, Wang H, Bredt DS (2012) AMPA receptor modulation by cornichon-2 dictated by transmembrane AMPA receptor regulatory protein isoform. The European journal of neuroscience 35:182-194.

Greger IH, Khatri L, Kong X, Ziff EB (2003) AMPA receptor tetramerization is mediated by Q/R editing. Neuron 40:763-774.

Greger IH, Khatri L, Ziff EB (2002) RNA editing at arg607 controls AMPA receptor exit from the endoplasmic reticulum. Neuron 34:759-772.

Greger IH, Ziff EB, Penn AC (2007) Molecular determinants of AMPA receptor subunit assembly. Trends in neurosciences 30:407-416.

Grove SJ, Jamieson C, Maclean JK, Morrow JA, Rankovic Z (2010) Positive allosteric modulators of the alpha-amino-3-hydroxy-5-methyl-4-isoxazolepropionic acid (AMPA) receptor. Journal of medicinal chemistry 53:7271-7279.

Hald H, Ahring PK, Timmermann DB, Liljefors T, Gajhede M, Kastrup JS (2009) Distinct structural features of cyclothiazide are responsible for effects on peak current amplitude and desensitization kinetics at iGluR2. Journal of molecular biology 391:906-917.

Hampson RE, Rogers G, Lynch G, Deadwyler SA (1998) Facilitative effects of the AMPAkine CX516 on short-term memory in rats: Enhancement of delayed-nonmatch-to-sample performance. Journal of Neuroscience 18:2740-2747.

Harms JE, Benveniste M, Maclean JK, Partin KM, Jamieson C (2013) Functional analysis of a novel positive allosteric modulator of AMPA receptors derived from a structure-based drug design strategy. Neuropharmacology 64:45-52.

Horning MS, Mayer ML (2004) Regulation of AMPA receptor gating by ligand binding core dimers. Neuron 41:379-388.

Hume RI, Dingledine R, Heinemann SF (1991) Identification of a site in glutamate receptor subunits that controls calcium permeability. Science 253:1028-1031.

Jamieson C, Basten S, Campbell RA, Cumming IA, Gillen KJ, Gillespie J, Kazemier B, Kiczun M, Lamont Y, Lyons AJ, Maclean JK, Moir EM, Morrow JA, Papakosta M, Rankovic Z, Smith L (2010a) A novel series of positive modulators of the AMPA receptor: discovery and structure based hit-to-lead studies. Bioorganic & medicinal chemistry letters 20:5753-5756.

Jamieson C, Campbell RA, Cumming IA, Gillen KJ, Gillespie J, Kazemier B, Kiczun M, Lamont Y, Lyons AJ, Maclean JK, Martin F, Moir EM, Morrow JA, Pantling J, Rankovic Z, Smith L (2010b) A novel series of positive modulators of the AMPA receptor: structure-based lead optimization. Bioorganic & medicinal chemistry letters 20:6072-6075.

Jamieson C, Maclean JK, Brown CI, Campbell RA, Gillen KJ, Gillespie J, Kazemier B, Kiczun M, Lamont Y, Lyons AJ, Moir EM, Morrow JA, Pantling J, Rankovic Z, Smith L (2011) Structure based evolution of a novel series of positive modulators of the AMPA receptor. Bioorganic & medicinal chemistry letters 21:805-811.

Jin R, Banke TG, Mayer ML, Traynelis SF, Gouaux E (2003) Structural basis for partial agonist action at ionotropic glutamate receptors. Nature neuroscience 6:803-810.

Jin R, Clark S, Weeks AM, Judman JT, Gouaux E, Partin KM (2005) Mechanism of positive allosteric modulators acting on AMPA receptors. The Journal of neuroscience : the official journal of the Society for Neuroscience 25:9027-9036.

Jin R, Singh SK, Gu S, Furukawa H, Sobolevsky AI, Zhou J, Jin Y, Gouaux E (2009) Crystal structure and association behaviour of the GluR2 amino-terminal domain. The EMBO journal 28:1812-1823.

Jourdi H, Hsu YT, Zhou M, Qin Q, Bi X, Baudry M (2009) Positive AMPA receptor modulation rapidly stimulates BDNF release and increases dendritic mRNA translation. The Journal of neuroscience : the official journal of the Society for Neuroscience 29:8688-8697.

Kato AS, Siuda ER, Nisenbaum ES, Bredt DS (2008) AMPA receptor subunit-specific regulation by a distinct family of type II TARPs. Neuron 59:986-996.

Kazi R, Jian D, Xiang Z, Wollmuth LP (2013) Subunit specificity in linker tension during NMDA receptor gating. 57th Annual Meeting of the Biophysical Society Abstract.

Kessels HW, Malinow R (2009) Synaptic AMPA receptor plasticity and behavior. Neuron 61:340-350.

Kessler M, Arai AC (2006) Use of [3H]fluorowillardiine to study properties of AMPA receptor allosteric modulators. Brain Res 1076:25-41.

Kessler M, Rogers G, Arai A (2000) The norbornenyl moiety of cyclothiazide determines the preference for flip-flop variants of AMPA receptor subunits. Neuroscience Letters 287:161-165.

Kessler M, Suzuki E, Montgomery K, Arai AC (2008) Physiological significance of high- and low-affinity agonist binding to neuronal and recombinant AMPA receptors. Neurochem Int 52:1383-1393.

Klein RM, Howe JR (2004) Effects of the *Lurcher* mutation on GluR1 desensitization and activation kinetics. JNeuralTransm 24:4941-4951.

Koike H, Iijima M, Chaki S (2011) Involvement of AMPA receptor in both the rapid and sustained antidepressant-like effects of ketamine in animal models of depression. Behavioural brain research 224:107-111.

Koike M, Tsukada S, Tsuzuki K, Kijima H, Ozawa S (2000) Regulation of kinetic properties of GluR2 AMPA receptor channels by alternative splicing. The Journal of neuroscience : the official journal of the Society for Neuroscience 20:2166-2174.

Lauterborn JC, Lynch G, Vanderklish P, Arai A, C.M. G (2000) Positive modulation of AMPA receptors increases neurotrophin expression by hippocampal and cortical neurons. Journal of Neuroscience 20:8-21.

Lynch G, Granger R, Ambros-Ingerson J, Davis MC, Kessler M, Schehr R (1997) Evidence that a positive modulator of AMPA-type glutamate receptors improves delayed recall in aged humans. Experimental Neurology 145:89-92.

Matsubara A, Laake JH, Davanger S, Usami S, Ottersen OP (1996) Organization of AMPA receptor subunits at a glutamate synapse: a quantitative immunogold analysis of hair cell synapses in the rat organ of Corti. The Journal of neuroscience : the official journal of the Society for Neuroscience 16:4457-4467.

Mayer ML (2011) Structure and mechanism of glutamate receptor ion channel assembly, activation and modulation. Current opinion in neurobiology 21:283-290.

Meyer AC, Frank T, Khimich D, Hoch G, Riedel D, Chapochnikov NM, Yarin YM, Harke B, Hell SW, Egner A, Moser T (2009) Tuning of synapse number, structure and function in the cochlea. Nature neuroscience 12:444-453.

Mitchell NA, Fleck MW (2007) Targeting AMPA receptor gating processes with allosteric modulators and mutations. Biophys J 92:2392-2402.

Montgomery KE, Kessler M, Arai AC (2009) Modulation of agonist binding to AMPA receptors by 1-(1,4-benzodioxan-6-ylcarbonyl)piperidine (CX546): differential effects across brain regions and GluA1-4/transmembrane AMPA receptor regulatory protein combinations. The Journal of pharmacology and experimental therapeutics 331:965-974.

Morrow JA, Maclean JK, Jamieson C (2006) Recent advances in positive allosteric modulators of the AMPA receptor. Current opinion in drug discovery & development 9:571-579.

Nusser Z (2000) AMPA and NMDA receptors: similarities and differences in their synaptic distribution. Current opinion in neurobiology 10:337-341.

Partin KM, Bowie D, Mayer ML (1995) Structural determinants of allosteric regulation in alternatively spliced AMPA receptors. Neuron 14:833-843.

Partin KM, Fleck MF, Mayer ML (1996) AMPA receptor flip/flop mutants affecting deactivation, desensitization and modulation by cyclothiazide, aniracetam and thiocyanate. Journal of Neuroscience 16:6634-6647.

Partin KM, Mayer ML (1996) Negative allosteric modulation of wild-type and mutants AMPA receptors by GYKI 53655. Molecular Pharmacology 49:142-148.

Penn AC, Balik A, Wozny C, Cais O, Greger IH (2012) Activity-mediated AMPA receptor remodeling, driven by alternative splicing in the ligand-binding domain. Neuron 76:503-510.

Plested AJ, Mayer ML (2009) AMPA receptor ligand binding domain mobility revealed by functional cross linking. The Journal of neuroscience : the official journal of the Society for Neuroscience 29:11912-11923.

Ptak CP, Ahmed AH, Oswald RE (2009) Probing the allosteric modulator binding site of GluR2 with thiazide derivatives. Biochemistry 48:8594-8602.

Quirk JC, Siuda ER, Nisenbaum ES (2004) Molecular determinants responsible for differences in desensitization kinetics of AMPA receptor splice variants. Journal of Neuroscience 24:11413-11420.

Robert A, Armstrong N, Gouaux JE, Howe JR (2005) AMPA receptor binding cleft mutations that alter affinity, efficacy, and recovery from desensitization. The Journal of neuroscience : the official journal of the Society for Neuroscience 25:3752-3762.

Robert A, Howe JR (2003) How AMPA receptor desensitization depends on receptor occupancy. The Journal of neuroscience : the official journal of the Society for Neuroscience 23:847-858.

Rogawski MA (2011) Revisiting AMPA receptors as an antiepileptic drug target. Epilepsy currents / American Epilepsy Society 11:56-63.

Sobolevsky AI, Rosconi MP, Gouaux E (2009) X-ray structure, symmetry and mechanism of an AMPA-subtype glutamate receptor. Nature 462:745-756.

Sommer B, Keinänen K, Verdoorn TA, Wisden W, Burnashev N, Herb A, Köhler M, Takagi T, Sakmann B, Seeburg PH (1990) Flip and flop: a cell-specific functional switch in glutamate-operated channels of the CNS. Science 249:1580-1585.

Staubli U, Perez Y, Xu FB, Rogers G, Ingvar M, Stone-Elander S, Lynch G (1994a) Centrally active modulators of glutamate receptors facilitate the induction of long-term potentiation in vivo. Proceedings of the National Academy of Sciences of the United States of America 91:11158-11162.

Staubli U, Rogers G, Lynch G (1994b) Facilitation of glutamate receptors enhances memory. Proceedings of the National Academy of Sciences of the United States of America 91:777-781.

Stern-Bach Y (2004) AMPA receptor activation; not a square dance. Neuron 41:309-311.

Stern-Bach Y, Bettler B, Hartley M, Sheppard PO, O'Hara PJ, Heinemann SF (1994) Agonist-selectivity of glutamate receptors is specified by two domains structurally related to bacterial amino acid binding proteins. Neuron 13:1345-1357.

Stern-Bach Y, Russo S, Neuman M, Rosenmund C (1998) A point mutation in the glutamate binding site blocks desensitization of AMPA receptors. Neuron 21:907-918.

Sukumaran M, Penn AC, Greger IH (2012) AMPA receptor assembly: atomic determinants and built-in modulators. Advances in experimental medicine and biology 970:241-264.

Sun Y, Olson R, Horning M, Armstrong N, Mayer ML, Gouaux E (2002) Mechanism of glutamate receptor desensitization. Nature 417:245-253.

Suzuki E, Kessler M, Arai AC (2005) C-terminal truncation affects kinetic properties of GluR1 receptors. Mol Cell Neurosci 29:1-10.

Suzuki E, Kessler M, Arai AC (2008) The fast kinetics of AMPA GluR3 receptors is selectively modulated by the TARPs gamma 4 and gamma 8. Mol Cell Neurosci 38:117-123.

Swanson GT, Kamboj SK, Cull-Candy SG (1997) Single-channel properties of recombinant AMPA receptors depend on RNA editing, splice variation, and subunit composition. Journal of Neuroscience 17:58-69.

Timm DE, Benveniste M, Weeks AM, Nisenbaum ES, Partin KM (2011) Structural and functional analysis of two new positive allosteric modulators of GluA2 desensitization and deactivation. Mol Pharmacol 80:267-280.

Tomita S, Adesnik H, Sekiguchi M, Zhang W, Wada K, Howe JR, Nicoll RA, Bredt DS (2005) Stargazin modulates AMPA receptor gating and trafficking by distinct domains. Nature 435:1052-1058.

Tomita S, Shenoy A, Fukata Y, Nicoll RA, Bredt DS (2007) Stargazin interacts functionally with the AMPA receptor glutamate-binding module. Neuropharmacology 52:87-91.

Traynelis SF, Wollmuth LP, McBain CJ, Menniti FS, Vance KM, Ogden KK, Hansen KB, Yuan H, Myers SJ, Dingledine R (2010) Glutamate receptor ion channels: structure, regulation, and function. Pharmacological reviews 62:405-496.

Verdoorn TA, Burnashev N, Monyer H, Seeburg PH, Sakmann B (1991) Structural determinants of ion flow through recombinant glutamate receptor channels. Science 252:1715-1718.

Ward SE, Bax BD, Harries M (2010) Challenges for and current status of research into positive modulators of AMPA receptors. British journal of pharmacology 160:181-190.

Ward SE, Harries M (2010) Recent advances in the discovery of selective AMPA receptor positive allosteric modulators. Current medicinal chemistry 17:3503-3513.

Ward SE, Harries M, Aldegheri L, Austin NE, Ballantine S, Ballini E, Bradley DM, Bax BD, Clarke BP, Harris AJ, Harrison SA, Melarange RA, Mookherjee C, Mosley J, Dal Negro G, Oliosi B, Smith KJ, Thewlis KM, Woollard PM, Yusaf SP (2011) Integration of lead optimization with crystallography for a membrane-bound ion channel target: discovery of a new class of AMPA receptor positive allosteric modulators. Journal of medicinal chemistry 54:78-94.

Xia YF, Arai AC (2005) AMPA receptor modulators have different impact on hippocampal pyramidal cells and interneurons. Neuroscience 135:555-567.

Xia YF, Kessler M, Arai AC (2005) Positive alpha-amino-3-hydroxy-5-methyl-4-isoxazolepropionic acid (AMPA) receptor modulators have different impact on synaptic transmission in the thalamus and hippocampus. The Journal of pharmacology and experimental therapeutics 313:277-285.

Yelshansky MV, Sobolevsky AI, Jatzke C, Wollmuth LP (2004) Block of AMPA receptor desensitization by a point mutation outside the ligand-binding domain. Journal of Neuroscience 24:4728-4736.

Zhang W, Cho Y, Lolis E, Howe JR (2008) Structural and single-channel results indicate that the rates of ligand binding domain closing and opening directly impact AMPA receptor gating. The Journal of neuroscience : the official journal of the Society for Neuroscience 28:932-943.

APPENDIX

SHORT COMMUNICATION WITH CRAIG JAMIESON

An email from Craig Jamieson (craig.jamieson@strath.ac.uk) in unedited format, regarding modeling conducted for the NC compounds mentioned in chapter 4.1.

AMPA Modeling Data

NC2-006 and JAMI1001A were docked in the active site of the flip (pdb code: 4FAT) and flop (pdb code: 3M3L) isoforms of the AMPA receptor using GOLD molecular modeling software. Docked poses of JAMI1001A in the flip structure are in good agreement with that of the crystallized ligand.

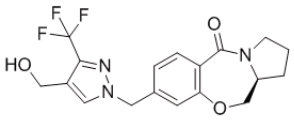

NC2-006

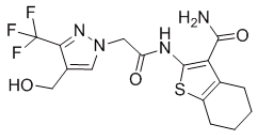

JAMI1001A

JAMI1001A

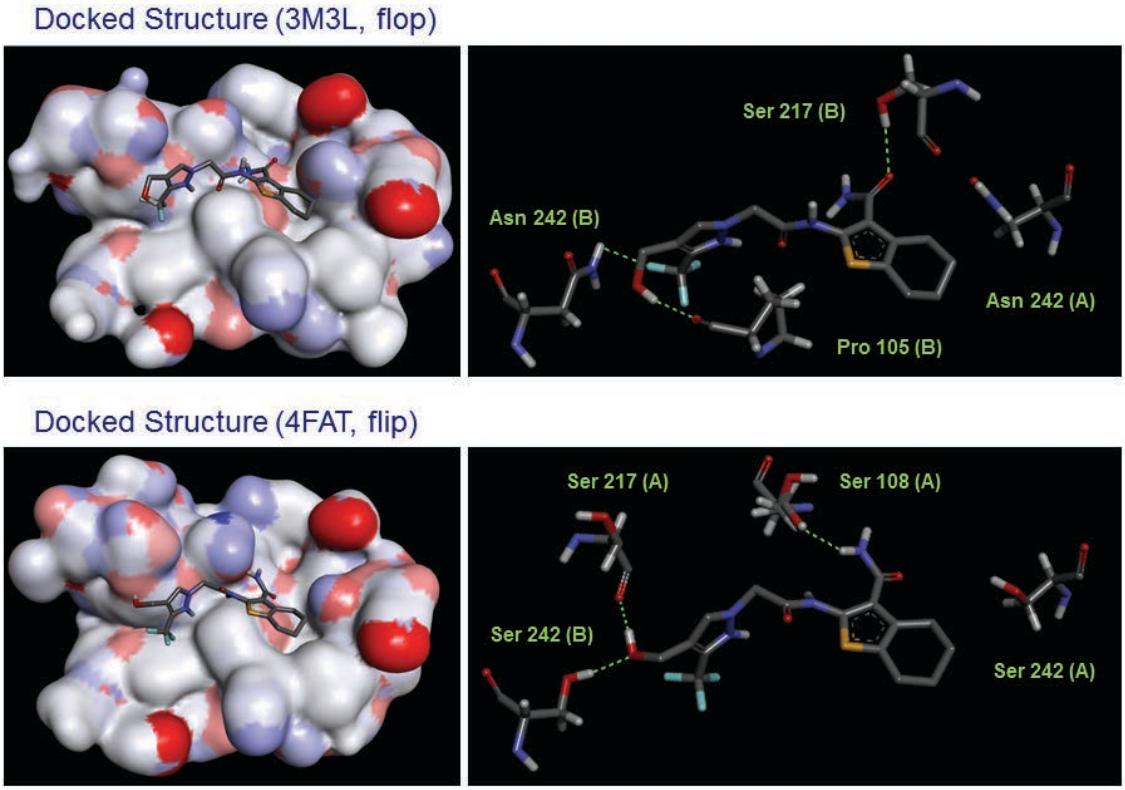

Docking results for JAMI1001A show similar poses in both forms of the receptor, with the compound binding across the 'saddle region' at the active site. This allows the fused ring system to bind in a pocket on the right hand side, and the trifluoromethyl group to point down into a hydrophobic region on the left. Hydrogen bonding interactions of the compound with active site residues are also similar for each isoform (letters (A) and (B) denote each chain of the dimer).

Noticeably, the mutation of an Asn (flop) to a Ser (flip) residue at the binding site is observed at position 242. The Asn residue appears to point upwards out of the pocket in the flop isoform, whilst the hydroxyl group of the Ser residue points into the binding site in the flip isoform.

NC2-006

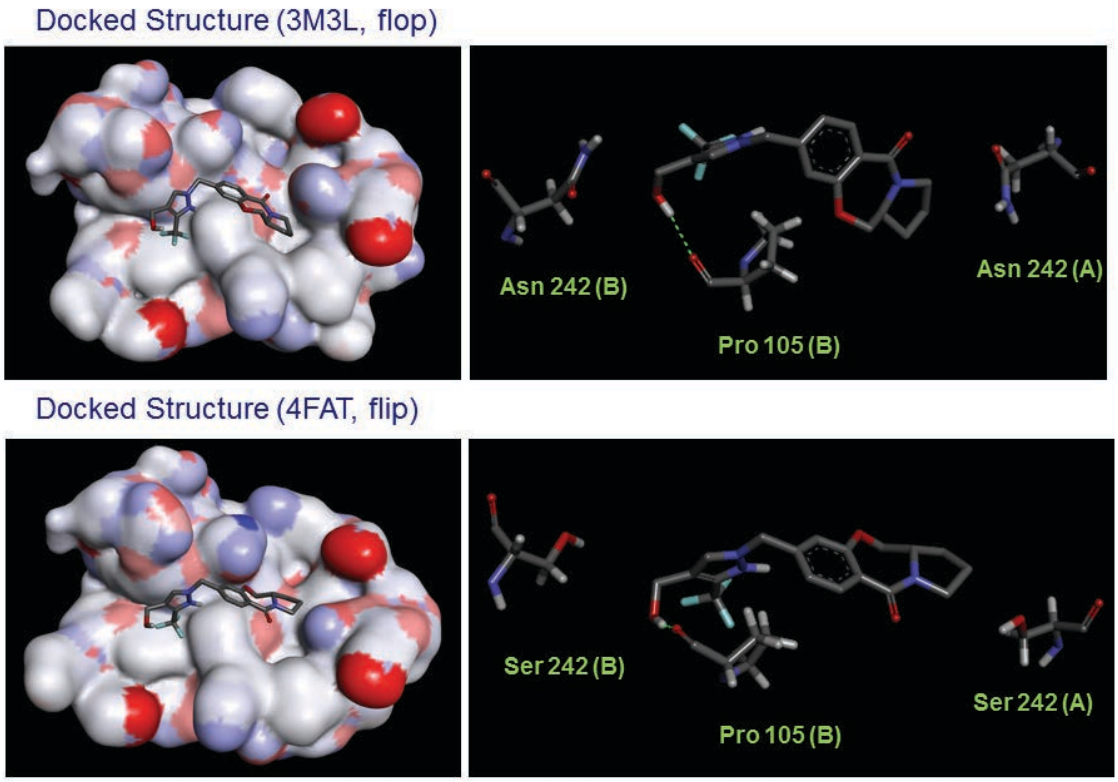

NC2-006 binds in a similar manner to JAMI1001, with the trifluoromethyl group pointing down into the hydrophobic region. The fused ring system binds in the pocket on the right as before, albeit in a slightly different conformation in each isoform of the receptor. The CH_2 linker group enables the compound to bind across the 'saddle region' as was the case with JAMI1001A. It is believed that removal of this linker (NC1-013) would prevent the compound adopting this conformation and make it difficult for this compound to fit in the binding pocket – which agrees with experimental data. NC2-006 shows less hydrogen bonding interactions with active site residues although these appear to be consistent with both the flip and flop forms.

Comparison of space-filling models

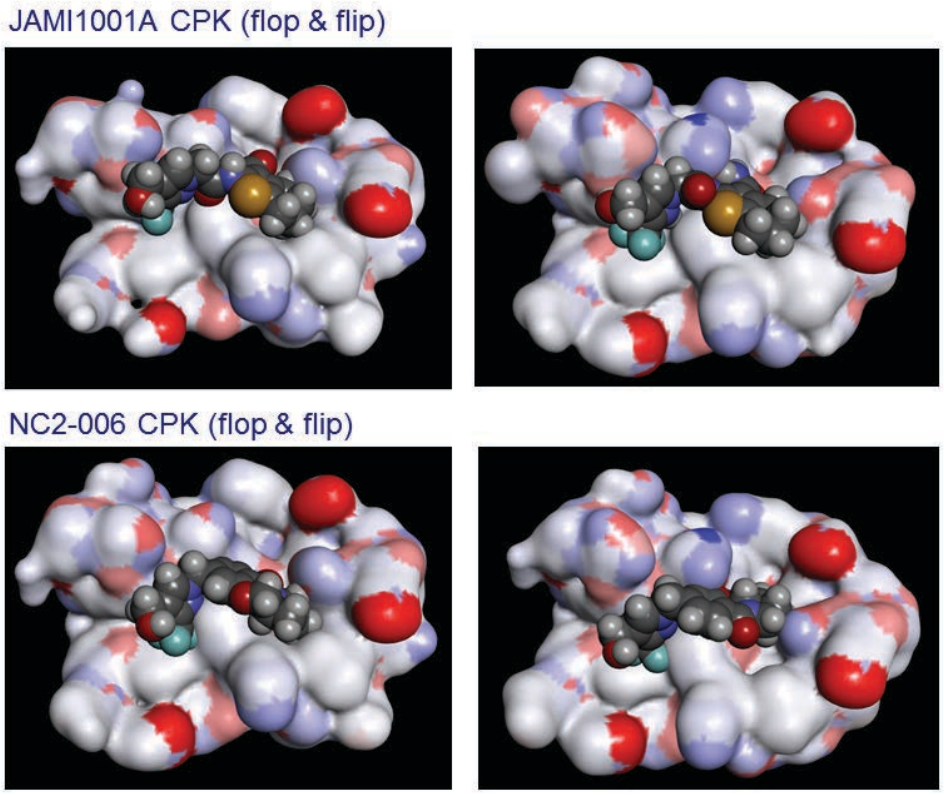

Hypothesizing that the enhanced selectivity of NC2-006 for the flop receptor may simply arise from sterics, space-filling models of each compound were examined in each isoform of the receptor. Whereas, JAMI1001A appears to fit well in the binding pockets of both, NC2-006 is slightly larger and only fits well in the binding site of the flop isoform. The mutated Ser residue which points into the binding pocket of the flip isoform means that the compound clashes with the right hand side of the pocket, suggesting that NC2-006 may not bind well to the flip receptor.

Overall, initial modelling data agrees well with experimental data for these compounds, rationalising why NC2-006 is only effective at the flop receptor whereas JAMI1001A is active at both. It also suggests why NC1-013 is inactive at both forms of the receptor.